



of these natural binding partners, we varied the size and targeting moiety of model drug carriers to determine how these parameters affect CAM-mediated endocytosis. Increasing ICAM-1-targeted carrier size slowed carrier uptake kinetics, reduced carrier trafficking to lysosomes, and increased carrier transport across ECs. Changing targeting moieties from antibodies to peptides decreased particle binding and uptake, lowered trafficking to lysosomes, and increased transport across ECs. Second, using cell culture models of leukocyte/EC interactions, inhibiting regulatory elements of the CAM-mediated pathway disrupted leukocyte sampling, a process crucial to leukocyte crossing of endothelial layers (transmigration). This inhibition also decreased leukocyte transmigration across ECs, specifically through the transcellular route, which occurs through a single EC without disassembly of cell-cell junctions. Third, fibrin meshes, which mimic blood clot fragments/remnants, bound to ECs at ICAM-1-enriched sites and were internalized by the endothelium. Inhibiting the CAM-mediated pathway disrupted this uptake. Following endocytosis, fibrin meshes trafficked to lysosomes where they were degraded. In mouse models, CAM-mediated endocytosis of fibrin meshes appeared to remove fibrin remnants at the endothelial surface, preventing re-initiation of the coagulation cascade. Overall, these results support a link between CAM-mediated endocytosis and leukocyte transmigration as well as uptake of fibrin materials by ECs. Furthermore, these results will guide the future design of ICAM-1-targeted carrier-assisted therapies.

ROLE OF ICAM-1-MEDIATED ENDOCYTOSIS IN ENDOTHELIAL FUNCTION AND  
IMPLICATIONS FOR CARRIER-ASSISTED DRUG DELIVERY.

by

Daniel Serrano

Dissertation submitted to the Faculty of the Graduate School of the  
University of Maryland, College Park, in partial fulfillment  
of the requirements for the degree of  
Doctor of Philosophy  
2014

Advisory committee:  
Professor Silvia Muro, Chair  
Professor Volker Briken  
Professor Peter Kofinas  
Professor Wenxia Song  
Professor Li Zhang

©Copyright by

Daniel Serrano

2014

## **Dedication**

*To my role models, Gioia and Jorge.*

## **Acknowledgements**

I would like to thank my advisor, Dr. Silvia Muro for her invaluable support and guidance during the course of these projects. Her teachings have truly shaped me as a scientist and a professional. I acknowledge Dr. Tridib Bhowmick, Dr. Carmen Garnacho and Dr. Ming Meng, postdoctoral fellows in the Muro lab who contributed to these projects. I also thank Rishi Chadha, Donna Motabar, Eden Paul, and especially Maria Ansar, undergraduate students whose help was invaluable for completing this work. Dr. Janet Hsu and Rasa Ghaffarian are two of the kindest people I have worked with, and their voluntary advice helped me develop my experiments more efficiently.

My graduate studies were supported by the National Science Foundation through their Bridge to the Doctorate and Graduate Research Fellowship initiatives, and also by the National Institutes of Health through their Research Supplements to Promote Diversity. I acknowledge the great contribution of these institutions to the success of my scientific career.

# Table of Contents

<b>Dedication .....</b>	<b>ii</b>
<b>Acknowledgements .....</b>	<b>iii</b>
<b>Table of Contents .....</b>	<b>iv</b>
<b>List of Tables .....</b>	<b>viii</b>
<b>List of Figures.....</b>	<b>ix</b>
<b>List of Abbreviations .....</b>	<b>xii</b>
<b>Chapter 1: Motivation and Goals.....</b>	<b>1</b>
<b>Chapter 2: Background.....</b>	<b>4</b>
2.1. <i>Intercellular Adhesion Molecule 1 (ICAM-1)</i> .....	4
2.2. <i>Cell Adhesion Molecule (CAM)-Mediated Endocytosis</i> .....	8
2.3. <i>Leukocyte Transendothelial Migration</i> .....	14
2.4. <i>Route of Leukocyte Transmigration</i> .....	18
2.5. <i>Coagulation and Fibrinolysis</i> .....	21
2.6. <i>Clot Dissolution and Remnant Clearance</i> .....	26
<b>Chapter 3: Methods .....</b>	<b>29</b>
3.1. <i>Antibodies and Reagents</i> .....	29
3.2. <i>Microscopy Equipment and Software</i> .....	30
3.3. <i>Iodination of Proteins for Radiotracing</i> .....	31
3.4. <i>Preparation of ICAM-1- or M6PR-Targeted Particles</i> .....	31
3.5. <i>Cell Culture</i> .....	34
3.6. <i>Binding of ICAM-1- or M6PR-Targeted Particles to Endothelial Cells</i> .....	35
3.7. <i>Uptake of ICAM-1 or M6PR-Targeted Particles by Endothelial Cells</i> .....	36
3.8. <i>Actin Staining and Ceramide Enrichment at Sites of ICAM-1 or M6PR-Targeted Particle Interaction with Endothelial Cells</i> .....	36

3.9	<i>Lysosomal Transport of ICAM-1-Targeted Particles.</i>	38
3.10.	<i>Transport of ICAM-1-Targeted Particles Across Endothelial Cells.</i>	38
3.11.	<i>Imaging of Lymphocyte Adhesion and Pre-transmigratory Interactions with Endothelial Cells.</i>	40
3.12.	<i>Quantification of Lymphocyte Transmigration Across Endothelial Cell Monolayers.</i>	41
3.13.	<i>Quantification of the Route of Lymphocyte Transmigration Across Endothelial Cells.</i>	42
3.14.	<i>Interaction of Fibrin Meshes or Microemboli with Endothelial Cells.</i>	43
3.15.	<i>Uptake of Fibrin Meshes or Microemboli by Endothelial Cells.</i>	44
3.16.	<i>Lysosome Trafficking of Fibrin Meshes in Endothelial Cells.</i>	45
3.17.	<i>SDS-PAGE and Western Blotting of Fibrin Meshes.</i>	46
3.18.	<i>Visualization of Fibrin Microemboli in Mice.</i>	47
3.19.	<i>Statistics.</i>	49
<b>Chapter 4: Role of Particle Size and Targeting Moiety on the Outcomes of ICAM-1-Mediated Endocytosis</b>		<b>50</b>
4.1.	<i>Background</i>	50
4.2.	<i>Results</i>	53
4.2.1.	Model to study the role of particle size and targeting moiety on CAM-mediated pathway outcomes.	53
4.2.2.	Role of particle size and targeting moiety on binding of ICAM-1-targeted particles.	54
4.2.3.	Role of particle size and targeting moiety on endothelial uptake of ICAM-1-targeted particles.	63
4.2.4.	Role of particle size and targeting moiety of ICAM-1-targeted particles on ceramide enrichment during CAM-mediated endocytosis.	66
4.2.5.	Role of particle size on the requirement for sphingomyelinase activity during endocytosis.	72
4.2.6.	Role of size and targeting moiety on intracellular trafficking of ICAM-1-targeted particles.	76

4.2.7. Size and targeting moiety of ICAM-1-targeted particles affect transport across endothelial cells. ....	80
4.3. <i>Conclusions</i> .....	84
<b>Chapter 5: Contribution of Regulatory Elements of the CAM-Mediated Pathway to Lymphocyte Transmigration across Endothelial Cells .....</b>	<b>86</b>
5.1. <i>Background</i> .....	86
5.2. <i>Results</i> .....	88
5.2.1. Contribution of CAM-mediated endocytosis to pre-transmigration interactions between lymphocytes and endothelial cells. ....	88
5.2.2. Contribution of CAM-mediated endocytosis to lymphocyte transmigration across endothelial cells. ....	98
5.2.3. Contribution of CAM-mediated endocytosis lymphocyte transcellular transmigration across endothelial cells. ....	103
5.3. <i>Conclusion</i> .....	107
<b>Chapter 6: Contribution by the CAM-Mediated Pathway to Endothelial Uptake and Degradation of Fibrin Polymers.....</b>	<b>110</b>
6.1. <i>Background</i> .....	110
6.2. <i>Results</i> .....	112
6.2.1. Initial interaction between fibrin meshes and endothelial cells. ....	112
6.2.2. Internalization of fibrin meshes by endothelial cells with contribution by the CAM-mediated pathway.....	118
6.2.3. Intracellular trafficking of fibrin meshes and contribution of lysosomes to fibrin mesh degradation. ....	126
6.2.4. Characterization of model fibrin microemboli for <i>in vivo</i> studies.....	133
6.2.5. Contribution by the CAM-mediated pathway to endothelial uptake of fibrin microemboli <i>in vivo</i> . ....	135
6.3. <i>Conclusion</i> .....	144
<b>Chapter 7: Overall Conclusions .....</b>	<b>146</b>
7.1. <i>Summary of Results, Significance, and Novelty</i> .....	146

7.1.1. Role of drug carrier size and targeting moiety on the outcomes of ICAM-1-mediated endocytosis.....	147
7.1.2. Role of ICAM-1-mediated endocytosis in leukocyte transmigration. ....	148
7.1.3. Role of ICAM-1-mediated endocytosis in clearance of blood clot fragments/remnants.....	150
7.2. <i>Future Directions</i> .....	152
<b>Literature Cited .....</b>	<b>156</b>

## List of Tables

Table 1. Comparison of endocytic pathways.....	12
Table 2. Characterization of ICAM-1 or M6PR-binding particles.....	33
Table 3. Injection treatments used for microscopy of mouse emboli models.....	48
Table 4. Particles used for the study of sphingomyelinase requirements in endocytosis.....	72

## List of Figures

Figure A. ICAM-1 structure, binding and signaling.....	5
Figure B. The CAM-mediated pathway of endocytosis.....	9
Figure C. Leukocyte recruitment at the endothelium and transmigration.....	16
Figure D. Structure of fibrin(ogen).....	21
Figure E. Coagulation and fibrinolysis.....	23
Figure 1. Binding of anti-ICAM particles to fixed endothelial cells.....	55
Figure 2. Binding of $\gamma 3$ particles to fixed endothelial cells.....	57
Figure 3. Association of anti-ICAM particles to live endothelial cells.....	59
Figure 4. Association of $\gamma 3$ particles to live endothelial cells.....	61
Figure 5. Comparison of binding of anti-ICAM versus $\gamma 3$ particles to endothelial cells.....	62
Figure 6. Uptake of anti-ICAM particles by endothelial cells.....	64
Figure 7. Uptake of $\gamma 3$ particles by endothelial cells and comparison with anti-ICAM particle uptake.....	65
Figure 8. Ceramide enrichment at sites of binding of ICAM-1-targeted particles to endothelial cells and effect on uptake.....	68
Figure 9. Uptake of anti-M6PR particles coated with neutral sphingomyelinase.....	73
Figure 10. Role of neutral sphingomyelinase on ceramide enrichment and actin for anti-M6PR particles.....	74
Figure 11. Role of particle size on neutral sphingomyelinase dependency for uptake.....	75
Figure 12. Lysosome trafficking of anti-ICAM particles.....	77
Figure 13. Lysosome trafficking of anti-ICAM versus $\gamma 3$ particles.....	79
Figure 14. Association of ICAM-1-targeted particles to endothelial cells on porous membranes.....	82
Figure 15. Transport of ICAM-1-targeted particles across endothelial cells.....	83
Figure 16. Enrichment of plasma membrane molecules as sites of interaction between lymphocytes and endothelial cells.....	89

Figure 17. Model to examine pre-transmigratory interactions between lymphocytes and endothelial cells.....	91
Figure 18. Effect of inhibitors on both lymphocytes and endothelial cells during pre-transmigratory interactions.....	93
Figure 19. Effect of inhibitors only on endothelial cells during pre-transmigratory interactions with lymphocytes.....	96
Figure 20. Model to examine transmigration of lymphocytes across endothelial monolayers.....	99
Figure 21. Effect of inhibitors on both lymphocytes and endothelial cells during binding and transmigration.....	100
Figure 22. Effect of inhibitors only on endothelial cells during lymphocyte binding and transmigration.....	101
Figure 23. Confocal microscopy of the route of lymphocyte transmigration across endothelial cells.....	104
Figure 24. Effect of inhibitors on the route of lymphocyte transmigration across endothelial cells.....	106
Figure 25. Formation of fibrin meshes on the surface of endothelial cells.....	113
Figure 26. Kinetics of fibrin mesh interaction with endothelial cells grown on porous membranes.....	115
Figure 27. Effect of blocking antibodies on the binding of fibrin meshes to endothelial cells.....	116
Figure 28. Enrichment of endothelial molecules at sites of fibrin mesh binding to endothelial cells.....	117
Figure 29. Kinetics of fibrin mesh internalization by endothelial cells.....	119
Figure 30. Role of fibrinolysis in the internalization of fibrin meshes by endothelial cells.....	121
Figure 31. Immunodetectability of endothelium-internalized fibrin meshes after permeabilization.....	123
Figure 32. Mechanism of fibrin mesh internalization by endothelial cells.....	125
Figure 33. Intracellular trafficking of fibrin meshes in endothelial cells.....	126
Figure 34. Effect of chloroquine on fibrin mesh colocalization with lysosomes in endothelial cells.....	128

Figure 35. Role of lysosomes in fibrin mesh degradation by endothelial cells.....	129
Figure 36. SDS-PAGE and Western blot characterization of fibrin mesh interaction with endothelial cells.....	131
Figure 37. Binding and internalization of fibrin microemboli by endothelial cells...	134
Figure 38. Confocal analysis of fibrin microemboli interaction with cells in mouse lungs.....	137
Figure 39. Model to study fibrin microemboli in the brain <i>in vivo</i> .....	140
Figure 40. Role of CAM-mediated endocytosis in fibrin microemboli clearance <i>in vivo</i> .....	142

## List of Abbreviations

ALCAM, Activated leukocyte cell adhesion molecule  
ASM, Acid sphingomyelinase  
BIM-1, Bisindolylmaleimide-1  
BSA, Bovine serum albumin  
CAM, Cell adhesion molecule  
Cdx, methyl- $\beta$ -cyclodextrin  
CPM, Counts per minute  
D1-D5, Domains 1 through 5 of ICAM-1  
EC, Endothelial cell  
EIPA, 5-(N-Ethyl-N-isopropyl)amiloride  
FBS, Fetal bovine serum  
GPRP, Glycine-proline-arginine-proline  
H-7, 1-(5-isoquinolylsulfonyl)-2-methyl-piperzine  
HBMEC, Human brain microvascular endothelial cell  
HBSS, Hank's balanced salt solution  
HEPES, (4-(2-hydroxyethyl)-1-piperazineethanesulfonic acid  
HUVEC, Human umbilical vein endothelial cell  
ICAM-1, Intercellular adhesion molecule 1  
IFN $\gamma$ , Interferon  $\gamma$   
IL-2, Interleukin 2  
LAMP-1, Lysosomal-associated membrane protein 1  
LFA-1, Lymphocyte function-associated antigen 1  
M6PR, Mannose 6-phosphate receptor  
Mac-1, Macrophage-1 antigen  
MAPK, Mitogen-activated protein kinase  
MDC, Monodansylcadaverine  
NHE1, Na<sup>+</sup>/H<sup>+</sup> exchanger 1  
NSM, Neutral sphingomyelinase  
PAI-1, Plasminogen activator inhibitor 1  
PBS, Phosphate-buffered saline

PECAM-1, Platelet-endothelial cell adhesion molecule-1  
PI3K, Phosphatidylinositol 3-phosphate kinase  
PKC, Protein kinase C  
PLGA, Poly(lactic-co-glycolic acid)  
PMA, Phorbol 12-myristate 13-acetate  
PSGL-1, P-selectin glycoprotein ligand 1  
ROCK, Rho-dependent kinase  
ROS, Reactive oxygen species  
SDF-1 $\alpha$ , stromal cell-derived factor 1-alpha  
SDS-PAGE, Sodium dodecyl sulfate polyacrylamide gel electrophoresis  
SHP-2, Src-homology domain 2 containing phosphatase 2  
TCA, Trichloroacetic acid  
TGF $\beta$ , Transforming growth factor  $\beta$   
TNF $\alpha$ , Tumor necrosis factor  $\alpha$   
tPA, Tissue plasminogen activator  
uPA, Urokinase plasminogen activator  
VCAM-1, Vascular cell adhesion molecule-1  
VE-cadherin, vascular endothelial cadherin  
VLA-4, Very late antigen 4  
WBC, leukocyte (white blood cell)

## Chapter 1: Motivation and Goals

Lining the interface between blood and tissues, vascular endothelial cells use a diverse set of molecules to achieve functions that are critical to organismal homeostasis [1]. One of these molecules is intercellular adhesion molecule 1 (ICAM-1), a glycoprotein of the immunoglobulin superfamily expressed on the surface of endothelial cells [2] that mediates recruitment of leukocytes to sites of inflammation [3]. Due to its localized upregulation during the inflammatory response [4], ICAM-1 has gained attention in the field of drug delivery; this molecule can be used to target therapeutics to diseased tissue by employing ICAM-1-binding drug delivery carriers [5]. The development of these targeting strategies has led to the discovery of a non-classical endocytic pathway known as cell adhesion molecule (CAM)-mediated endocytosis, which is activated when drug carriers bind multiple copies of ICAM-1 on the surface of endothelial cells [6]. Uptake of carriers through this pathway depends on Na<sup>+</sup>/H<sup>+</sup> exchanger 1 (NHE1), acid sphingomyelinase (ASM)-driven production of ceramide, and rearrangement of actin into stress fibers [6-8]. After uptake, drug carriers undergo trafficking to lysosomes, as well as transcytosis across cell barriers [9-11].

Although significant efforts have been made to understand and optimize the use CAM-mediated endocytosis for drug delivery, several questions remain about the regulation of this pathway. Furthermore, CAM-mediated endocytosis has been associated with endocytic phenomena, such as recycling of this molecule at the immunological synapse [12] and entry of human rhinovirus into cells [13, 14], but the physiological role

of the CAM-mediated pathway in the endothelium is still obscure. The objective of the work presented in this dissertation was to expand our understanding of CAM-mediated endocytosis in the context of drug delivery, and to explore the physiological relevance of this pathway in the endothelium.

To achieve this, we focused on two important natural ligands of ICAM-1: leukocytes, which bind to ICAM-1 via  $\beta_2$  integrins, and fibrin polymers, which bind to ICAM-1 via the fibrin(ogen)  $\gamma_3$  sequence. While  $\alpha_L\beta_2$  is found in multiple copies on the surface of leukocytes [15], fibrin polymers are the main component of the blood clot matrix [16]. Thus, both leukocytes and blood clots have the potential to bind multiple copies of ICAM-1 on the surface of cells, similar to drug carriers that elicit the CAM-mediated pathway. In addition to this, leukocyte or fibrin(ogen) interaction with endothelial cells elicits similar signaling and responses seen during CAM-mediated endocytosis [17, 18], including massive rearrangement of the actin cytoskeleton [19, 20]. In the case of leukocytes, this signaling has been linked to the process of transmigration across endothelial cells, which requires membrane and vesicular dynamics [21]. In the case of fibrin clots, it has been shown that interaction with endothelial cells leads to clot extravasation [22]. Thus, it is plausible that CAM-mediated endocytosis is activated upon binding of leukocytes and fibrin polymers to ICAM-1, and that this pathway is involved in endothelial functions associated with leukocytes and/or blood clots.

Inspired by notable properties of these ICAM-1 natural binding partners, we first explored how the parameters of size and targeting moiety can affect binding, internalization and intracellular trafficking of drug carriers targeted to CAM-mediated endocytosis (Aim 1). Then, we explored the potential role of regulatory elements of the

CAM-mediated pathway in the interaction between the endothelium and leukocytes (Aim 2) or fibrin polymers (Aim 3). Improving our understanding of CAM-mediated endocytosis can allow for the optimization of drug delivery strategies that use ICAM-1 as a target. Furthermore, increasing our knowledge of leukocyte and blood clot interaction with the endothelium may expand our basic understanding of endothelial cells and has important clinical relevance.

The following section (Chapter 2) will provide a background on ICAM-1, CAM-mediated endocytosis, and the interaction of the endothelium with leukocytes and blood clots. Chapter 3 will summarize the methodologies used in our studies. Then, chapters 4, 5 and 6 will describe and discuss the results found for each respective aim. Finally, Chapter 7 will present the conclusions of this work, and provide future directions that ramify from the present findings.

## Chapter 2: Background

### 2.1. Intercellular Adhesion Molecule 1 (ICAM-1)

Intercellular adhesion molecule 1 (ICAM-1; CD54) is a glycoprotein of the immunoglobulin superfamily first characterized in 1986 as a 90 kDa antigen necessary for homotypic aggregation of leukocytes [23]. Contemporary studies revealed that ICAM-1 was expressed on the surface of fibroblasts and endothelial cells (among others), and showed its role in lymphocyte adhesion to non-hematopoietic cells and its upregulation in the presence of several cytokines [2, 24], forecasting its importance in the inflammatory response. Within five years of its discovery, a variety of studies consolidated ICAM-1 as a molecule crucial to immune function, highlighting its role in T cell-mediated cytotoxicity [25] and B cell activation [26], T cell activation [27-30], lymphocyte-endothelium interactions [3, 26], and various pathologies [4, 31-34].

Structurally, ICAM-1 is a type I transmembrane protein, whose extracellular region consists of five Ig-like domains (D1 at the N-terminus, through D5 adjacent to the plasma membrane) [35-37]. These domains are arranged linearly in a kinked rod-like conformation that extends from the cell surface (Figure A), positioning ICAM-1 in a manner suitable for its function as an adhesive co-receptor for leukocytes on both hematopoietic and non-hematopoietic cells [26, 38]. The five extracellular domains are connected via a single transmembrane region to the cytosolic C-terminal tail of ICAM-1. Consisting of 28 residues [36], the ICAM-1 cytosolic domain lacks conventional protein-protein interaction sequences. However, it contains several positively charged residues

and one tyrosine, which seem to account for its protein-binding and signaling activities [39-43], as described below.

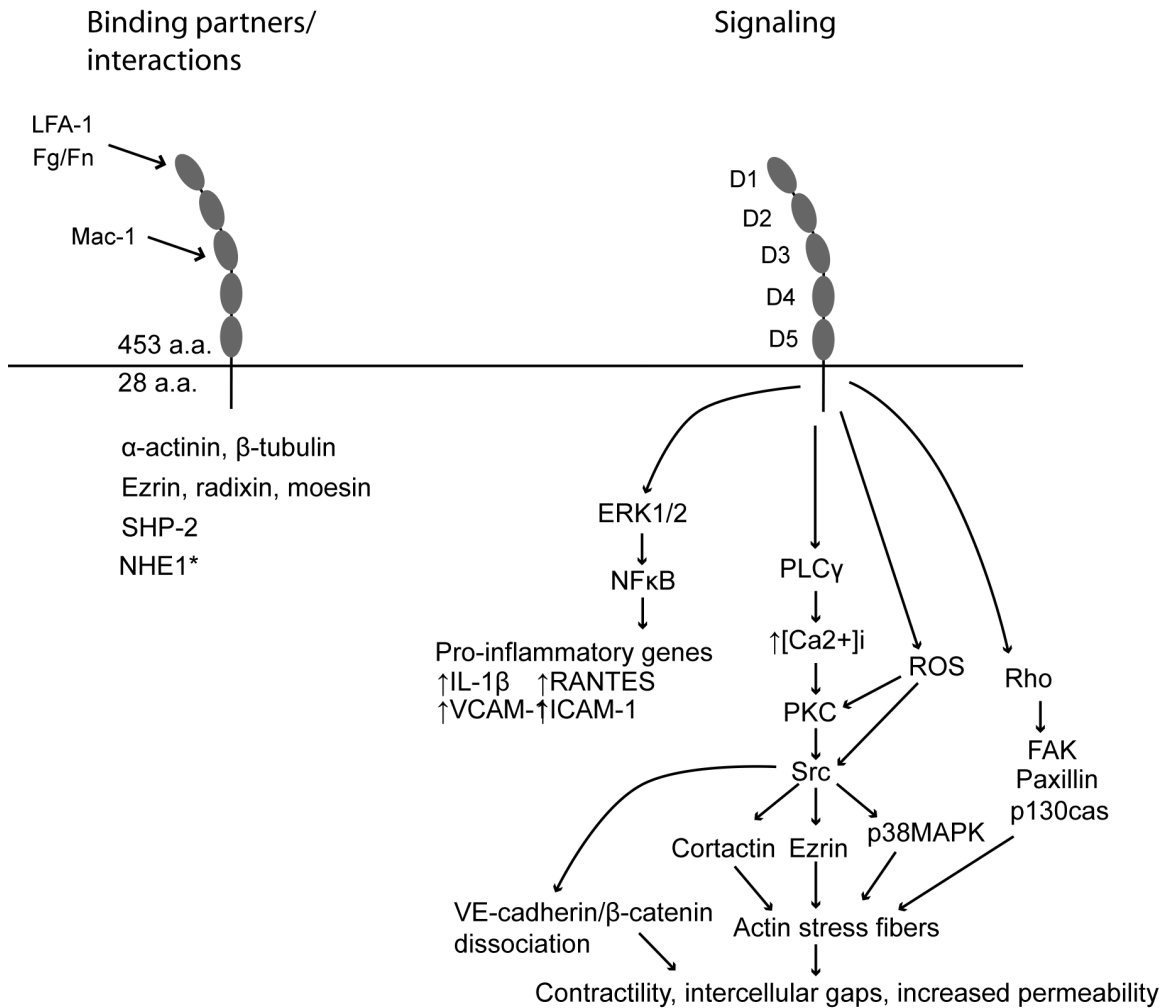


**Figure A. ICAM-1 structure, binding and signaling.** Intercellular adhesion molecule 1 (ICAM-1) on the plasma membrane (horizontal line). Domains D1 through D5 are found on the extracellular side of the plasmalemma and comprise 453 amino acids (a.a.). ICAM-1 can interact with integrins LFA-1 and Mac-1 as well as fibrin(ogen). A transmembrane domain is followed by a C-terminal short cytosolic tail (28 a.a.), which can interact with cytosolic proteins (\*NHE1 is not cytosolic, but transmembrane). ICAM-1 signals through a variety of molecules, most of which converge in rearrangement of the actin cytoskeleton, often associated with opening of endothelial cell-cell junctions. ICAM-1 signaling also induces overexpression of inflammatory molecules. Adapted from Serrano and Muro [5].

Endothelial expression of ICAM-1 is constitutive, yet low, but its expression is upregulated during inflammatory and thrombogenic states by cytokines and other factors, including TNF $\alpha$ , IFN $\gamma$ , TGF $\beta$ , thrombin, fibrin and fibrinogen, and reactive oxygen species [2, 44-46]. In addition to being expressed on endothelial cells and leukocytes,

ICAM-1 is also found on dendritic and epithelial cells, fibroblasts, neurons, myocytes and other cell types [2, 47]. Furthermore, several isoforms of this protein have been identified, including splicing and post-translational glycosylation variants, along with a soluble form of ICAM-1 that can appear in circulation and corresponds to the full extracellular domain of this protein, and which is thought to compete against endothelial ICAM-1 for integrin binding as a means of regulating inflammatory events [34, 48].

Natural ligands that bind to ICAM-1 include leukocyte integrins  $\alpha_L\beta_2$  (lymphocyte function-associated antigen 1, LFA-1) and  $\alpha_M\beta_2$  (macrophage-1 antigen, Mac-1) which bind, respectively, to the extracellular domains D1 and D3 of the molecule [38, 49]. Fibrinogen and fibrin also bind to domain D1 and serve as an additional bridge between leukocytes (macrophages) and endothelial cells, improving binding and transmigration [50, 51]. In addition, some pathogens exploit the prevalence and luminal binding availability of ICAM-1, including human rhinovirus [52], plasmodium falciparum-infected erythrocytes [53], and possibly polioviruses and HIV [54, 55].

Interaction with cytosolic molecules accounts for certain functions of ICAM-1. In particular, most proteins known to bind the cytosolic tail of ICAM-1 serve as cytoskeleton adaptors:  $\alpha$ -actinin [41],  $\beta$ -tubulin [40], and ezrin [56]. Radixin and moesin, the two other members of the ezrin-radixin-moesin (ERM) family of actin adaptors, have been found to colocalize with ICAM-1 [57, 58]. These interactions with members of the cytoskeleton or cytoskeleton-adaptor proteins appear to be important for ICAM-1 distribution on the plasma membrane, as ICAM-1 is normally found enriched in microvilli structures, while deletion of its cytoplasmic domain results in homogeneous distribution on the cell surface [41, 56, 59]. Scanning electron microscopy reveals that

this redistribution is itself associated with a loss in microvilli structures [59], suggesting a link between ICAM-1 and the formation of membrane protrusions.

Signal transduction is also associated with ICAM-1 cytosolic residues.

Multivalent binding of ICAM-1 at the surface of endothelial cells using antibodies activates xanthine oxidase activity, generating reactive oxygen species (ROS) that in turn activate Src-kinases [60-63]. ICAM-1 cross-linking also activates small GTPase Rho [19, 57, 58, 64], RhoA [58] and perhaps other Rho proteins [60, 65], and mitogen-activated protein kinases (MAPK) [63, 66]. In turn, p38 MAPK phosphorylates HSP27 and this leads to cytoskeletal rearrangement [67]. Along with MAPK, cytoskeleton-associated proteins ezrin, cortactin, focal adhesion kinase, paxillin, and p130Cas are also phosphorylated downstream of Src [60, 62, 63], consistent with multiple reports that cross-linking ICAM-1 elicits rearrangement of the actin cytoskeleton [6, 68-70]. Wittchen [17] as well as Lawson and Wolf [71] have recently summarized the current signaling paradigms associated with ICAM-1, which often converge in the opening of endothelial cell-cell junctions.

These signaling events occur in parallel to ICAM-1 redistribution to detergent-resistant membrane fractions, a phenomenon likely to be important for signaling through ICAM-1. For instance, Src activation seems to depend on Src-homology domain 2 containing phosphatase 2 (SHP-2), which binds to ICAM-1 upon cross-linking and entry into detergent-resistant membrane fractions [39, 72]. This is followed by SHP-2-dependent Src activation and ERK1/2 signaling, leading to increased expression of inflammation-related genes like IL-1 $\beta$ , RANTES, VCAM-1, and ICAM-1 itself [73, 74]. Specialized lipid domains might serve as rigid platforms required for localized

maintenance of ICAM-1-dependent signaling events and cytoskeletal remodeling [75]. Our recent findings also suggest that these cytoskeletal rearrangements depend on ICAM-1-mediated production of ceramide [7], a signaling lipid also known to promote the formation of membrane microdomains [76]. Although a comprehensive mapping of the signals mediated by ICAM-1 and their respective functional significance remains to be performed, the following sections will illustrate the several of the cascades mentioned above can be ascribed to the functions of this protein.

## 2.2. Cell Adhesion Molecule (CAM)-Mediated Endocytosis

ICAM-1 was initially thought to serve only as an adhesive molecule, but subsequent work revealed signaling properties associated with it [71]. In addition, studies on the use of ICAM-1 for endothelium-targeted delivery of therapeutics led to the discovery of its endocytic activity: a pathway known as cell adhesion molecule (CAM)-mediated endocytosis is activated upon engagement of multiple copies of ICAM-1 by ICAM-1-targeted drug carriers (Figure B) [6]. This multivalent engagement, which can be achieved by the interaction between antibody-coated nano- or microparticles and ICAM-1 on the endothelial cell surface, elicits the recruitment of Na<sup>+</sup>/H<sup>+</sup> exchanger 1 (NHE1) to particle binding sites [8]. This occurs with concomitant mobilization of acid sphingomyelinase from perinuclear regions of the cell and enrichment of this enzyme at NHE1- and ICAM-1-rich sites of the plasma membrane where particles bind [7]. The activity of acid sphingomyelinase is responsible for subsequent enrichment of ceramide at sites of binding, which results in endocytosis of drug carriers as small as 100 nm and as large as 10 μm in diameter [7, 77]. The mechanism that results in uptake is dependent on

vesicle formation and rearrangement of the actin cytoskeleton, both of which were initially mapped downstream of Rho and rho-dependent kinase (ROCK), protein kinase C (PKC) and Src, as well as dynamin [6], and now are also attributed to sphingomyelinase activity [7]. Such signaling cascades are in agreement with historical reports using antibodies to cross-link ICAM-1 [68, 78, 79].

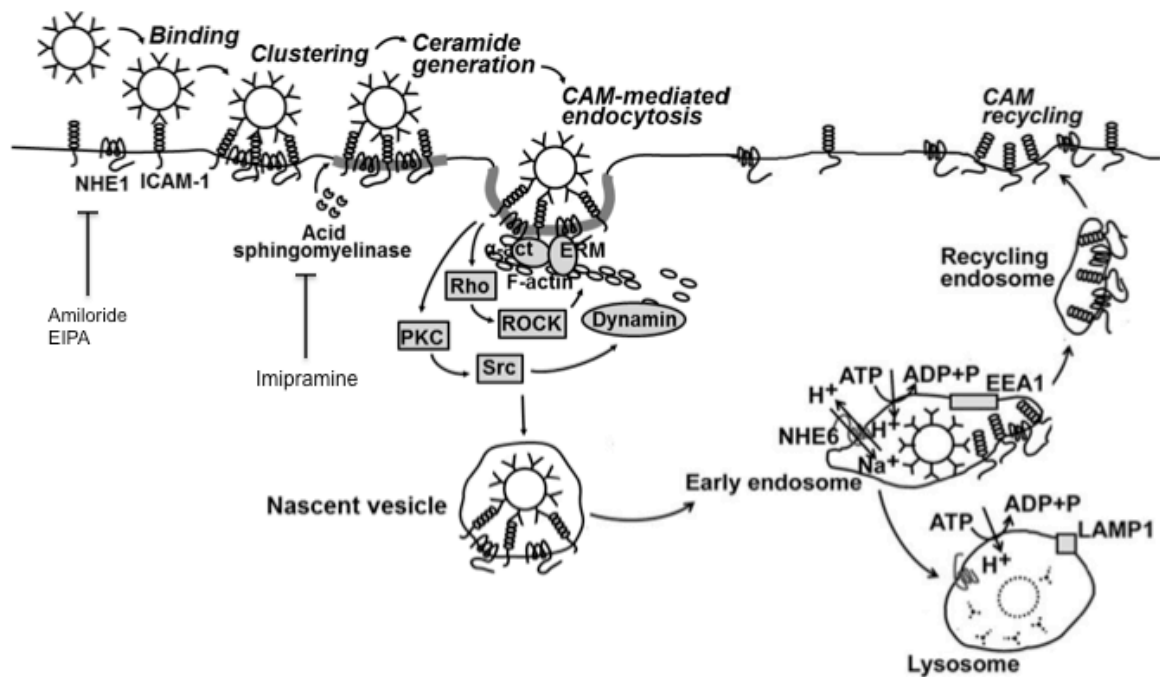


**Figure B. The CAM-mediated pathway of endocytosis.** CAM-mediated endocytosis is initiated upon multivalent engagement of ICAM-1 by ICAM-1-binding drug carriers. ICAM-1 engagement elicits the recruitment of NHE1, which is itself an adaptor of the actin cytoskeleton. Concomitant mobilization of acid sphingomyelinase to sites of carrier binding leads to conversion of sphingomyelin to ceramide. This leads to vesicle formation and rearrangement of actin. Signaling through Rho/ROCK, PKC, and Src elicits actin rearrangement and dynamin-dependent endocytosis. Internalized vesicles fuse into early endosomes, where ICAM-1 dissociates from anti-ICAM particles and recycles back to the plasma membrane. Early endosomes mature into/fuse with lysosomes in an NHE6-dependent manner. The final trafficking destination of particles is the lysosome. In addition to lysosome trafficking, transport of carriers across cells occurs. Inhibitors of NHE1 include amiloride and EIPA. Inhibitors of acid sphingomyelinase include imipramine. Not shown, CAM-mediated endocytosis also occurs with PECAM-1-binding carriers. Adapted from Ding et al. [80].

Although the biophysical properties that promote vesicle detachment from the plasma membrane and/or fusion into larger compartments to internalize both nanometric and micron-sized objects have not been fully elucidated, they are likely associated with

the involvement of ceramide in this pathway. In other systems, generation of ceramide produces changes in the plasma membrane suitable for flexible uptake, such as promotion of large lipid domains [81, 82], modification of the membrane curvature resulting in ATP-independent vesiculation [81, 83, 84], vesicular fusion [85, 86], and also cytoskeletal rearrangement [87, 88].

Following CAM-mediated uptake, drug carriers are trafficked to early endosomes in a microtubule-dependent manner, and later colocalize with lysosomes, reaching maximum accumulation at approximately 3 hours after internalization [6, 9, 89]. This trafficking pattern is slow compared to typical pathways such as pinocytosis, where accumulation in lysosomes can occur as early as 15 minutes after uptake [89].

Meanwhile, it appears that ICAM-1 detaches from carriers in maturing endosomes [8] and recycles to the plasma membrane [9]. Recent studies also indicate that a fraction of carriers internalized by CAM-mediated endocytosis undergo transport across epithelial and endothelial cells [10, 11], but the trafficking itinerary followed within cells during this transport remains unexplored. It should be noted that although the majority of work regarding CAM-mediated endocytosis has focused on ICAM-1, the engagement of multiple copies of another immunoglobulin superfamily protein, platelet/endothelial cell molecule 1 (PECAM-1), on endothelial cells also leads to this endocytic pathway [6]. Whether or not other immunoglobulin superfamily CAMs elicit CAM-mediated endocytosis remains unknown.

CAM-mediated uptake is categorized as a non-classical endocytic pathway (Table 1). The pathway is unrelated to clathrin- and caveolae-dependent uptake, as pharmacological inhibitors of caveolae- (filipin and genistein) or clathrin-mediated ( $K^+$

depletion and monodansylcadaverine) endocytosis do not inhibit internalization elicited by multivalent binding of ICAM-1 [6]. Furthermore, fluorescently labeled anti-ICAM particles do not colocalize with clathrin heavy chain or caveolin-1 during the process of internalization or intracellular trafficking [6]. This is confirmed by transmission electron microscopy images of the mouse pulmonary endothelium, which show that anti-ICAM particles are contained in endothelial cell invaginations and vesicles not associated with typical morphological features of these two classical endocytic pathways, such as caveolar pits and clathrin coats [77]. Furthermore, endocytosis of anti-ICAM particles is not inhibited in caveolin knockout mice [7].

Due to the close association between CAM-mediated endocytosis and the actin cytoskeleton, this pathway shares certain features with macropinocytosis and phagocytosis, in particular PKC dependence, as PKC inhibitors bisindolylmaleimide-1 (BIM-1) and 1-(5-isoquinoline-sulphonyl)-2-methylpiperazine (H-7) reduce, and PKC stimulator phorbol 12-myristate 13-acetate (PMA) increases, internalization of anti-ICAM particles [6]. However, CAM-mediated endocytosis does not exhibit the formation of phagocytic actin cups or membrane ruffling, as the two other pathways [6]. Furthermore, CAM-mediated endocytosis is independent of microtubules for internalization to occur, unlike macropinocytosis, and of phosphatidylinositol 3-phosphate kinase (PI3K) signaling, unlike phagocytosis, but depends on dynamin [6]. Further differentiation between CAM-mediated uptake and classical pathways of endocytosis comes from its association with acid-sphingomyelinase-driven generation of ceramide [7], although growing evidence is connecting sphingomyelinases and ceramide to many modes of endocytosis [90, 91].

**Table 1. Comparison of endocytic pathways.**

	CR-mediated phagocytosis	FcR-mediated phagocytosis	Macropinocytosis	Caveolae-mediated endocytosis	Clathrin-mediated endocytosis	CAM-mediated endocytosis	CME Differs from
Uptake objects >1 $\mu$ m	+	+	+	-	-	+	Cav, Clat
Receptor-mediated	+	+	-	+	+	+	M
Dynamin-2	+	+	-	+	+	+	M
NHE	-	-	+	-	-	+	C, F, Cav, Clat
PKC	+	+	+	+	+	+	n
Actin	+	+	+	+	+	+	n
Actin cup	+	+	+	-	-	-	C, F, M
Microtubules	+	-	+	+	+	-	C, M, Cav, Clat
Src kinase	-	+	+	+	+	+	C
PI3 kinase	+	+	+	?	-	-	C, F, M
Rho/ROCK	+	-	?	?	?	+	F
Caveolin-1	-	-	-	+	-	-	Cav
Sensitive to MDC/K <sup>+</sup> depletion	-	-	-	-	+	-	Clat
Sensitive to filipin/genistein	?	?	-	+	-	-	Cav
Sensitive to LatA/CytD	+	+	+	+	+	+ (LatA) / - (CytD)	C, F, M, Cav, Clat
Sphingomyelinase/ceramide pathway	-	+	-	?	?	+	C, M

Adapted from Caron and Hall [92], and Muro et al [6]

+, required for uptake/event observed; -, not required for uptake/event not observed; ?, no definitive data found in the literature/not previously tested.

MDC, monodansylcadaverine; LatA, latrunculin A; CytD, cytochalasin D; C, complement receptor (CR)-mediated phagocytosis; F, FcR-mediated phagocytosis; M, macropinocytosis; Cav, caveolae-mediated endocytosis; Clat, clathrin-mediated endocytosis; CME, CAM-mediated endocytosis; n, none.

An important aspect differentiating CAM-mediated uptake from other modes of endocytosis is its promiscuity regarding the size of drug carriers internalized. While clathrin- and caveolae-mediated endocytosis are mechanically restricted to internalize objects below a few hundred nanometers in diameter [93], macropinocytosis and phagocytosis are associated with uptake of micron-sized objects [94, 95]. A clear example of these limitations of this comes from the internalization of IgG-coated particles by macrophages, where increasing particle size shifts the uptake mechanism from clathrin-dependent to phagocytic [96]. In the case of CAM-mediated endocytosis, particles that bind ICAM-1 use this mechanism regardless of their size. These particles can range between 100 nm and 10  $\mu\text{m}$  in diameter, and still share signaling features as well as uptake kinetics, efficiencies, and molecular dependencies [77].

With its flexible limitations on particle size for uptake, CAM-mediated endocytosis has been a suitable tool for understanding the role of size and shape on post-endocytic trafficking. This is important, as the field of drug delivery aims to understand the role of geometry on endocytic outcomes in order to optimize therapeutic strategies [77, 97-100]. Following CAM-mediated entry into cells, large ligands, such as those 1  $\mu\text{m}$  and 3  $\mu\text{m}$  in diameter traffic to lysosomes more slowly than nanometric counterparts and they reach a plateau of lower colocalization with lysosomes [77], indicating differences in trafficking for objects of different sizes. Furthermore, disc-shaped carriers exhibit lower uptake efficiencies compared to spherical carriers of a similar diameter [77], implicating object shape in the outcomes that follow CAM-mediated uptake.

Other evidence indicates that besides ligand geometry, the receptor epitope targeted by a drug carrier can also affect CAM-mediated endocytic outcomes [101].

Particles coated with antibodies to different epitopes of PECAM-1 exhibit different binding properties, with some antibodies providing low, while others providing high, carrier binding to endothelial cells despite the fact that all antibodies behaved similarly when presented as free molecules in solution [101]. Out of the population of antibodies that elicit substantial carrier binding, some reveal efficient CAM-mediated uptake, while others are not internalized by cells. Finally, out of the population of anti-PECAM carriers that induce similar endocytosis, some undergo efficient trafficking of carriers to endothelial lysosomes, while others do not, depending on the PECAM-1 epitope bound [101].

As illustrated here, a large body of work has described the properties of drug carrier-induced CAM-mediated endocytosis. However, gaps in knowledge remain regarding its biological function. If cells are equipped with the machinery necessary to induce an endocytic pathway upon the binding of ICAM-1, it is likely that this mechanism occurs in nature and has a relevant physiological significance. As will be described, understanding the phenomena behind ICAM-1 binding to its natural ligands can guide the efforts to fill this gap.

### 2.3. Leukocyte Transendothelial Migration

Two notable natural ligands of ICAM-1 are leukocyte integrins  $\alpha_L\beta_2$  (LFA-1) and  $\alpha_M\beta_2$  (Mac-1) [38, 49, 102], which bind at domains D1 and D3, respectively [103, 104]. Initially, these interactions were thought to contribute only to the firm adhesion of leukocytes to the endothelium, but signaling functions have now been attributed to ICAM-1-integrin binding. Since a single leukocyte exhibits multiple copies of these

integrins, it can engage multiple copies of ICAM-1 on the same endothelial cell. Thus, some of the signaling events observed during ICAM-1 multivalent binding by antibodies, as described in Section 2.1, and by antibody-coated drug carriers (Section 2.2) match with those associated with leukocyte binding to endothelial cells [71]. ICAM-1 engagement by leukocytes mediates signaling involving  $\text{Ca}^{2+}$ , Src kinases and PKC, Rho/ROCK-mediated formation of actin stress fibers, and binding of actin crosslinkers to the cytosolic domain of ICAM-1 [105-107]. These signaling events are important for leukocytes to move from the bloodstream into tissues, a process known as transmigration.

Since leukocytes must perform a variety of functions outside of their sites of origin and beyond the circulation, transmigration is crucial for proper functioning of the immune system. This process can occur both under normal conditions for surveillance, and during abnormal conditions, such as the inflammatory response [108, 109]. In both cases, it is necessary for leukocytes to travel outside of the bloodstream in a regulated manner to minimize or prevent pathology [110]. This regulated recruitment of leukocytes into tissues is described as a sequential series of events that results in transmigration (Figure C) [111]. In this model, leukocytes undergo tethering, followed by rolling interactions, strong adhesion, lateral crawling, and finally transmigration, which can occur through a paracellular or a transcellular route [17, 112].

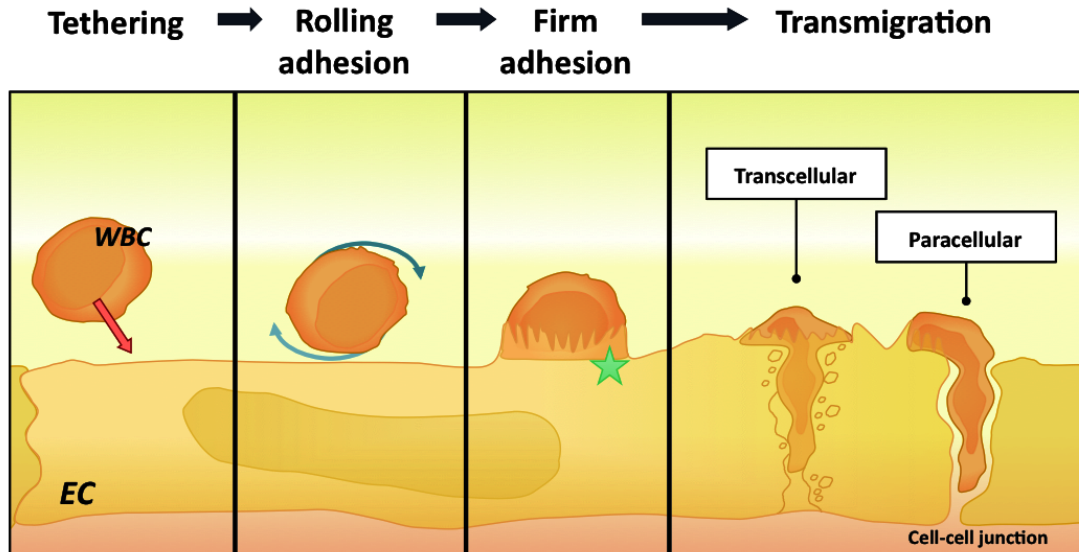


**Figure C. Leukocyte recruitment at the endothelium and transmigration.** Leukocytes (white blood cells, WBC) undergo selectin-mediated tethering and rolling, followed by integrin-mediated firm adhesion, which leads to formation of endothelial docking structures (star). After firm adhesion, crawling (not shown) involves lateral migration of leukocytes to sites suitable for transmigration. Finally, transendothelial migration can occur by two means. The transcellular route involves tractive forces by docking structures, and endothelial cell vesicular fusion into transcellular pores. The paracellular route involves opening of endothelial cell-cell junctions and crossing of the endothelium through these junction openings. Taken from Serrano [113].

The initial steps of tethering and rolling involve the interaction of leukocyte L-selectin or endothelial cell P-selectins with PSGL1 (P-selectin glycoprotein ligand 1) and other glycosylated ligands complementarily expressed on either leukocytes or endothelial cells [111, 114-116]. At sites of inflammation, activated endothelial cells additionally express E-selectin, which supports slow leukocyte rolling [117].

The transient leukocyte-endothelial cell interaction imparted by rolling mechanisms allows for activation of leukocyte integrins, which leads to firm adhesion [109]. The most commonly studied interactions in firm adhesion are those of leukocyte integrins  $\alpha_1\beta_2$  (LFA-1) and  $\alpha_4\beta_1$  (very late antigen 4, VLA-4) with ICAM-1 and vascular adhesion molecule 1 (VCAM-1), respectively [38, 118]. Despite its name, firm adhesion does not imply absolute immobilization of the leukocyte on the endothelial surface.

Instead, lateral movement of the leukocyte, even against blood flow, occurs prior to crossing of the endothelial barrier [109].

The step of transmigration features notable signaling cascades, as well as membrane changes at the protein/lipid composition and morphological levels in both the leukocyte and the endothelium. For instance, the lateral crawling of leukocytes on the endothelial surface changes leukocyte morphology from round to flattened [59, 119, 120]. Along with this, leukocytes extend protrusions (~0.2-1  $\mu\text{m}$  in diameter and up to several microns in length [121]) against the plasmalemma of endothelial cells, which is thought to allow for the leukocyte to probe for sites suitable for transmigration [121, 122].

Interestingly, the process of transmigration is also dependent on active participation by the endothelial cell. This reflects the regulated nature of the event, where the leukocyte does not force itself across the endothelial barrier, but must instead be granted access. At sites of leukocyte probing, endothelial cells develop ICAM-1-enriched invaginations and vesicles from 200 nm to 1  $\mu\text{m}$  in diameter that coalesce to form pores through which leukocytes transmigrate [121]. Simultaneously to leukocyte probing, endothelial cells extend protrusions around leukocytes, which form a structure known as the trans migratory cup, or docking structure, whose presence is necessary for transmigration [105, 123, 124]. These structures can form by a single endothelial cell, or be composed of contributing adjacent endothelial cells, and could serve as a directional track for the leukocyte to follow, or a plug to prevent crossing of blood components into tissue [123, 125]. The formation of the trans migratory cup, which is enriched in ICAM-1 and VCAM-1 likely due to profuse integrin-CAM interactions, is associated with

rearrangement of the actin cytoskeleton to form stress fibers, and depends on the cytosolic tail of ICAM-1 [59, 105, 123, 126, 127]. The maintenance of these large regions of specific molecular enrichment is associated with protein/lipid rearrangement to form specialized lipid domains at the plasma membrane that allow for ICAM-1-dependent signaling events. This is manifested in the enrichment of ICAM-1, VCAM-1, tetraspanin CD9, actin, RhoG, ezrin, and moesin [105, 123, 124, 126], and a redistribution of ICAM-1 to detergent-resistant membrane fractions [128].

In addition to VCAM-1 and ICAM-1, PECAM-1 also has a role in transmigration. This molecule is expressed on endothelial junctions, and its homophilic interaction serves in the maintenance of monolayer integrity [129]. During transmigration, PECAM-1 contained in so-called lateral border recycling compartments traffics to sites of leukocyte interaction with endothelial cells, and promotes crossing of the endothelial barrier [109, 130]. The mechanism of involvement by PECAM-1 remains to be fully understood, but it is thought that transient leukocyte PECAM-1 interactions with endothelial PECAM-1 may serve as a track for crossing through the endothelium. In addition, it may be possible that multivalent homophilic interactions induce vesicle formation to open a path in the endothelial barrier, possibly implicating PECAM-1 in the opening of endothelial pores [6, 130-132].

#### 2.4. Route of Leukocyte Transmigration

For decades, transmigration was accepted to occur solely through the paracellular pathway, which involves dissociation of cell junctions between endothelial cells, and passage of leukocytes in between these opened junctions [111, 133]. This satisfies a

model in which leukocytes transmigrate through a path of least resistance, and is in agreement with many of the signaling events ascribed to ICAM-1 and VCAM-1, which are associated with disassembly of endothelial cell-cell junctions [134, 135].

However, even early studies suggested an alternative route of transmigration independent of junctional disruption, with electron micrographs showing lymphocytes inside the endothelial cytoplasm or in vacuoles [136, 137]. This evidence was treated cautiously until cell culture studies proved the crossing of endothelial layers by leukocytes not only without disruption of cell-cell junctions, but also at sites distant from the endothelial border [123, 127, 138]. In this route, a leukocyte moves across the body of an individual endothelial cell through a process that involves fusion of endothelial vesicles into a so-called transcellular pore, whose dimensions vary but can be as large as several microns in diameter [122, 123, 138]. Recent evidence suggests that the mechanisms behind the transcellular and paracellular pathways might be similar, as junctional proteins migrate from cell-cell junctions to sites of transcellular transmigration [130], but this has not been seen in all instances of transmigration [139].

The extent to which the two routes of transmigration are used by leukocytes, the conditions in which one is favored over the other, and the regulation between paracellular versus transcellular migration remain controversial [111, 133, 140]. Despite methodological difficulties in characterizing these phenomena and a lack of systematic studies attempting to define their regulation, it is likely that the differences in route preference rates observed in different studies depend on factors such as endothelial and white blood cell type, flow conditions, and cell activation states. For instance, the transcellular route can be as low as 10% or as high as 100% of all transmigration events,

depending on the conditions used [17]. In addition, only recent studies have successfully quantified transcellular transmigration *in vivo* [141], agreeing with the lower rate found in cell culture studies (less than 10%), yet this technique remains to be used to categorize transmigration in a variety of endothelial beds and leukocyte types.

Despite discrepancies, the role of ICAM-1 in leukocyte transcellular transmigration is well recognized. TNF $\alpha$ -activation of HUVECs to induce ICAM-1 overexpression increases the percentage of polymorphonuclear leukocytes that migrate using the transcellular route [127]. Further, blocking or deleting the cytoplasmic domain of ICAM-1 reduces primarily transcellular transmigration events, suggesting that transcellular migration depends on ICAM-1 signaling and/or association with actin [127]. During the transcellular pathway, ICAM-1 becomes internalized and undergoes transcytosis to the basal membrane of endothelial cells [138], which is likely a manifestation of transcellular pore aperture.

Some works suggest a contribution of caveolar endocytosis [138, 142] and/or the related vesiculo-vacuolar organelle [143] in the formation of the transcellular pore. Other works, however, have shown more partial association between ICAM-1 and caveolin-1 in structures that form during transmigration [121, 123]. Thus, although there is consensus on the key role of ICAM-1 and vesicle formation in leukocyte transcellular migration, the nature of the transcellular pore and the vesicular pathway regulating its dynamic formation is still unclear. Due to similarities in signaling and features such as vesicle formation/fusion and transcytosis, it is possible that CAM-mediated endocytosis could contribute to the generation of transcellular pores.

## 2.5. Coagulation and Fibrinolysis

The second known ICAM-1 physiological ligand is fibrinogen, a molecule central in the coagulation cascade, which is crucial for maintenance of fluid within the vasculature upon injury. Fibrinogen is a 340 kDa protein made up of two identical dimers linked by multiple disulfide bonds (Figure D) [16]. Each subunit is in turn composed of three chains (A $\alpha$ , B $\beta$  and  $\gamma$ ) also stabilized by disulfide bonds [144]. A binding site for ICAM-1 is found in the  $\gamma$  chains, so that one fibrinogen molecule has binding potential for two molecules of ICAM-1 [145]. Cleavage of fibrinogen by thrombin generates fibrin, which polymerizes to form the matrix of blood clots. Since this cleavage removes small peptides at the N-terminus of fibrinogen, the  $\gamma$  chains and the ICAM-1-binding site are retained when fibrin is formed [146]. Due to polymerization of fibrin into a mesh during blood clot formation, ICAM-1 binding capacity is increased, allowing for engagement of multiple copies of ICAM-1 during interaction with endothelial cells.

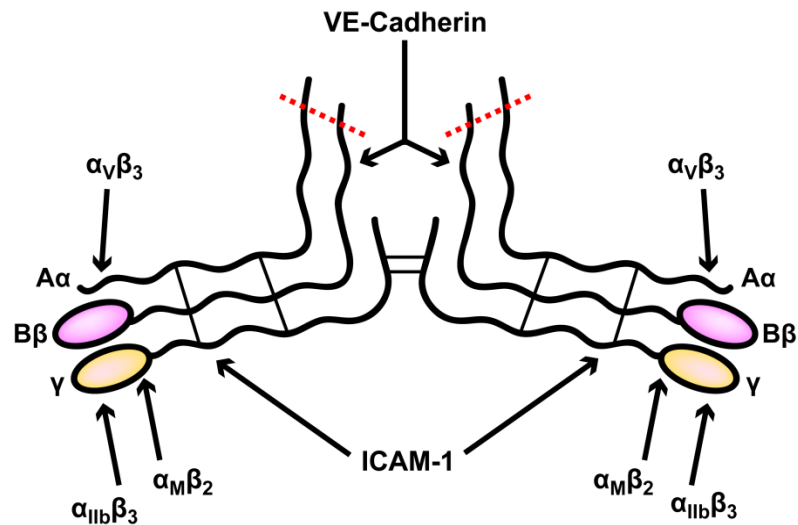


**Figure D. Structure of fibrin(ogen).** Fibrinogen consists of two identical dimers, each composed of three chains (A $\alpha$ , B $\beta$ , and  $\gamma$ ). Waved lines versus ovals represent coiled coil versus globular structure, respectively. Straight lines between chains represent disulfide linkages. Red dashed lines represent the cleavage sites for fibrin generation. Arrows point at binding sites of molecules as indicated. VE-cadherin and ICAM-1 are found on endothelial cells.  $\alpha_v\beta_3$  (also found on endothelial cells) and  $\alpha_M\beta_2$  are leukocyte integrins.  $\alpha_{IIb}\beta_3$  is found on platelets.

Fibrinogen can also interact directly with vascular endothelial (VE)-cadherin and integrin  $\alpha_V\beta_3$ , both of which are found on the surface of endothelial cells, like ICAM-1 [147-149]. Finally, fibrin(ogen) can interact indirectly with endothelial cells by binding to receptors of tissue plasminogen activator (tPA) or urokinase (u)PA, or thrombomodulin [150, 151]. Besides the endothelium, fibrin(ogen) can interact with leukocytes through  $\alpha_V\beta_3$  and  $\alpha_M\beta_2$  (Mac-1) [152], and platelets through  $\alpha_{IIb}\beta_3$  [149].

Although fibrinogen and fibrin are central elements of the coagulation cascade, this mechanism is composed of a large number of molecules that interact in a complex manner [153]. This is due to the required balance between formation of fibrin to create clot polymers, and degradation of these polymers in order to spatially and temporally confine the gelatinization of blood and cell aggregation [154]. Biochemical characterization of the clotting cascade is thorough and well documented [155, 156], whereby the phenomenon is described as a two-branched mechanism depending on the signal that ignites coagulation: a) exposure to tissue factor (the extrinsic pathway), or b) contact activation by exposure to a negatively-charged surface (the intrinsic pathway). The two branches converge in the hydrolysis of prothrombin to thrombin, the protease responsible for generating fibrin, the main protein component of the clot (the common pathway). Current views on this system emphasize the interconnectedness of the two branches and the importance of cellular surfaces on which the biochemical reactions can occur and be compartmentalized. Three phases are recognized in the process of coagulation: Initiation, amplification, and propagation (Figure E) [156].

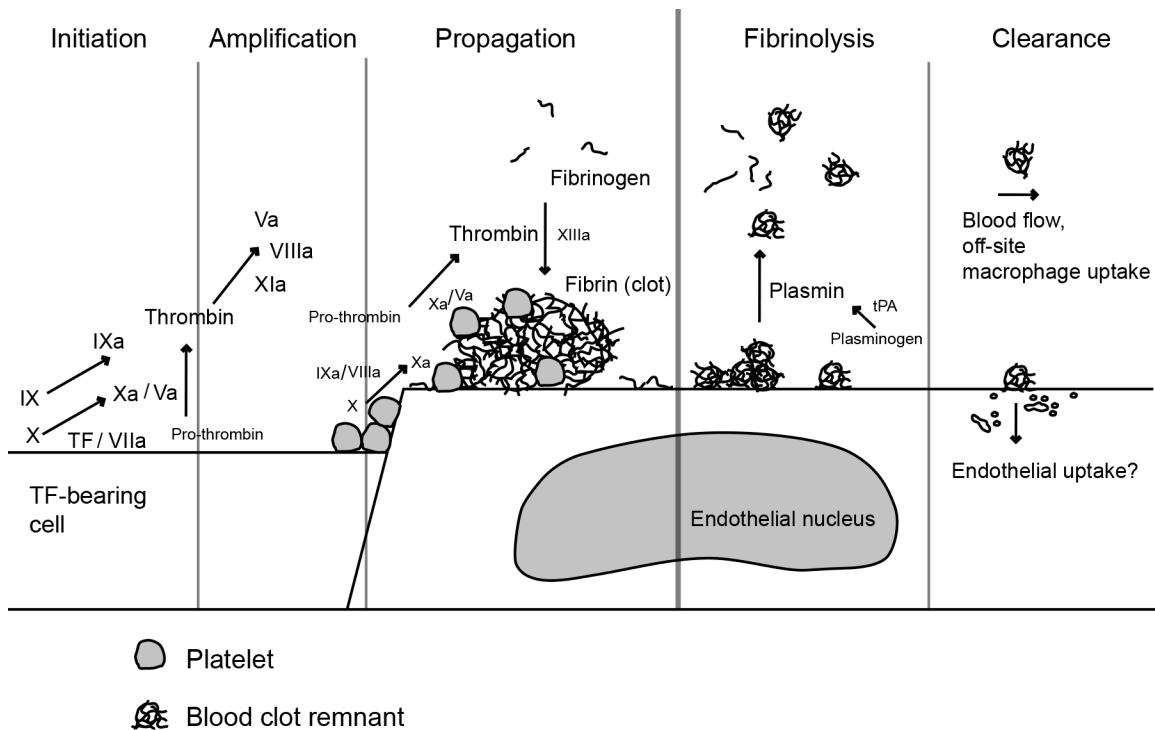


**Figure E. Coagulation and fibrinolysis.** The model of coagulation has three stages. *Initiation* involves exposure of tissue factor (TF) to components of the blood. TF complexes with active factor VII ('a' indicates activation) to activate factors IX and X. Factors Xa and Va complex to generate small thrombin quantities. *Amplification* involves thrombin-mediated generation of factors Va, VIIIa, and XIa. IXa from initiation (and from XIa activity) complexes with VIIIa to generate more Xa. *Propagation* occurs when sufficient Xa and Va are produced to induce a thrombin burst. After wound repair, plasminogen is converted to plasmin by tPA (and uPA), which leads to clot fibrinolysis. Blood clot remnants become soluble and are cleared by blood flow and endocytosed by macrophages downstream. It is unknown what happens to clot remnants still attached to the endothelium.

After injury and platelet plug formation, initiation proceeds when the ubiquitous transmembrane protein tissue factor, normally confined to the non-circulating environment, is exposed to blood. This occurs due to vessel injury, or due to induced expression of tissue factor on endothelial or blood cells [157-159]. Tissue factor forms a complex with factor VII, leading to activation of factors IX and X. At this point, active factor IX is not crucial, but instead diffuses and comes into play during propagation. Interaction of active factors X and V results in the formation of small quantities of thrombin [156]. Amplification involves the thrombin-mediated activation of platelets and also factors V, VIII and XI. This is coupled with deposition of circulating fibrinogen on

the endothelial cell surface, which induces the production of pro-inflammatory and pro-coagulant molecules, leading to recruitment of leukocytes and platelets, and increased binding of fibrinogen [160, 161]. Active factor XI can generate more active factor IX, which interacts with active factor VIII to generate more active factor X. Sufficient concentration of active factors V and X leads to propagation, which involves a massive burst of thrombin production, cleaving sufficient fibrinogen to generate fibrin polymers

Cleavage by thrombin involves the proteolysis of 16 residues at the N-terminal region of fibrinogen, exposing polymerization sites that allow for the initial formation of simple double-stranded fibrils [146]. Cleavage of a second 14-residue fragment allows for inter-fibril associations to produce more complex, branching networks of fibrin, creating the blood clot matrix, whose porosity and architecture depend on fibrinogen and thrombin concentrations [162]. In parallel, the polymerization of fibrin is consolidated by factor XIII, which generates covalent bonds between fibrin molecules, generating the fibrin meshes tethered to the endothelial surface. These meshes serve as docks for platelets and erythrocytes in the growth of a blood clot.

The specific endothelial responses to interaction with these fibrin polymers have been documented for over three decades, yet they remain relatively sparse. Contact of polymerized fibrin with endothelial cells in culture causes disorganization of the monolayer, cell retraction, junction disassembly, and migrational behavior of endothelial cells. This was proposed as a mechanism for delivery of tPA to sites where fibrin clots are present, or a potentiator of coagulation itself by opening of the endothelial barrier and exposure to tissue factor [163], yet to our knowledge these hypotheses have not been formally tested. In addition to this, fibrin induces release of von Willebrand factor [164],

a molecule crucial for clotting due to its role in platelet recruitment and factor VIII regulation [165, 166]. Fibrin also increases endothelial expression of ICAM-1 [167], supporting the role of clots in self-propagation and promotion of inflammation.

In terms of molecule-specific responses, VE-cadherin interaction with fibrin induces the rearrangement of endothelial cell cultures into capillary-like tubes [168] through effects on endothelial cytoskeleton [169]. Binding of fibrinogen to  $\alpha_v\beta_3$  on the endothelium induces the production of prostacyclin by endothelial cells (which inhibits platelet activation) [170], and this interaction has also been linked to disorganization of the endothelial layer and formation of capillary-like structures [171].

The interaction between endothelial ICAM-1 and fibrin(ogen) has been more thoroughly characterized. First, it is known that fibrinogen can serve as a bridging molecule between ICAM-1 on the surface of lymphocytes and ICAM-1 on endothelial cells (or Mac-1 on monocytes and ICAM-1 on endothelial cells), increasing the adhesion between these two cell types [172]. It was later found that the interaction between fibrinogen and ICAM-1 on endothelial cells requires the clustering of ICAM-1 (which is actin-dependent), indicating that fibrinogen might not constitutively bind to the endothelium, but requires a surface of activated (i.e.: inflamed) endothelium for binding [173], and binding occurs at domain D1 of ICAM-1 [50], at an epitope different from those responsible for integrin binding [51]. It also appears that fibrinogen and fibrin may interact differently with ICAM-1. Fibrin, but not fibrinogen, binding to endothelial cells induces overexpression of ICAM-1 to similar levels as potent cytokines [44]. This phenomenon is dependent not only on thrombin-mediated cleavage of fibrinogen, but polymerization of fibrin into meshes. Thus, although it has not been formally shown,

fibrin-dependent upregulation of ICAM-1 is likely mediated by ICAM-1 itself, as the kinetics and degree of activation mimic those seen in ICAM-1 autoregulation after clustering [44]. In addition to this, fibrinogen interaction with ICAM-1 is known to induce mitogenic and proliferative pathways [72, 174].

## 2.6. Clot Dissolution and Remnant Clearance

Following vascular repair, fibrinolysis is required for dissolution of clots (Figure E). The fibrinolytic machinery consists of plasmin and plasminogen activators, which are active even during clot formation, so a shift in equilibrium is required to favor clot degradation. Here, the abundant circulating molecule plasminogen (which can embed itself in the clot during clot formation [175]) is converted to plasmin by uPA or tPA, both of which can be secreted by endothelial cells [176, 177], and factor XII. Both plasminogen and tPA can bind fibrin, localizing the fibrinolytic reaction, while plasmin can cleave uPA and tPA to generate more active forms, serving as a positive feedback mechanism [178]. In turn, platelets in the vicinity of the clot can release plasminogen activator inhibitor 1 (PAI-1), to keep fibrinolytic reactions in check [179].

A series of fragments result from plasmin fibrinolytic activity depending on the cleavage site within the complex mesh [180]. The best characterized fragments are the D-dimer, the E fragment, and B $\beta$ 15-42, which are known to have pro- and anti-inflammatory as well as pro- and anti-coagulant activities [181], highlighting the complex regulation of the clotting system up to its final steps. Yet these smaller fragments comprise a small percentage of the total plasmin-derived fibrin mesh products. *In vitro* studies show that a heterogeneous selection of less-characterized fragments of larger size are produced, and

their size distribution can range by two orders of magnitude in molecular weight [180]. Indeed, since complete clot solubilization requires cleavage of only 25% of the fragment D-fragment E connections, it is expected that a majority of fibrinolysis material is composed of large fibrin polymer meshes. This is supported by the lateral (and not outside-in) mode in which clot digestion occurs [182] and electron microscopy studies characterizing the released clot fragments which can be up to 400 nm in diameter [183].

Despite a clear understanding of the biochemical features of fibrinolysis, and some aspects of clot architecture during this process *in vitro* [178], the interactions of this system within a cellular context are not fully understood. For instance, it is not known how the binding between clots and endothelial surface molecules, such as ICAM-1, can affect their degradation, or retention of clot fragments on the endothelial wall. The solubilized fragments that shed from the degrading clot may be removed by blood flow [160, 184, 185], followed by off-site uptake by neutrophils through pinocytosis and monocytes through integrin Mac-1, and lysosomal degradation [186, 187]. However, the postfibrinolytic clot fragments that remain bound to the endothelial surface could be responsible for re-ignition of the coagulation cascade, unless they are removed. Under pathological conditions this may be the cause of disease, as suggested by the consequences of hypofibrinolysis, where there is an increased risk of venous thrombosis [188]. Indeed, it appears that the healthy endothelium is equipped to transport blood clots from the vasculature into tissue in a process that involves formation of endothelial cell membrane protrusions similar to those observed during leukocyte transmigration [22]. Thus, if endothelial cells are equipped with mechanisms to perform clearance of these fibrin meshes, ICAM-1-dependent CAM-mediated endocytosis could be a possible

candidate. Indeed, there is similarity in binding to ICAM-1 and subsequent signaling between fibrin polymers (clots and their remnants) and drug carriers that elicit CAM-mediated endocytosis.

## Chapter 3: Methods

### 3.1. Antibodies and Reagents.

Monoclonal antibodies used in these studies were: mouse anti-ceramide (IgM; Sigma-Aldrich, Inc., Saint Louis, MO), mouse anti-human fibrin  $\beta$  chain (Sekisui Diagnostics, Lexington, MA), mouse anti-human ICAM-1 clone LB-2 (Santa Cruz Biotechnology, Inc., Santa Cruz, CA), mouse anti-human ICAM-1 clone R6.5 (ATCC, Manassas, VA), mouse anti-human integrin  $\alpha_4\beta_1$  (VLA-4; Millipore, Billerica, MA), mouse anti-human integrin  $\alpha_L\beta_2$  (LFA-1; Millipore), mouse anti-human integrin  $\beta_3$  (Millipore), mouse anti-human mannose 6-phosphate receptor (M6PR) clone 2G11 (Novus Biologicals, Littleton, CO), mouse anti-human thrombomodulin (Abcam, Cambridge, MA), mouse anti-human tPA receptor (BD Biosciences, Franklin Lakes, NJ), mouse anti-human uPA receptor (Sekisui Diagnostics), mouse anti-human VCAM-1 (Millipore), and mouse anti-human VE-cadherin clone BV9 (Abcam). Polyclonal antibodies were: rabbit anti-human acid sphingomyelinase (Santa Cruz), rabbit anti-human NHE1 (Santa Cruz), and rabbit anti-human VE-cadherin clone H-72 (Santa Cruz). All non-labeled and labeled secondary antibodies were from Jackson ImmunoResearch Laboratories, Inc. (West Grove, PA), except for FITC-labeled rabbit anti-mouse IgM from Santa Cruz. The 17-residue peptide containing the ICAM-1-binding sequence of fibrin(ogen) (NNQKIVNLKEKVAQLEA [145]), known as  $\gamma_3$ , and a peptide containing the corresponding scrambled sequence ALENAEVQNLVKKIQKN ( $\gamma_3S$ ) were synthesized by United Biochemical Research, Inc. (Seattle, WA). Calcein AM, AF594 phalloidin, DAPI, AF594 or AF488 fibrinogen, and Texas Red dextran (10,000 MW)

were from Life Technologies (Grand Island, NY). Polystyrene latex beads were from Polysciences, Inc. (Warrington, PA). Na<sup>125</sup>I was from Perkin Elmer (Waltham, MA) and Pierce iodination tubes were from Thermo Scientific (Rockford, IL). Unless otherwise stated, all other reagents were from Sigma-Aldrich.

### 3.2. Microscopy Equipment and Software.

Phase-contrast and epifluorescence microscopy were performed using an Olympus IX81 inverted microscope (Olympus, Inc., Center Valley, PA) with 40× or 60× oil immersion objectives (UPlanApo; Olympus, Inc.) and filters in the red (excitation BP360-370 nm, dichroic DM570 nm, emission BA590-800+ nm; Semrock, Rochester, NY), green (excitation BP460-490 nm, dichroic DM505 nm, emission BA515-550 nm; Semrock), or blue (excitation 355-375 nm, dichroic 380 nm, emission 400-480 nm; Chroma, Bellows Falls, VT) channels. Micrographs were taken with an ORCA-ER camera (Hamamatsu Corporation, Bridgewater, NJ) and SlideBook™ 4.2 (Intelligent Imaging Innovations, Inc., Denver, CO). Confocal microscopy was performed on a Zeiss LSM700 confocal laser scanning microscope (Zeiss, Thornwood, NY) equipped with 555, 405, and 488 lasers, using a 40× air or a 63× oil immersion objective (Zeiss). Micrographs were captured using Zen 2012 (Zeiss). Two-photon microscopy was performed using a two-photon microscope system equipped with a Ti:sapphire laser (Mira 900F; Coherent Inc., Santa Clara, CA) operating at 785 nm wavelength, 165 fs pulse width, and 76 MHz repetition rate. The excitation laser beam was focused with a 40×/1.0NA oil immersion objective (Olympus) and the fluorescence signal was detected with a photomultiplier (PMT) after a 572-642 nm optical band-pass filter.

Epifluorescence and two-photon image processing analysis were performed using Image-Pro Analyzer 6.3 or 7.0 (MediaCybernetics, Rockville, MD), while confocal processing and analysis were performed using Zen 2012.

### 3.3. Iodination of Proteins for Radiotracing.

Proteins were labeled with  $^{125}\text{I}$  for radiotracing by mixing 100  $\mu\text{g}$  of 1  $\mu\text{g}/\mu\text{L}$  protein with 2  $\mu\text{Ci}$  of  $\text{Na}^{125}\text{I}$  in iodination tubes for 5 minutes. The reaction mixture was passed through Tris buffer size-exclusion polyacrylamide bead columns of molecular weight limit 6 kDa (Bio-Spin® P-6; Bio-Rad) 4 minutes at 1,000 g to separate free  $^{125}\text{I}$ . To determine the protein activity, iodinated protein was mixed with 3% bovine serum albumin (BSA) in phosphate-buffered saline (PBS) and (1-to-6 volume/volume) trichloroacetic acid (TCA). This precipitates protein, leaving free  $^{125}\text{I}$  in the supernatant, which allows for determination of the radioactive counts per minute (CPM) only in the protein fraction using a gamma counter (PerkinElmer Wizard<sup>2</sup>, Waltham, MA). Then, the concentration of iodinated protein was determined using a standard Bradford assay. Using protein concentration and activity, the specific activity of the iodinated protein was calculated as CPM per  $\mu\text{g}$  of protein.

### 3.4. Preparation of ICAM-1- or M6PR-Targeted Particles.

Particles targeting ICAM-1, associated with CAM-mediated endocytosis, or M6PR, associated with clathrin-mediated endocytosis (as an example of an endocytic receptor associated to a non-CAM-mediated pathway [189]), were used for this thesis.

Particles were prepared by adsorbing antibodies to ICAM-1 (clone R6.5; hereby referred to as anti-ICAM particles), peptide  $\gamma$ 3, or antibodies to M6PR (anti-M6PR) on the surface of 100 nm, 500 nm, 1  $\mu$ m or 4.5  $\mu$ m polystyrene-latex particles, as described [6, 77]. As controls for binding specificity, particles were coated with non-specific mouse IgG, or  $\gamma$ 3S (scrambled  $\gamma$ 3). Particles of 100 nm and 500 nm in diameter had a green fluorescent FITC-derived labeled core to allow for detection via microscopy.

In the case of anti-ICAM and  $\gamma$ 3 particles, the adsorption reaction only contained each respective molecule, yielding a particle whose surface coverage was 100% antibody or peptide. In the case of anti-M6PR particles, they were coated in three different manners: (a) 100% with the antibody, (b) 80% with anti-M6PR and 20% with IgG (anti-M6PR:IgG) or neutral sphingomyelinase (NSM; anti-M6PR:NSM), or (c) 50% with anti-M6PR and 50% with IgG or neutral sphingomyelinase [189, 190, 191]. We have previously titrated the molar ratios to which antibodies and enzyme need to be combined in the adsorption reaction mixture in order to achieve these values [191].

After adsorption, non-coated antibodies or peptides were separated by centrifugation and coated particles were resuspended using 1% BSA in PBS and sonicated to prevent particle aggregation. The effective diameter of antibody- or peptide-coated particles was measured by dynamic light scattering (for nanometric particles; Malvern Zetasizer Nano-ZS90, Westborough, MA) or phase-contrast microscopy (for micron-sized particles). Particles 100 nm in diameter ranged from 230-260 nm after coating; hence, they are referred to as 200 nm in diameter.

Antibodies,  $\gamma$ 3 or neutral sphingomyelinase used for coating were  $^{125}$ I-labeled for determination of the antibody or peptide density on particles using a gamma counter as

previously described [189, 191]. Briefly, a known concentration particles coated with  $^{125}\text{I}$ -labeled protein (whose specific activity is known) is passed through a gamma counter to determine the CPMs per particle. Since CPM/ $\mu\text{g}$  of protein is known, one can calculate the  $\mu\text{g}$  of protein (and, by extension, the number of molecules) associated per particle. This number divided by the surface area of the particle yields the coating density.

Antibodies were also  $^{125}\text{I}$ -labeled for radiotracing in transport experiments. Also, in certain cases as indicated, it was necessary to add a fraction of non-specific mouse IgG to the surface of  $\gamma 3$  particles in order to allow for immunostaining or radiotracing ( $^{125}\text{I}$ -IgG). The fraction of IgG was small (1,000  $\gamma 3$  to 1 IgG by mass) and preliminary data showed no effects of this IgG on the binding of  $\gamma 3$  particles. The characterization of used formulations is provided below:

**Table 2. Characterization of ICAM-1- or M6PR-binding particles.**

Size	Coat	Surface coverage	Molecules/ $\mu\text{m}^2$ of particle		Diameter ( $\mu\text{m}$ )
			Antibody	IgG or NSM	
200 nm	Anti-ICAM	100	7,393	-	0.264
500 nm	Anti-ICAM	100	25,944	-	0.561
1 $\mu\text{m}$	Anti-ICAM	100	30,564	-	1.098
4.5 $\mu\text{m}$	Anti-ICAM	100	25,827	-	4.410
200 nm	$\gamma 3$	100	262,384	-	0.239
1 $\mu\text{m}$	$\gamma 3$	100	4,953,739	-	1.001
4.5 $\mu\text{m}$	$\gamma 3$	100	34,153,702	-	4.394
1 $\mu\text{m}$	Anti-M6PR	100	23,544	-	1.144
1 $\mu\text{m}$	Anti-M6PR:IgG	80:20	19,608	1,632	1.156
1 $\mu\text{m}$	Anti-M6PR:IgG	50:50	12,616	4,328	1.095
1 $\mu\text{m}$	Anti-M6PR:NSM	80:20	16,052	2,532	1.051
1 $\mu\text{m}$	Anti-M6PR:NSM	50:50	11,498	5,658	1.142

NSM = Neutral sphingomyelinase; Surface coverage = approximate fraction of particle surface that a molecule type occupies.

### 3.5. Cell Culture.

Human umbilical vein endothelial cells (HUVECs) purchased from Lonza Walkersville, Inc. (Walkersville, MD) were cultured in M-199 basal medium supplemented with 15% fetal bovine serum (FBS), 15 µg/mL endothelial cell growth supplement, 2 mM L-glutamine, 100 µg/mL heparin, 100 U/mL penicillin, and 100 µg/mL streptomycin. Human brain microvascular endothelial cells (HBMECs) from Applied Cell Biology Research Institute (Kirkland, WA) were cultured in RPMI-1640 medium supplemented with 20% FBS, 2 mM glutamine, 30 µg/mL endothelial cell growth supplement, 100 µg/mL heparin, 100 U/mL penicillin, and 100 µg/mL streptomycin. For microscopy, HUVECs were seeded on 12-mm<sup>2</sup> 1%-gelatin-coated glass cover slips in 24-well plates. For SDS-PAGE (sodium dodecyl sulfate polyacrylamide gel electrophoresis), HUVECs were seeded on 1%-gelatin-coated 6-well plates. For lymphocyte transmigration, HUVECs were seeded on 8-µm pore Transwell® filters (Corning, Inc., Lowell, MA). For particle transcytosis, HBMECs were seeded on 3-µm pore Transwell® filters (Corning, Inc.). In all cases, endothelial cells were grown to confluence at 37°C, 5% CO<sub>2</sub>, and 95% relative humidity, and treated for 16 hours with 10 ng/mL TNFα (BD Biosciences) to induce endothelial activation and up-regulate ICAM-1 expression.

Lymphocytes were obtained from the blood of healthy volunteers (under International Review Board approval) using standard protocols [192]. Briefly, blood was extracted into sodium citrate-coated tubes followed by density gradient centrifugation over Ficoll-Paque™ PLUS (GE Healthcare Amersham Biosciences Corp., Piscataway, NJ) or Polymorphprep (Accurate Chemical & Scientific Corporation, Westbury, NY).

The layer of peripheral blood mononuclear cells was isolated and washed, followed by incubation on gelatin-coated culture bottles to separate adherent monocytes. Non-adherent cells were cultured in RPMI-1640 supplemented with 10% FBS (Mediatech, Inc., Manassas, VA) in the presence of 0.5  $\mu\text{g}/\text{mL}$  phytohemagglutinin for 48 hours to activate and differentiate T lymphocytes into T lymphoblasts, followed by addition of 10 U/mL interleukin 2 (IL-2) for 8-12 days for continued enrichment and activation. Non-migratory K562 erythroid leukemia cells were obtained from Sigma-Aldrich (Inc., Saint Louis, MO) and cultured as done with lymphocytes.

### 3.6. Binding of ICAM-1- or M6PR-Targeted Particles to Endothelial Cells.

For binding experiments, TNF $\alpha$ -activated HUVECs growing on glass cover slips were fixed to prevent confounding results due to concomitant endocytosis. After fixation, cells were incubated for 30 minutes, 3 or 24 hours with 200 nm, 1  $\mu\text{m}$ , or 4.5  $\mu\text{m}$  anti-ICAM,  $\gamma$ 3, anti-M6PR, anti-M6PR:IgG (50:50 or 80:20), or anti-M6PR:NSM (50:50 or 80:20) particles, followed by washing of non-bound particles. Phase-contrast and epifluorescence microscopy were used to determine the number of particles bound per cell. For fluorescent particles, a custom-made algorithm was used that detects and counts fluorescent objects regardless of their intensity as long as they are above a specified background fluorescence threshold [6].

Alternatively, for experiments on live cells, HUVECs were not fixed, and were incubated for 30 minutes, 3 or 24 hours with 200 nm, 1  $\mu\text{m}$ , or 4.5  $\mu\text{m}$  anti-ICAM or  $\gamma$ 3 particles, followed by washing of non-bound particles, and fixing before microscopy.

### 3.7. Uptake of ICAM-1 or M6PR-Targeted Particles by Endothelial Cells.

For uptake studies, TNF $\alpha$ -activated HUVECs growing on glass cover slips were incubated with 200 nm, 1  $\mu$ m, or 4.5  $\mu$ m anti-ICAM,  $\gamma$ 3, anti-M6PR, anti-M6PR:IgG (50:50 or 80:20), or anti-M6PR:NSM (50:50 or 80:20) particles at 37°C for 30 minutes or 3 hours. Cells were washed and fixed, followed by staining with Texas Red-labeled goat anti-mouse, which can recognize the antibodies coated on the particle. This labels surface-bound, but not internalized, particles since antibodies cannot cross the cell membrane. This allows differentiation between particles inside versus those outside of cells for quantification of percent uptake through microscopy as described before [6, 189]. Briefly, for 1  $\mu$ m or 4.5  $\mu$ m particles, total particles were counted using phase contrast and surface-bound non-internalized particles were counted using Texas Red fluorescence. For 200 nm particles, total particles versus non-internalized particles were counted using green and Texas Red fluorescence, respectively using the same algorithm as Section 3.6 [189]. Internalized particles were calculated by subtracting non-internalized particles (Texas Red immunostained) from total particles. Percent internalization was calculated as: internalized particles divided by total particles  $\times$  100.

### 3.8. Actin Staining and Ceramide Enrichment at Sites of ICAM-1 or M6PR-Targeted Particle Interaction with Endothelial Cells.

TNF $\alpha$ -activated HUVECs growing on cover slips were incubated for 30 minutes at 37°C with 200 nm, 1  $\mu$ m or 4.5  $\mu$ m anti-ICAM,  $\gamma$ 3, anti-M6PR:IgG, or anti-M6PR:NSM particles. When indicated, HUVECs were pre-incubated for 30 minutes in the presence of 20  $\mu$ M imipramine to inhibit acid sphingomyelinase, and imipramine was

kept during the binding incubation. Non-bound particles were washed, and cells were fixed and blocked overnight with 2% BSA in PBS. Cells were permeabilized with 0.2% Triton X-100 and then F-actin was stained with red AF594 phalloidin or ceramide was immunostained using mouse anti-ceramide (IgM) followed by green FITC-labeled goat anti-mouse IgM [7]. For ceramide staining experiments, 200 nm particles had a red, not green, fluorescent core for detection.

Microparticles were located using phase-contrast, while nanoparticles were located using epifluorescence microscopy. Fluorescence micrographs at these positions were then obtained to visualize ceramide or actin. Semi-quantitative analysis of ceramide enrichment at binding sites was performed as described previously [7]. Briefly, a reference line of 5  $\mu\text{m}$  was drawn crossing the equatorial axis of the identified particle (and also centered with the center of the particle). The fluorescence intensity was obtained for every pixel found on this line. This was done for  $\geq 30$  particle binding sites and averaged. Enrichment was then calculated as the fold increase (represented as  $\Delta$  in graphs) between the average intensity of surrounding background areas of the plasma membrane and the average intensity where particles bound the HUVEC membrane.

In order to graph the relationship between ceramide enrichment and ICAM-1 binding density, we estimated the potential ICAM-1-binding capacity of each particle as the antibody density (determined through radiolabeling, as described in Section 3.4, Table 2) multiplied by 2 (each antibody has two potential ICAM-1-binding sites).

### 3.9 Lysosomal Transport of ICAM-1-Targeted Particles.

TNF $\alpha$ -activated HUVECs grown on cover slips were incubated with Texas Red-labeled dextran (10,000 MW) for 45 minutes, followed by washing and incubation for 45 minutes to label lysosomes. This ensures that internalized dextran has fully trafficked to lysosomes, a technique shown to be a suitable alternative to lysosomal-associated membrane protein 1 (LAMP-1) immunostaining [9, 89, 193]. Then, cells were incubated with 200 nm, 1  $\mu$ m or 4.5  $\mu$ m anti-ICAM or  $\gamma$ 3 particles for 1 hour (pulse, to allow for synchronized binding and uptake), followed by washing and incubation for 0, 2, or 4 hours (chase, to allow for intracellular trafficking). After fixation, surface-bound, non-internalized particles were immunostained. Epifluorescence microscopy was used to determine the percentage of internalized particles (obtained by subtracting non-internalized particles from the total particle count) that colocalized with Texas Red-labeled lysosomes as done previously [9]. Briefly, green fluorescent pixels (total particles) above a given intensity threshold are counted. Then, then red pixels above the same intensity threshold, but only those overlapping with green (only red lysosomes that colocalize with green particles), are counted. Percent colocalization is the area of yellow pixels (green pixels that overlap with red) divided by the area of total pixels (all green pixels)  $\times$  100.

### 3.10. Transport of ICAM-1-Targeted Particles Across Endothelial Cells.

TNF $\alpha$ -activated HBMECs grown on 3- $\mu$ m pore Transwell® filters were incubated with 200 nm, 500 nm, or 1  $\mu$ m <sup>125</sup>I-anti-ICAM or  $\gamma$ 3:<sup>125</sup>I-IgG particles for 30 minutes (pulse, to allow for binding), followed by washing of both apical and basal chambers, and

incubation for 4.5 hours (chase, to allow for internalization and transport). Washing of both apical and basal chambers removes non-bound particles from the medium to ensure that the transport observed after chase only originates from ICAM-1-bound particles. This washing minimizes confounding results due to leakage of non-bound particles.

Apical and basal fractions were collected and the porous membrane was excised and incubated in 1% Triton X-100 to lyse cells, freeing internalized particles. All fractions were quantified using a gamma counter (to obtain total CPMs), followed by precipitation of proteins in TCA (1-to-6 volume/volume). The non-precipitated fractions were quantified using a gamma counter in order to determine the free (non-protein-bound) iodine CPMs. This allows to calculate the counts in each fraction contributed only by proteins (by subtracting the free iodine CPMs from the original total CPMs). Protein CPM values of each fraction can be divided by the pre-established CPM/particle values to determine how many particles are in each fraction. Detailed protocols of this procedure are published [194].

Although this technique does not trace the particle itself but antibodies coating the particle surface, it is acceptable to assume that the detected free-iodine-corrected CPMs are from non-degraded proteins on the particle surface [10, 195]: previous data show high antibody coating stability of anti-ICAM particles in different solutions (including cell medium and blood serum) and pH for extended periods of time [195], while microscopy evidence shows that these particles retain their antibody coat inside cells before they reach lysosomes [89].

3.11. Imaging of Lymphocyte Adhesion and Pre-transmigratory Interactions with Endothelial Cells.

IL-2-activated lymphocytes were stained with 4  $\mu$ M (green fluorescent) calcein AM, washed, and added over TNF $\alpha$ -activated HUVECs growing on glass cover slips at 1.5-lymphocyte to 1-HUVEC ratio. Cells were incubated for 30 minutes at 37°C, followed by fixation with 2% paraformaldehyde, and washing to remove non-adhered lymphocytes. For inhibition, HUVECs were pre-treated for 30 minutes with 1  $\mu$ g/mL filipin to inhibit caveolae-mediated endocytosis, 5 mM methyl- $\beta$ -cyclodextrin (Cdx) to chelate cholesterol and disrupt lipid domains, 3 mM amiloride or 20  $\mu$ M 5-(N-Ethyl-N-isopropyl)amiloride (EIPA) to inhibit NHE1, or 50  $\mu$ M imipramine to inhibit acid sphingomyelinase. The inhibitors were either washed away before adding lymphocytes or maintained through the experiment, as indicated. After fixing, samples were permeabilized with 0.2% Triton X-100 and stained using anti-VE-cadherin, anti-ICAM, anti-NHE1, anti-acid sphingomyelinase, or anti-ceramide, plus fluorescently labeled secondary antibodies as indicated (ceramide immunostaining involved an overnight pre-blocking at 4°C in 2% BSA PBS).

Samples were analyzed by phase-contrast and epifluorescence microscopy with a 40 $\times$  objective. The total number of lymphocytes left on the HUVEC monolayer firmly bound after washing was quantified to obtain binding data. Lymphocytes exhibiting flat, spread-out morphologies, suggestive of lateral movement on the endothelium or pre-transmigratory probing, were scored as 'sampling' cells. Meanwhile, lymphocytes showing round morphologies, indicative of no transmigration, were scored as simply 'adhered' cells. Both adhered and sampling lymphocytes were additionally spatially

scored at either the HUVEC border (in contact with or within 1  $\mu\text{m}$  of HUVEC borders) or away from it (HUVEC 'body';  $\geq 1 \mu\text{m}$  away from the cell border). Location of lymphocytes at these sites and presence of podosome-like structures in sampling lymphocytes were visualized in parallel by scanning electron microscopy.

### 3.12. Quantification of Lymphocyte Transmigration Across Endothelial Cell Monolayers.

IL-2-activated lymphocytes (or the erythroid leukemia cell line K562, which does not transmigrate) were added at a 1.5-lymphocyte to 1-HUVEC ratio to the apical chamber above a confluent monolayer of TNF $\alpha$ -activated HUVECs grown on 8- $\mu\text{m}$  pore Transwell® filters. Recombinant lymphocyte chemoattractant stromal cell-derived factor 1-alpha (SDF-1 $\alpha$ ; R&D Systems, Inc., Minneapolis, MN) was added at 200 ng/mL to the basal chamber under HUVECs. Transmigration was assessed by counting lymphocytes in the bottom chamber after incubation with HUVECs for 30 minutes at 37°C. For inhibition, HUVECs were pre-treated with 1  $\mu\text{g/mL}$  filipin, 5 mM Cdx, 3 mM amiloride, 20  $\mu\text{M}$  EIPA, or 50  $\mu\text{M}$  imipramine, and the inhibitors were either washed before addition of lymphocytes or maintained through the experiment. Alternatively, lymphocytes were pre-treated with 40 ng/ $\mu\text{L}$  anti- $\alpha_4\beta_1$  (to block binding to VCAM-1) or anti- $\alpha_L\beta_2$  (to block binding to ICAM-1), then washed and incubated over HUVECs. Experiments were also performed in the absence of a HUVEC monolayer to determine the effect of inhibitors or antibody blocking on lymphocyte motility across the porous membrane.

### 3.13. Quantification of the Route of Lymphocyte Transmigration Across Endothelial Cells.

IL-2-activated lymphocytes were added over TNF $\alpha$ -activated HUVECs growing on glass cover slips at a 1.5-lymphocyte to 1-HUVEC ratio. Cells were incubated for 15 minutes at 37°C, followed by fixation with 2% cold paraformaldehyde and then washing to remove non-bound lymphocytes. For inhibition, HUVECs were pre-treated with 1  $\mu$ g/mL filipin, 5 mM Cdx, 3 mM amiloride, 20  $\mu$ M EIPA, or 50  $\mu$ M imipramine for 30 minutes, and the inhibitors were washed away before adding lymphocytes. Samples were stained (after fixation and permeabilization) using DAPI (to identify nuclei), AF594 phalloidin (to identify endothelial and lymphocyte actin), and anti-VE-cadherin followed by green fluorescent secondary antibody (to identify cell-cell junctions).

Samples were analyzed by confocal microscopy using a 63 $\times$  objective by obtaining 1024 $\times$ 1024 pixel z-sections starting at the bottom of the HUVEC monolayer in contact with the cover slip, and reaching the top of the monolayer, where endothelial actin cannot be detected, but adhered lymphocyte actin is still visible (total thickness  $\sim$ 5  $\mu$ m, 6-7 stacks). Micrographs were used to quantify the total number of lymphocytes, and those transmigrating (lymphocyte actin observed on top of and beneath HUVECs) versus those not transmigrating (lymphocyte actin observed only on top of HUVECs). All transmigration events not occurring directly on cell-cell borders were counted as transcellular. In addition, the population of transmigrating lymphocytes on borders was classified as transcellular if VE-cadherin staining was intact at the transmigration site, or paracellular if VE-cadherin was disrupted. Fully detailed procedures are published [192].

### 3.14. Interaction of Fibrin Meshes or Microemboli with Endothelial Cells.

TNF $\alpha$ -activated HUVECs growing on glass cover slips were incubated in the presence of 0.5  $\mu$ M AF488 (green fluorescently labeled) fibrinogen, 2 mM CaCl<sub>2</sub>, 0.063 nM plasminogen, and 0.034 nM thrombin in 25 mM (4-(2-hydroxyethyl)-1-piperazineethanesulfonic acid (HEPES) Hank's balanced salt solution (HBSS), hereby referred to as fibrin mesh forming mixture, for 30 minutes at 37°C to form fibrin meshes [196]. Fibrin mesh formation was also performed in the presence of 40 U/mL hirudin (EMD Chemicals, Gibbstown, NJ) to inhibit thrombin, and, thus, production of fibrin, or 3 mM glycine-proline-arginine-proline (GPRP; EMD Chemicals) to inhibit fibrin polymerization. For blocking of endothelial surface molecules, HUVECs were pre-treated with 33.3  $\mu$ g/mL of mouse IgG, anti-ICAM-1 (LB-2 clone), anti-VE-cadherin (BV9 clone), anti-integrin  $\beta_3$ , anti-tPA receptor, anti-uPA receptor, or anti-thrombomodulin at 4°C 15 minutes prior to mesh formation, and antibodies were maintained during the assay. This was also done with 0.33  $\mu$ g/ $\mu$ L or 0.067  $\mu$ g/ $\mu$ L  $\gamma_3$  or  $\gamma_3$ S to directly block the ICAM-1 fibrin(ogen) epitope.

Alternatively, fibrin mesh forming mixture was pre-incubated in test tubes for 30 minutes and then added to HUVECs (final concentration of fibrin was equivalent to the meshes formed *in situ* as described above) for 30 minutes to allow binding. These are referred to as fibrin microemboli, as the fibrin mesh polymers are formed prior to coming in contact with endothelial cells, mimicking the interaction between a circulating pre-formed fibrin polymer and the endothelium.

Cells were washed, fixed and permeabilized, followed by immunostaining of ICAM-1, NHE1, acid sphingomyelinase, or VCAM-1, as done in Section 3.11. Analysis

was done by epifluorescence microscopy and images were used to quantify the binding of fibrin meshes (calculated as the total number of fluorescent objects (meshes or microemboli) detected in the green channel), as well as their mean diameter. Enrichment of the described molecules at binding sites of fibrin meshes was also determined using custom-made algorithms that determine the percent colocalization between green and red staining as done previously [89]. Briefly, green fluorescent pixels (total fibrin meshes) above a given intensity threshold are counted. Then, then red pixels (immunostained membrane proteins) above the same intensity threshold, but only those overlapping with green, are counted. Percent colocalization is the area of yellow pixels (green pixels that overlap with red) divided by the area of total pixels (all green pixels)  $\times 100$ .

### 3.15. Uptake of Fibrin Meshes or Microemboli by Endothelial Cells.

TNF $\alpha$ -activated HUVECs growing on glass cover slips were incubated in the presence of fibrin mesh forming mixture or fibrin microemboli for 30 minutes at 37°C. Cells were washed and incubated in complete medium for 0, 30 minutes, 1, 3, 5 or 24 hours (chase). Incubation at 3 hours was also performed in the presence of 0.15 U/mL aprotinin and 50 ng/mL PAI-1 (EMD Chemicals) to inhibit serine proteases and tPA, respectively. To probe mechanisms of endocytosis, incubation at 3 hours was performed in the presence of 1  $\mu$ g/mL filipin to inhibit caveolae-mediated uptake, 50  $\mu$ M monodansylcadaverine (MDC) to inhibit clathrin-mediated endocytosis, 3 mM amiloride to inhibit NHE1, 50  $\mu$ M imipramine to inhibit acid sphingomyelinase, or 0.5  $\mu$ M wortmannin to inhibit PI3K-dependent uptake (which is associated with macropinocytosis and phagocytosis).

After washing and fixing, cells were incubated with anti-fibrin  $\beta$  chain, followed by a red fluorescent secondary antibody to label only surface-bound, non-internalized fibrin meshes for percent internalization analysis. Samples were analyzed by phase-contrast and epifluorescence microscopy using a 40 $\times$  objective. Using this technique, micrographs reveal non-internalized fibrin meshes as green and red (yellow), while internalized meshes are only green. Images were used to quantify percent internalization as green meshes divided by total (green and yellow) meshes  $\times$  100 (as done with particles in Section 3.7).

Alternatively, cells were permeabilized prior to staining to determine the immunolabeling by anti-fibrin of internalized fibrin meshes. Analysis was performed on micrographs to quantify the percent immunolabeling, calculated as follows: Immunolabeled fibrin meshes (green meshes that are immunolabeled in red, appearing as yellow) divided by total fibrin meshes (all green meshes)  $\times$  100.

### 3.16. Lysosome Trafficking of Fibrin Meshes in Endothelial Cells.

TNF $\alpha$ -activated HUVECs growing on glass cover slips were pre-treated with Texas Red labeled dextran (10,000 MW) for 45 minutes, followed by washing and incubation for 45 minutes in dextran-free medium. This ensures that dextran fully traffics to lysosomes. Then, cells were incubated in the presence of fibrin mesh forming mixture 30 minutes at 37 $^{\circ}$ C. Cells were washed and incubated in complete medium for 0, 30 minutes, 1, 3, 5, or 24 hours (chase). Alternatively, cells were not pre-treated with dextran, but instead were permeabilized after fixing, followed by incubation with anti-fibrin  $\beta$  chain and red fluorescently labeled secondary antibody. When noted, cells were

treated with 10  $\mu$ M chloroquine (to disrupt lysosome-mediated hydrolysis), 0.15 U/mL aprotinin plus 50 ng/mL PAI-1 (to inhibit non-specific and tPA-mediated proteolysis), or all three reagents.

Epifluorescence microscopy was used to analyze the colocalization between green fibrin meshes and red lysosomes (as done in Section 3.9 for particles), or green fibrin meshes and red anti-fibrin immunostaining (as done in Section 3.15).

### 3.17. SDS-PAGE and Western Blotting of Fibrin Meshes.

TNF $\alpha$ -activated HUVECs growing on 6-well plates were incubated in the presence of fibrin mesh mixture 30 minutes at 37°C. Cells were washed and incubated in complete medium for 4.5 hours under control conditions, or in the presence of 3 mM amiloride, 10  $\mu$ M chloroquine, 50 ng/mL PAI-1 plus 0.15 U/mL aprotinin, amiloride with PAI-1 plus aprotinin, or chloroquine with PAI-1 plus aprotinin. Wells were washed in PBS, followed by HUVEC lysis with radio-immunoprecipitation (RIPA) buffer in the presence of protease inhibitor cocktail (AEBSF, aprotinin, bestatin, E-64, leupeptin, pepstatin A; Thermo Scientific). Cell residue was separated by centrifugation (13,300 g for 15 minutes) and the protein fraction was prepared for reducing SDS-PAGE by incubating at 70°C in the presence of 0.1 M dithiothreitol for 10 minutes to denature protein and reduce disulfide linkages. Gel electrophoresis was done in TrisHCl 4%-15% polyacrylamide gels (Bio-Rad Laboratories, Inc., Hercules, CA) at 60 V (constant voltage), TrisHCl buffer. After PAGE, gels were directly imaged using fluorescence detection in a Typhoon Trio imager (GE Healthcare Life Sciences, Pittsburgh, PA). Alternatively, protein was transferred to polyvinyl difluoride membranes at 250 mA

(constant current) in 80% TrisHCl:20% methanol. This was followed by Western blotting with anti-fibrin  $\beta$  chain, followed by horse radish peroxidase (HRP)-conjugated secondary, and detection by chemiluminescence. Densitometry analysis was performed using ImageJ (National Institutes of Health, Bethesda, MD).

In order to test the activity of PAI-1, we incubated fibrin mesh mixture in the absence (control) or presence of tPA or tPA plus PAI-1 plus aprotinin in test tubes. After 8 hours of incubation, fibrin mesh mixtures were processed for SDS-PAGE and Western blotting with anti-fibrinogen as done above.

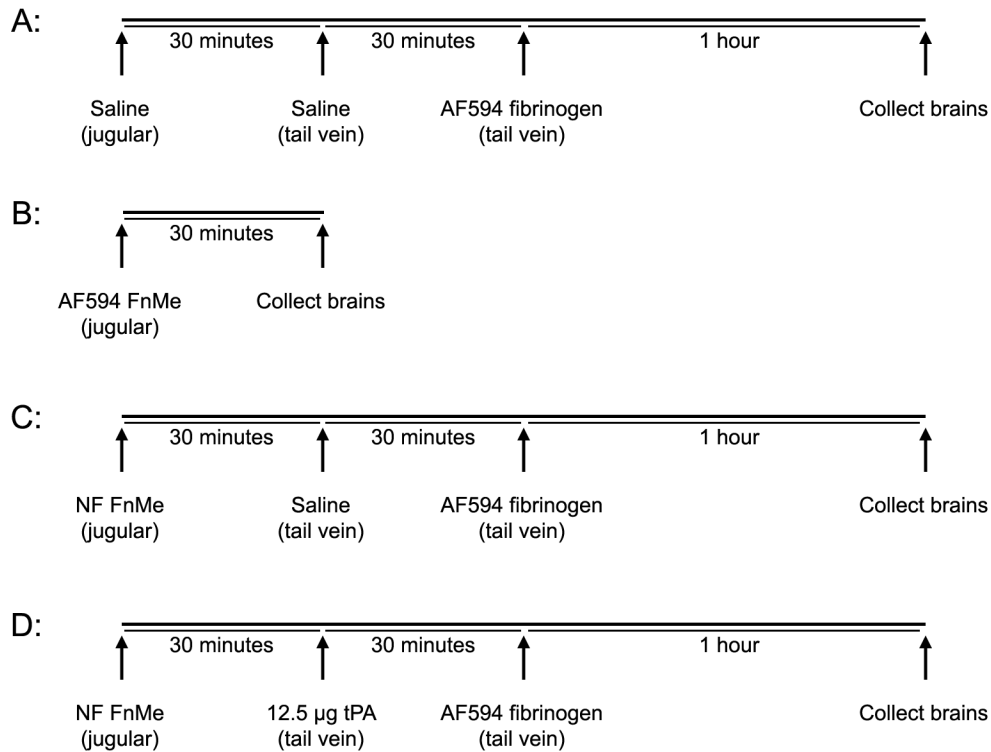
### 3.18. Visualization of Fibrin Microemboli in Mice.

For confocal microscopy of pulmonary emboli models, wild-type C57BL/6 (Jackson Laboratory, Bar Harbor, ME), ICAM-1 knockout (B6.129S4-Icam1<sup>tm1Jcgr/J</sup>, Jackson Laboratory), or acid sphingomyelinase (ASM) knockout (kindly provided by Dr. Edward Schuchman, Mount Sinai School of Medicine, New York, NY [197]) mice were anesthetized and injected via jugular vein with pre-formed green fibrin microemboli (made by incubating fibrin mesh mixture for 30 minutes in test tubes, see Section 3.14). After 1.5 hours, mice were injected with 50  $\mu$ g AF594 (red fluorescently labeled) fibrinogen. One hour later, mice were sacrificed and lungs were dissected, followed by fixation overnight in 4% paraformaldehyde. Lungs were submerged in DAPI for 1 hour, and washed. Confocal microscopy was used to identify fibrin microemboli found in alveolar regions. Then, individual frames were selected to obtain z-stacks starting at the top of the fibrin microembolus of interest, and ending at the plane of the nuclei in the

same frame. Images were used to determine overlap between green fibrin microemboli and red fibrinogen.

For two-photon microscopy of brain emboli models, C57BL/6, ICAM-1 knockout, or ASM knockout mice were anesthetized and injected with one of the treatments indicated in Table 3.

**Table 3. Injection treatments used for microscopy of mouse emboli models.**



NF = Non-fluorescent, FnMe = fibrin microemboli

After the last injection, mice were sacrificed and brains were dissected and fixed in 4% paraformaldehyde overnight prior to imaging using two-photon fluorescence microscopy. For each mouse, the brain surface was scanned to find a region where blood vessels could be clearly identified. At this location, an image was obtained ~100 μm deep into the tissue, where preliminary experiments consistently showed abundant brain

capillaries. Then, four more images were similarly obtained above, below, left, and right of this central location. The process was repeated at 2 different brain regions, yielding 15 images per mouse, each image comprising a field of 400  $\mu\text{m}$  by 400  $\mu\text{m}$  of tissue.

Analysis was performed on each image to quantify the number and mean diameter of fluorescent fibrin microemboli above a background fluorescence threshold in each field.

All animal studies were performed according to the Guide for the Care and Use of Laboratory Animals, as well as Institutional Animal Care and Use Committee-approved protocols and University regulations.

### 3.19. Statistics.

For microscopy, each experiment was repeated at minimum two times and contained duplicate cover slips per treatment ( $\geq 4$  cover slips total). From each cover slip, with a population of  $\sim 10^5$  cells under confluence, a minimum of 5 frames containing confluent cells ( $\sim 5$ -10 cells per field) were obtained randomly. Depending on the analysis, frames were analyzed as a whole ( $\geq 20$  frames total), or a minimum of 2 cells were analyzed per frame ( $\geq 40$  cells total). For Transwell® experiments, each experiment was repeated at minimum two times and contained four replicate wells per treatment ( $\geq 8$  wells total). Mouse experiments used a minimum of two mice per treatment, and a minimum of 15 images were obtained per organ ( $\geq 30$  frames total). Data were calculated as mean  $\pm$  standard error of the mean. For two-way comparisons, statistical significance was determined using Student's *t*-test with a threshold of  $p < 0.05$ . For multiple comparisons, statistical significance was determined using One-way ANOVA followed by Tukey's test ( $p < 0.05$ ).

## **Chapter 4: Role of Particle Size and Targeting Moiety on the Outcomes of ICAM-1-Mediated Endocytosis**

### *4.1. Background*

A major goal in the field of drug delivery is to optimize the therapeutic effect of a cargo drug, which can be achieved by varying parameters such as dose, administration route, cell- or tissue-targeting capacities, etc. [198, 199], and a clear understanding of biological systems often facilitates these optimizations [200]. When intracellular drug delivery relies on endocytic receptors, knowledge about the mechanism of endocytosis associated with a given targeted receptor can inform drug carrier design. For instance, clathrin- and caveolae-mediated endocytosis are adapted for the uptake of nanometric nutrients, proteins and other small molecules, and thus internalize objects no larger than ~70-200 nm in diameter due to the physical limitations in their vesicular machineries [93, 201]. Drug carriers targeted to receptors associated with these pathways must be below 200 nm in diameter to achieve efficient intracellular delivery. Conversely, it can result beneficial to use drug carriers above 200 nm if delivery is desired in the vicinity of, but not inside, cells that express said receptors.

In a similar fashion, tools used in the field of drug delivery can help elucidate natural phenomena thanks to the ability to generate mimicking entities, and modulate physical and chemical properties of these objects when they interact with biological systems. An example of this is the use of spherical inert particles coated with selectin-

binding and/or Ig-like CAM-binding molecules that have given insight into the binding properties behind leukocyte interaction with the endothelium [202-205].

The characterization of cell adhesion molecule (CAM)-mediated endocytosis, which occurs when drug carriers bind multiple copies of ICAM-1 on the cell surface, has thus far only occurred in the context of drug delivery [6-8]. Therefore, the design parameters used for drug delivery through this pathway have not benefitted from in-depth biological knowledge of the mechanism, but rather have served to elucidate its regulation. Furthermore, no systematic studies have been performed to link ICAM-1 binding and subsequent endocytosis to a physiological function. However, since binding ICAM-1 is the initial driving step of CAM-mediated uptake, it is possible that the properties of natural binding partners of ICAM-1 could shed light on this endocytic mechanism.

With this in mind, the first goal of this work was to study how two physical parameters can affect CAM-mediated endocytosis of drug carriers, based on knowledge about two important natural ICAM-1 ligands: integrin  $\alpha_L\beta_2$ , found on the surface of leukocytes, and fibrin, the main component of blood clot polymers. As suggested above, this strategy could provide two-fold benefits: first, to gain knowledge about CAM-mediated endocytosis that can be applied for the optimization of drug delivery; second, to gain insight into the possible mechanisms that regulate the physiological functions of the CAM-mediated pathway.

The two parameters we selected were drug carrier size and the targeting moiety used to bind ICAM-1. Regarding size, leukocytes range from 5 to 20  $\mu\text{m}$  diameter before spreading on the endothelial cell surface [206], and they produce podosomes against the endothelial cell plasmalemma which range from 0.2 to 1  $\mu\text{m}$  in diameter [123]. Blood

clots range from hundreds of nanometers to hundreds of microns [207], so that blood clot degradation (fibrinolytic) fibrin mesh remnants can be expected to fall within a wider range compared to leukocytes, but exhibiting smaller sizes at the lower (nanometric) end [183]. This makes it plausible for outcomes of CAM-mediated endocytosis elicited by ICAM-1 binding to depend on ligand size.

Regarding targeting moiety, leukocytes and fibrin(ogen) bind ICAM-1 through different means. First, leukocytes use integrin-mediated binding, which depends on integrin activation states [208, 209] and is regulated by changing the distribution of integrins on the leukocyte plasma membrane, generating changes in avidity [210]. Meanwhile, fibrin(ogen) has a binding site for ICAM-1 on its  $\gamma$  chain [145] and the density of fibrin clots could affect how these binding sites are presented to ICAM-1. In addition to this, while both leukocytes and fibrin bind domain D1 of ICAM-1, they do so at different epitopes. Certain antibodies that bind/disrupt D1 of ICAM-1, such as clone LB-2, can block binding of both  $\alpha_L\beta_2$  and fibrin(ogen), while others, such as clone R6.5, inhibit  $\alpha_L\beta_2$ , but not fibrinogen, binding [51]. Use of ICAM-1 peptides for competition experiments, mutagenesis, and crystallography, also suggests that the sites for  $\alpha_L\beta_2$  and fibrin(ogen) binding both reside near the N terminus of D1, but are different and might slightly overlap at most [50]. Thus, if natural systems are in place to bind different regions of ICAM-1 and with potential variety of binding strengths, it is possible the CAM-mediated pathway can be regulated based on the used ICAM-1-targeting moiety that coats drug carriers.

In support of these ideas, previous evidence shows that size and bound epitope can significantly affect aspects of CAM-mediated endocytosis of drug carriers. For

example, spherical carriers of a wide range of sizes (100 nm to 10  $\mu\text{m}$ ) enter cells with similar efficiency, yet trafficking to lysosomes is slower and less efficient for 1  $\mu\text{m}$  carriers compared to 100 nm carriers [77]. In a different scenario, carriers targeted to PECAM-1 to induce CAM-mediated endocytosis have different uptake and trafficking efficiencies depending on the epitope on PECAM-1 bound by antibodies coating drug carriers [101].

Drug carrier size and targeting moiety appear to be important factors that could help modulate CAM-mediated drug delivery strategies, and they represent easily manipulatable parameters in the design of drug carriers. Thus, in this chapter we examine how ligand size and targeting moiety affect binding, uptake, ceramide enrichment, and intracellular trafficking associated with CAM-mediated endocytosis.

## 4.2. Results

### 4.2.1. Model to study the role of particle size and targeting moiety on CAM-mediated pathway outcomes.

In order to perform our studies, we used inert polystyrene-latex spherical particles, a ubiquitous and economical model to study targeting and intracellular transport of ICAM-1-targeted polymer drug carriers. These particles behave in a similar fashion as the clinically relevant biodegradable poly(lactic-co-glycolic acid) (PLGA) drug carriers, yet they do not introduce confounding effects of degradation [190]. We chose particles of four sizes, spanning the range in which typical drug carriers, leukocytes, and fibrin meshes fall (200 nm, 500 nm, 1  $\mu\text{m}$ , and 4.5  $\mu\text{m}$ ). To differentiate targeting moieties, we

coated on the surface of these particles either of two targeting molecules: Antibodies to ICAM-1 (clone R6.5) bind the same epitope as integrin  $\alpha_L\beta_2$  without blocking fibrin(ogen) binding, while the 17-residue peptide  $\gamma_3$  is directly derived from the ICAM-1-binding sequence of fibrinogen. While anti-ICAM is a divalent 150 kDa molecule,  $\gamma_3$  is a monovalent 1.93 kDa peptide, such that differences in size and valency between these two molecules could affect CAM-mediated uptake.

The properties of particles used in each section will be detailed correspondingly, but Table 2 in the Methods section (page 33) serves as an overall reference.

#### 4.2.2. Role of particle size and targeting moiety on binding of ICAM-1-targeted particles.

The induction of CAM-mediated endocytosis depends on initial binding of drug carriers to ICAM-1. As shown in other scenarios, the efficiency of endocytosis may be dependent on the total number of receptors bound, strength of binding, and other phenomena at the interface between ligands (e.g.: drug carriers, leukocytes, or fibrin meshes) and the plasma membrane [211]. Thus, it is important to understand binding events separately from subsequent endocytosis. In order to achieve this, we first examined binding of ICAM-1-targeted particles using fixed endothelial cells, where uptake and membrane dynamics are abolished. We chose particles of three sizes spanning the range in which typical drug carriers and ICAM-1 natural binding partners fall: 200 nm, 1  $\mu\text{m}$ , and 4.5  $\mu\text{m}$ . In order to better determine the effect of size, we adjusted the concentration of each size formulation in order to normalize the total particle surface area added to cells. That is, each cell was exposed to the same net particle surface area regardless of particle size.

As shown in Figure 1A, anti-ICAM particles of 200 nm, 1  $\mu\text{m}$  and 4.5  $\mu\text{m}$  in diameter all bound to fixed TNF $\alpha$ -activated HUVECs. This binding was specific, as determined by comparing binding levels of anti-ICAM particles to those of particles coated with non-specific IgG (fold-increase in binding between IgG and anti-ICAM was  $87\pm3$ ,  $92.3\pm6.1$ , and  $45.3\pm3.2$  for 200 nm, 1  $\mu\text{m}$  and 4.5  $\mu\text{m}$  particles, respectively). Although all particle sizes bound specifically, the total number of anti-ICAM particles bound per cell was lower with increasing particle size at all time-points (Figure 1B).

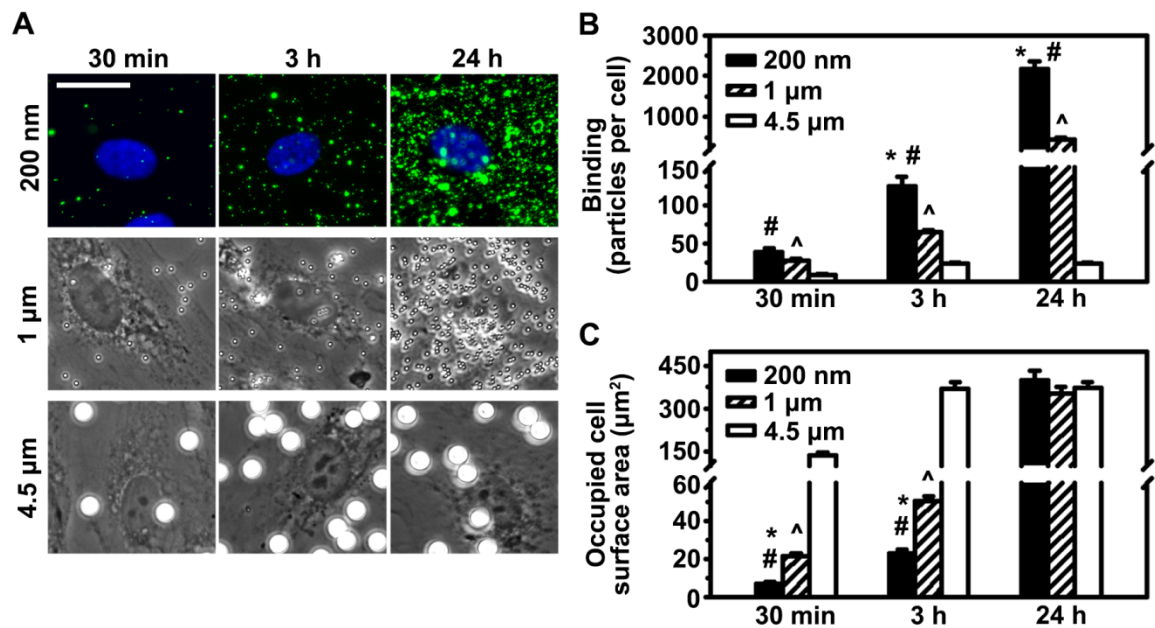


**Figure 1. Binding of anti-ICAM particles to fixed endothelial cells.** (A) Fluorescence (top) or phase-contrast (middle, bottom) microscopy showing binding of 200 nm, 1  $\mu\text{m}$  or 4.5  $\mu\text{m}$  anti-ICAM particles after 30 minutes, 3 hours or 24 hours incubation at room temperature with fixed activated HUVECs. Scale bar = 20  $\mu\text{m}$ . Green = particles. Blue = nuclei. (B) Quantification of total particles bound per cell. (C) Total (top-down) cell surface area occupied by bound particles on each cell. Data represent mean  $\pm$  standard error of the mean. \* compares 200 nm to 1  $\mu\text{m}$ , # compares 200nm to 4.5  $\mu\text{m}$ , and ^ compares 1  $\mu\text{m}$  to 4.5  $\mu\text{m}$  ( $p < 0.05$  by Tukey's test after One-way ANOVA).

This result is not surprising since each individual particle of a larger size occupies more surface area than a smaller counterpart. Thus, in order to better compare binding, we calculated the top-down cell surface area occupied by all the particles bound per cell (Figure 1C). This revealed that at 30 minutes and 3 hours, micron-sized particles occupied a larger surface area of the cell compared to nanoparticles. However, allowing

sufficient binding time (24 hours incubation) led to equal occupancy by particles of all three sizes ( $\sim 370 \mu\text{m}^2$ ), which may represent a saturation level. Since we originally exposed cells to equal particle surface areas regardless of size, this indicated that particles of larger sizes exhibit earlier stronger binding than those in the nanoscale. This result is in line with the additive binding properties of antibodies since each individual particle of larger size exhibits more antibody-ICAM-1 interactions than a smaller counterpart, likely making its avidity higher. However, it appears from these data, that given sufficient time, the binding interactions become stabilized regardless of size.

When we examined binding of  $\gamma 3$  particles, they also bound specifically as compared to particles coated with  $\gamma 3\text{S}$ , a  $\gamma 3$  scrambled peptide sequence (binding for 200 nm  $\gamma 3\text{S}$  particles was not quantifiable, while 1  $\mu\text{m}$   $\gamma 3$  particles bound  $3.6 \pm 0.3$ -fold more than  $\gamma 3\text{S}$ ). Similar to anti-ICAM particles, there was a size-dependent pattern in terms of binding to HUVECs (Figure 2A and B). However, binding was much lower for both sizes of  $\gamma 3$  particles even though the  $\gamma 3$  peptide density on the particle surface (and, thus, potential for binding a number of ICAM-1 molecules) far surpassed that of antibodies (Table 2, page 33). This result might be expected since the dissociation constant of R6.5 for ICAM-1 is 4 orders of magnitude lower than that of  $\gamma 3$  in solution (6.3 nM vs 34  $\mu\text{M}$  [145, 212]), so the affinity of  $\gamma 3$  for ICAM-1 is predicted to be lower compared to an antibody when presented on the surface of particles.

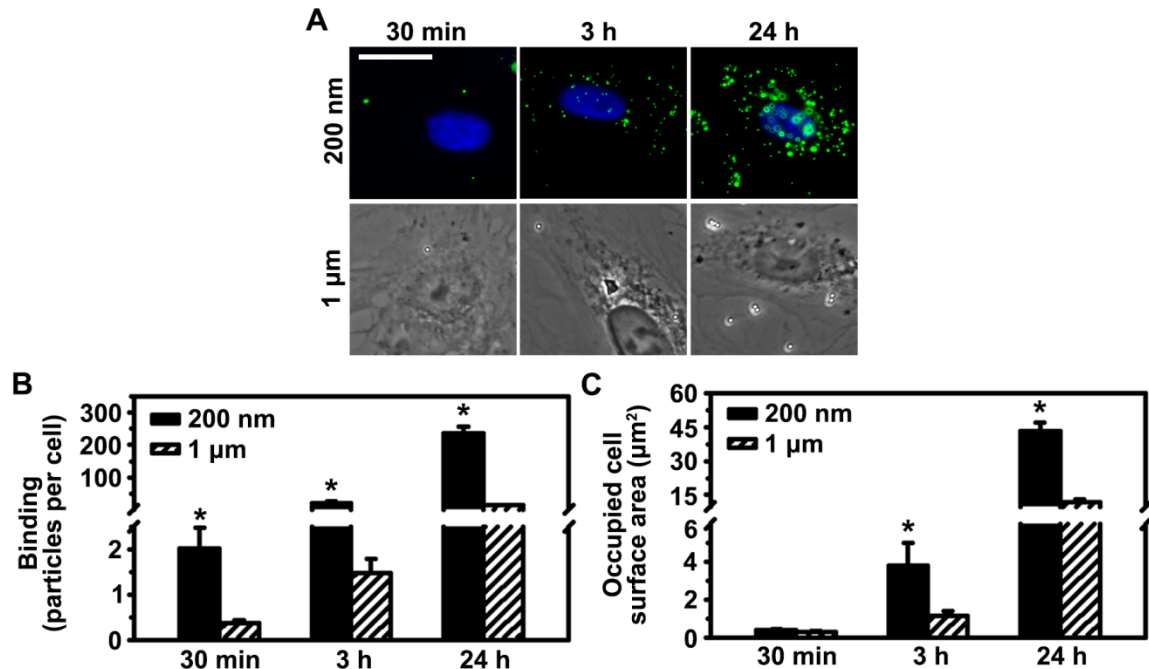


**Figure 2. Binding of  $\gamma 3$  particles to fixed endothelial cells.** (A) Fluorescence (top) or phase-contrast (bottom) microscopy showing binding of 200 nm or 1  $\mu\text{m}$   $\gamma 3$  particles after 30 minutes, 3 hours or 24 hours incubation at room temperature with fixed activated HUVECs. Scale bar = 20  $\mu\text{m}$ . Green = particles. Blue = nuclei. (B) Quantification of total particles bound per cell. (C) Total (top-down) cell surface area occupied by bound particles on each cell. Data represent mean  $\pm$  standard error of the mean. \* compares 200 nm to 1  $\mu\text{m}$  ( $p < 0.05$  by Student's *t*-test).

We also observed that the difference in binding between 200 nm versus 1  $\mu\text{m}$  particles was much larger for  $\gamma 3$  than for anti-ICAM particles. Even after calculating the total cell surface area occupied by particles per cell,  $\gamma 3$  nanometer-sized particles occupied a larger surface area than  $\gamma 3$  microparticles (compare black versus dashed columns in Figures 1C and 2C). This suggested that, unlike anti-ICAM, there was not such an acute increase in particle avidity as size (and, thus, number of ICAM-1 engaged per particle) increased. Due to this, it seemed that binding through  $\gamma 3$  is more sensitive to increasing particle size compared to anti-ICAM, a reflection of the differences in binding potential between the two molecules coating the particles. It is also possible that a small peptide such as  $\gamma 3$  might have more difficulty accessing its ICAM-1 binding epitope than a large antibody when presented on a large particle compared to a small one.

Next, we repeated binding experiments using live HUVECs to verify these results and in order to understand how membrane dynamics and concomitant endocytosis may affect particle association with endothelial cells. Important factors that may affect this are (a) lateral mobility of proteins in the plasma membrane, which could allow particles to bind more molecules of ICAM-1 and increase avidity, (b) concomitant endocytosis that may retain carriers inside cellular compartments regardless of how firmly bound they are to ICAM-1, and/or (c) internalization of ICAM-1 molecules, reducing the available binding pool of this molecule. As shown in Figure 3A and B, the pattern of total anti-ICAM particle binding levels was the same as that seen with fixed cells, where fewer microparticles bound per cell compared to nanoparticles. Despite this similar trend, there were differences in the total number of particles associated with cells between fixed versus live cells depending on particle size. Submicrometer-sized particles showed an enhancement in cell association when cells were live, in agreement with the expected particle accumulation within cells due to concomitant endocytosis, while this was not the case (or less dramatic) for microparticles (Figure 3C). Specifically, at 30 minutes, 200 nm particles showed a 2.9-fold enhancement in association with cells, while 1  $\mu\text{m}$  and 4.5  $\mu\text{m}$  showed comparatively no/lower enhancement (0.97-fold and a 1.79-fold enhancement, respectively). Even by 3 hours, 200 nm particles retained a 1.7-fold enhancement, while both microparticle sizes showed equal binding between live and fixed cells.

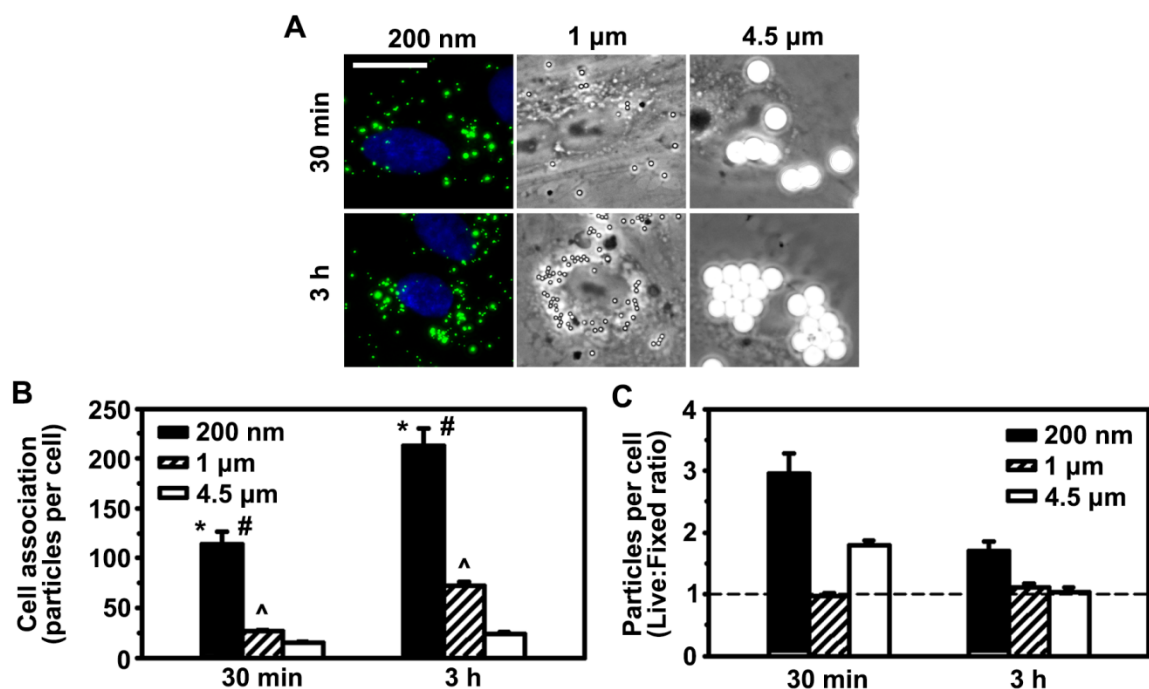


**Figure 3. Association of anti-ICAM particles to live endothelial cells.** (A) Fluorescence (right) or phase-contrast (middle and left) microscopy showing association of 200 nm, 1 μm or 4.5 μm anti-ICAM particles after 30 minutes or 3 hours incubation at 37°C with activated HUVECs. Scale bar = 20 μm. Green = particles. Blue = nuclei. (B) Quantification of total particle binding per cell. (C) Ratio of particles per cell in living versus fixed HUVECs. Dashed line = 1. Data represent mean ± standard error of the mean. In B, \* compares 200 nm to 1 μm, # compares 200 nm to 4.5 μm, and ^ compares 1 μm to 4.5 μm ( $p < 0.05$  by Tukey's test after One-way ANOVA).

A lower enhancement between fixed and live cells for micron-sized particles suggests that perhaps endocytosis for this size is not as efficient as that observed for 200 nm particles. However, previous evidence shows that the CAM-mediated pathway is capable of internalizing drug carriers of a wide range of sizes [77]. Thus, it is possible that the concomitant endocytosis of anti-ICAM particles led to a depletion of ICAM-1 at the cell surface, preventing new particles in solution from engaging the cell. Although previous work has shown that ICAM-1 rapidly recycles back to the plasma membrane after drug carrier uptake [9], this was only explored in the case of nanocarriers (which agrees with our data showing binding enhancement even after 3 hours in live cells for 200 nm particles). It may be possible that ICAM-1 recycling kinetics are slower or trafficking itinerary differs for micron-sized particles, preventing replenishment of the

receptor on the plasma membrane. This could also be associated with different trafficking patterns for internalized particles depending on size after CAM-mediated uptake, which we explore in subsequent sections.

The idea that  $\gamma 3$  particles may exhibit lower avidity compared to anti-ICAM particles was further supported after examining their binding in live cells (Figure 4A). Similar to anti-ICAM particles, micron-sized  $\gamma 3$  particles bound to live HUVECs at lower levels than nanometric counterparts (Figures 4B). However, the enhancement in cell association for  $\gamma 3$  particles between fixed and living cells was quite prevalent, for both particle sizes and at both time-points (compare Figures 3C and 4C). For a particle exhibiting low binding strength, it may have been of greater benefit to allow for the lateral migration and clustering of more ICAM-1 molecules at the particle binding site compared to high-affinity antibody particles. It may also be possible that endocytic retention of particles increased their association with cells. Furthermore, it should be noted that unlike 1  $\mu\text{m}$  anti-ICAM particles, 1  $\mu\text{m}$   $\gamma 3$  particles bound more in live versus fixed cells even after 3 hours. This suggests that  $\gamma 3$  particles might not deplete ICAM-1 from the plasma membrane, as could be expected from their lower binding levels, or that ICAM-1 recycling patterns may differ depending on the targeting moiety used to engage ICAM-1.

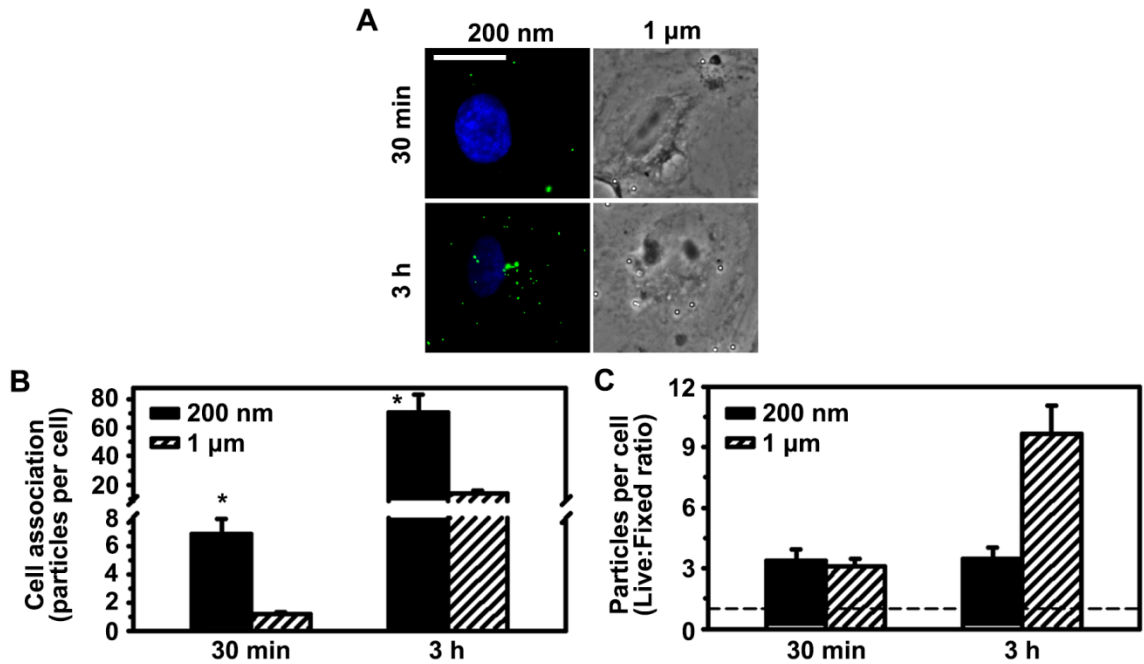


**Figure 4. Association of  $\gamma 3$  particles to live endothelial cells.** (A) Fluorescence (left) or phase-contrast (right) microscopy showing association of 200 nm or 1  $\mu\text{m}$   $\gamma 3$  particles after 30 minutes or 3 hours incubation at 37°C with activated HUVECs. Scale bar = 20  $\mu\text{m}$ . Green = particles. Blue = nuclei. (B) Quantification of total particle binding per cell. (C) Ratio of particles per cell in living versus fixed HUVECs. Dashed line = 1. Data represent mean  $\pm$  standard error of the mean. In B, \* compares 200 nm to 1  $\mu\text{m}$  at each time-point ( $p < 0.05$  by Student's  $t$ -test).

When comparing the binding levels, anti-ICAM particles always bound at higher levels than  $\gamma 3$  counterparts regardless of size (anti-ICAM particles per cell divided by  $\gamma 3$  particles per cell  $> 1$  for all cases; Figure 5A). Also, this difference was always higher for 1  $\mu\text{m}$  versus 200 nm particles, supporting the idea that  $\gamma 3$  particles are more sensitive to increasing particle size regarding binding outcomes. It was interesting to note that this difference was mitigated over time even in fixed cells, suggesting that initial weak interactions between  $\gamma 3$  and ICAM-1 are stabilized over time to a greater degree than the originally strong antibody-ICAM-1 interaction.

As mentioned earlier, endocytic entrapment of particles or ICAM-1 membrane mobility may also enhance cell association. Indeed, the difference in binding between anti-ICAM and  $\gamma 3$  particles was further reduced in living cells (Figure 5B). Furthermore,

the gap between 200 nm and 1  $\mu\text{m}$  particle binding was lower in living cells than fixed cells (compare the jump between black columns and dashed columns in Figure 5A versus 5B), suggesting endocytic accumulation (or increased avidity due to ICAM-1 lateral mobility) can mitigate the size-dependent binding sensitivity of  $\gamma 3$  particles.

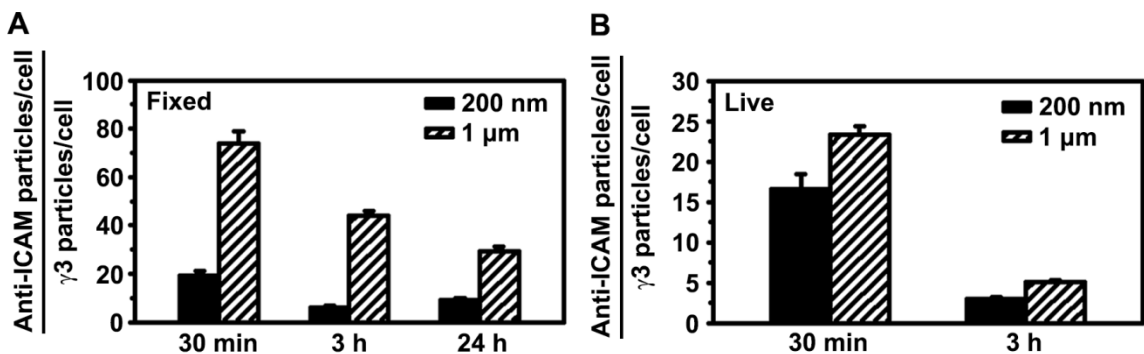


**Figure 5. Comparison of binding of anti-ICAM versus  $\gamma 3$  particles to endothelial cells.** (A) Ratio of binding of 200 nm or 1  $\mu\text{m}$  anti-ICAM versus  $\gamma 3$  particles after 30 minutes, 3 hours or 24 hours incubation at room temperature with fixed activated HUVECs. (B) Ratio of cell association of 200 nm or 1  $\mu\text{m}$  anti-ICAM versus  $\gamma 3$  particles after 30 minutes or 3h incubation at 37°C with activated HUVECs. Data represent mean  $\pm$  standard error of the mean.

In short, these results provide insight into the optimization of drug delivery strategies that target ICAM-1, where overall lower binding of  $\gamma 3$  particles may affect their performance compared to antibody particles, especially for larger particle sizes. Although pure binding data showed that  $\gamma 3$  particles may not be as advantageous as anti-ICAM counterparts for high levels of therapeutic delivery, their association with cells thanks to membrane dynamics and/or CAM-mediated endocytic retention reduces these binding deficiencies and makes them similarly suitable for ICAM-1-targeted intracellular drug delivery. The apparent differences in binding strength between these two targeting moieties call for in-depth examination of the behavior of these particles under the shear stress of blood flow. This will be particularly important because drug carriers with lower affinity/avidity may accumulate more acutely at desired delivery sites, since they are less likely to interact and be retained at sites with low expression of the targeted molecule.

#### 4.2.3. Role of particle size and targeting moiety on endothelial uptake of ICAM-1-targeted particles.

Next, we determined the role of size and targeting moiety on CAM-mediated uptake by incubating anti-ICAM or  $\gamma 3$  particles with HUVECs for 30 minutes or 3 hours, followed by fixing and immunostaining to differentiate surface-bound from internalized particles (see Methods, Section 3.7). Since particles of different sizes and targeting moieties associated with cells at different total numbers, we calculated their rate of uptake (percent internalized particles out of the total cell-associated), which has been shown to be unaffected by how many particles are bound per cell in the case of CAM-mediated endocytosis [7].

As shown in Figure 6, we found that at initial time-points, the percent internalization for anti-ICAM particles was dependent on particle size (~70% for 200 nm and 1  $\mu\text{m}$  versus 31.9% for 4.5  $\mu\text{m}$ ). Nonetheless, by 3 hours, uptake of all particles was the same regardless of size, in agreement with previous reports [77], and showing that given enough time, CAM-mediated endocytosis is capable of internalizing a wide range of object sizes with high efficiency. These internalization patterns shed some light on our results seen with binding fixed versus live cells. The fact that by 3 hours all particles showed levels of uptake near 100%, yet only nanoparticles exhibited enhanced binding in live versus fixed cells, as discussed above (recall Figure 3C), is intriguing. This supports the idea that large particles a) might have depleted ICAM-1 from the cell membrane more readily than small particles and/or b) may elicit different trafficking patterns that do not recycle ICAM-1 back to the plasma membrane as readily as nano-meter sized particles. Such properties of CAM-mediated uptake could hold importance in the design of drug

delivery strategies as, for instance, previous studies have shown that ICAM-1 recycling following CAM-mediated endocytosis can be exploited for the administration of multiple therapeutic doses [9]. Thus, it will be important for future work to study the ICAM-1 plasma membrane depletion/recycling properties of large versus small ICAM-1-targeted particles.

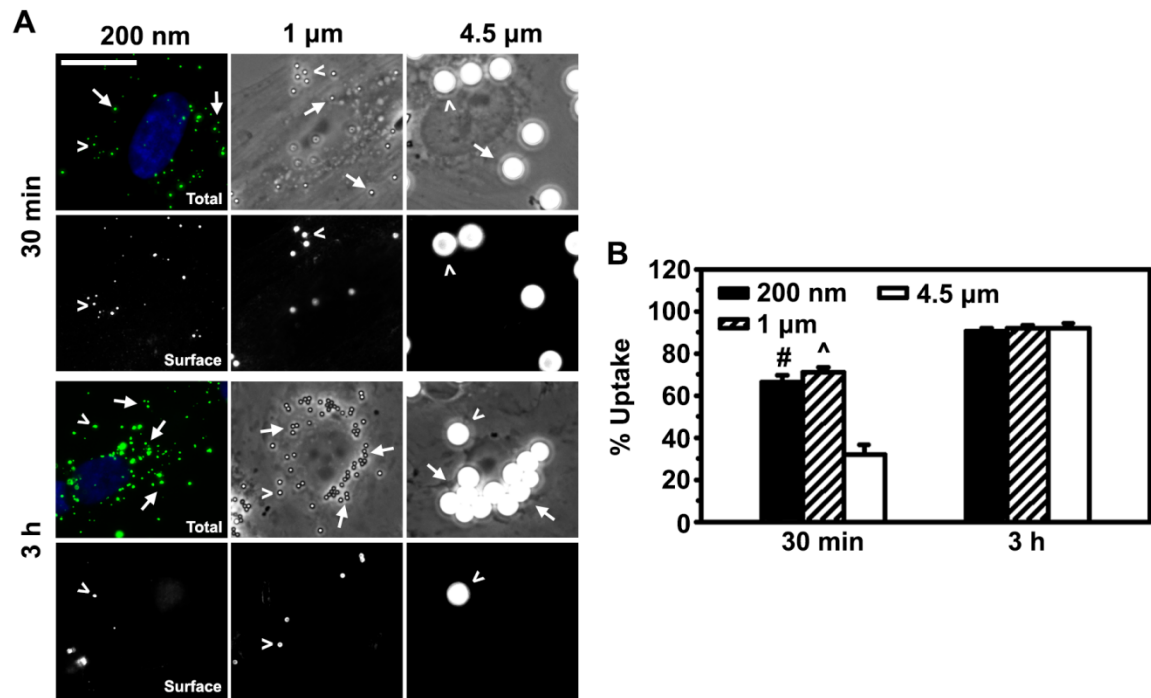


**Figure 6. Uptake of anti-ICAM particles by endothelial cells.** Activated HUVECs were incubated with 200 nm, 1 μm or 4.5 μm anti-ICAM particles for 30 minutes or 3 hours at 37°C. Surface-bound, but not internalized, particles were immunostained to quantify percent uptake. (A) Sample micrographs showing total particles (top panels for each time-point) or only surface-bound non-internalized particles (bottom panels for each time-point). Arrows indicate internalized particles and arrowheads indicate non-internalized particles. Scale bar = 20 μm. Green = particles. Blue = nuclei. (B) Quantification of uptake expressed as the percent of particles inside cells out the total cell-associated particles. Data represent mean ± standard error of the mean. # compares 200 nm to 4.5 μm, and ^ compares 1 μm to 4.5 μm ( $p < 0.05$  by Tukey's test after One-way ANOVA).

Compared to anti-ICAM particles, which showed similar uptake for 200 nm and 1 μm particles by 30 minutes, the endocytosis of  $\gamma 3$  particles appeared to be more sensitive to size. Particles 1 μm in diameter showed significantly lower levels of uptake at 30 minutes compared to 200 nm particles (Figure 7A and B). As seen with anti-ICAM particles, the uptake efficiency of nano- and micro-particles was brought closer over time,

indicating that CAM-mediated uptake is equipped for internalization of objects of a wide range of sizes, regardless of the ICAM-1-targeting moiety used to elicit the pathway.

However, since the percent uptake of 200 nm versus 1  $\mu\text{m}$   $\gamma\text{3}$  particles at 3 hours was still significantly higher, this suggests that binding ICAM-1 via  $\gamma\text{3}$ , slower, or weaker particle binding, may lead to more size-sensitive CAM-mediated uptake rates.

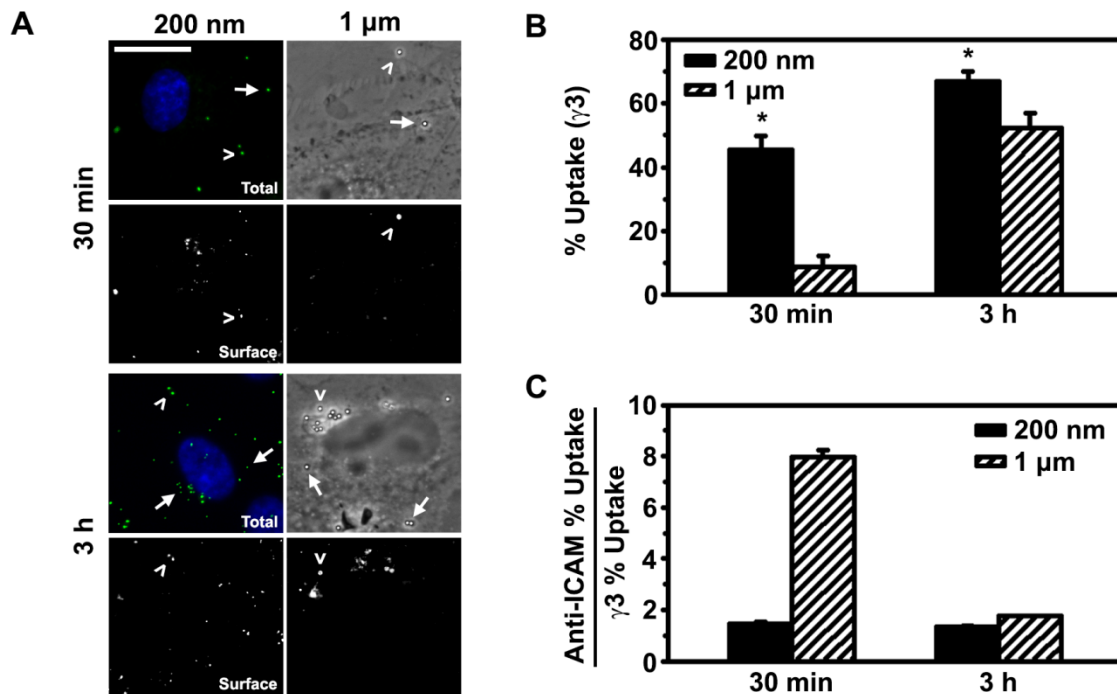


**Figure 7. Uptake of  $\gamma\text{3}$  particles by endothelial cells and comparison with anti-ICAM particle uptake.** Activated HUVECs were incubated with 200 nm or 1  $\mu\text{m}$   $\gamma\text{3}$  or anti-ICAM particles for 30 minutes or 3 hours at 37°C. Surface-bound, but not internalized, particles were immunostained (see Methods) to quantify percent uptake. (A) Sample micrographs showing total particles (top panels for each time-point) or only surface-bound non-internalized particles (bottom panels for each time-point). Arrows indicate internalized particles and arrowheads indicate non-internalized particles. Scale bar = 20  $\mu\text{m}$ . Green = particles. Blue = nuclei. (B) Quantification of uptake expressed as the percent of particles inside cells out of the total cell-associated particles. (C) Ratio of uptake of anti-ICAM versus  $\gamma\text{3}$  particles. Data represent mean  $\pm$  standard error of the mean. \* compares 200 nm to 1  $\mu\text{m}$  at each time-point ( $p < 0.05$  by Student's *t*-test).

In support of these targeting moiety differences regarding particle size, a comparison of the uptake levels of anti-ICAM versus  $\gamma\text{3}$  particles, showed only a slight (1.5-fold) higher efficiency of uptake for 200 nm as early as 30 minutes, yet 1  $\mu\text{m}$  particles took 3 hours to reach this level (from an original 8-fold difference; Figure 7C).

This suggests that in addition to particle size, the CAM-mediated endocytic machinery is sensitive to targeting moiety, particularly at early time-points.

These results should be considered in the development of ICAM-1-targeted carrier-assisted drug delivery, as the use of peptides instead of antibodies could prove beneficial in order to prevent potential effects on the immune system [213], yet our data indicate generally lower uptake efficiency of  $\gamma 3$  versus anti-ICAM model drug carriers, and specifically slower uptake with micron-sized formulations. For instance, increasing the concentration of  $\gamma 3$  carriers administered may attenuate these differences.

#### 4.2.4. Role of particle size and targeting moiety of ICAM-1-targeted particles on ceramide enrichment during CAM-mediated endocytosis.

Thus far, our data showed that particle size and targeting moiety affect particle binding outcomes, suggesting differences in ICAM-1 engagement. Since ICAM-1 signaling depends on the multivalent engagement of this molecule [6], it is possible that these particle size and targeting moiety differences affect signaling properties of CAM-mediated uptake. Such differences in signaling could be manifested in the downstream events of membrane deformability and actin rearrangement, both of which are likely to affect the efficiency of internalization, particularly in a size-dependent manner. Our published data show that ICAM-1 signaling leads to acid sphingomyelinase recruitment and production of ceramide during CAM-mediated uptake, and this is a major aspect in the regulation of membrane deformability and actin rearrangement [7]. With that in mind, we next explored ceramide in the context of size and targeting moiety.

In order to compare ceramide production for particles of different sizes, we incubated HUVECs with 200 nm, 1  $\mu\text{m}$ , and 4.5  $\mu\text{m}$  anti-ICAM or  $\gamma 3$  particles for 30 minutes. Then, we immunostained ceramide (Figure 8A, left) and measured the fold increase ( $\Delta$ ) between background levels of plasma membrane ceramide at the vicinity of binding sites versus ceramide intensity at regions where particles bound (Figure 8A, right).

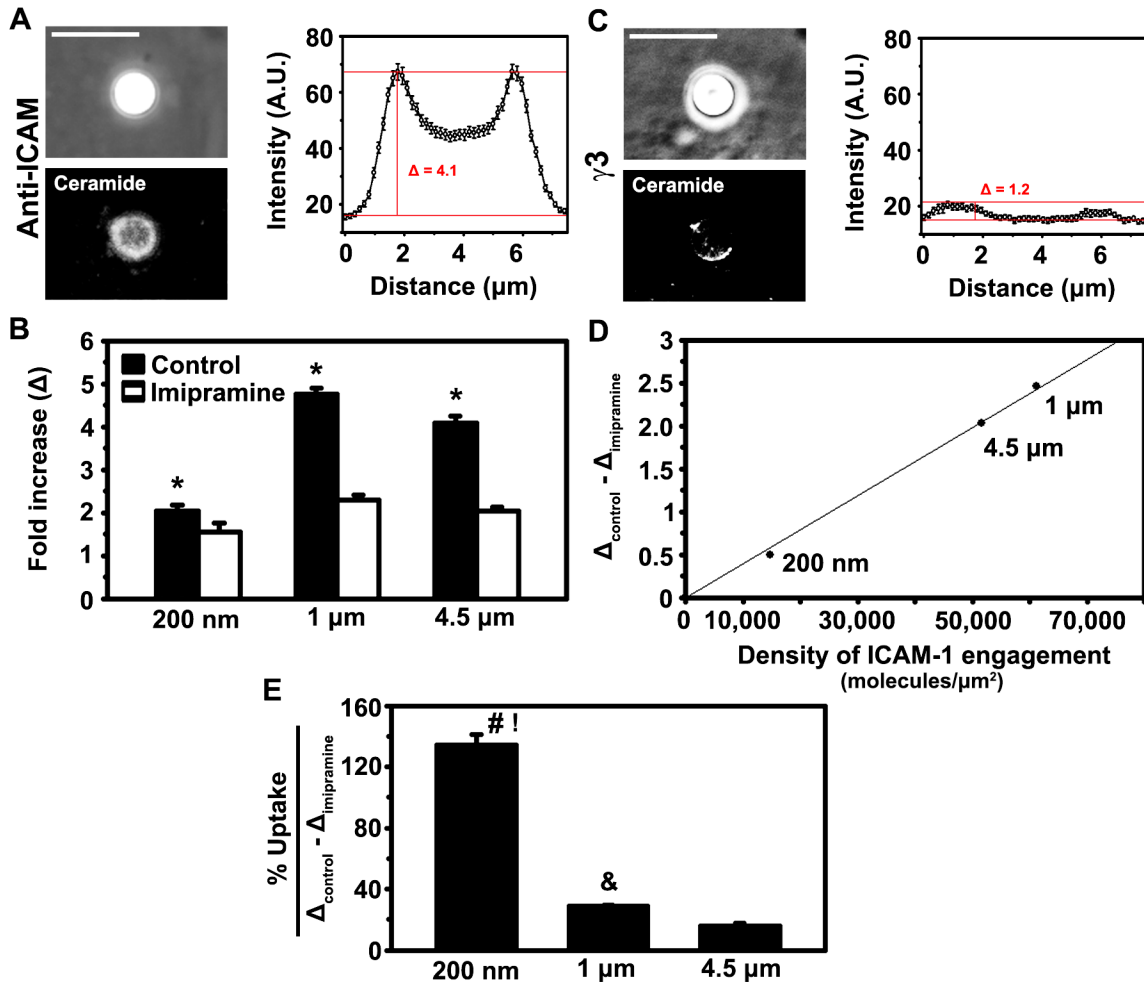


**Figure 8. Ceramide enrichment at sites of binding of ICAM-1-targeted particles to endothelial cells and effect on uptake.** Activated HUVECs were incubated with 200 nm, 1 μm or 4.5 μm anti-ICAM or  $\gamma 3$  particles for 30 minutes at 37°C in the absence (control) or presence of imipramine. After fixing, ceramide was immunostained for fluorescence microscopy. (A) Left: Example of a 4.5 μm anti-ICAM particle (phase-contrast; upper panel) colocalizing with enriched ceramide (fluorescence; bottom panel) at the endothelial plasma membrane. Right: Quantification of ceramide enrichment, where  $\Delta$  indicates fold increase in fluorescence intensity over background levels (adjacent plasmalemma). (B) Ceramide enrichment at sites of 200 nm, 1 μm or 4.5 μm anti-ICAM particle binding in the absence or presence of imipramine. (C) Left: Example of a 4.5 μm  $\gamma 3$  particle (upper panel) colocalizing with enriched ceramide (bottom panel) at the endothelial plasma membrane. Right: Quantification of ceramide enrichment, where  $\Delta$  indicates fold increase in fluorescence intensity over background levels. (D) Plot of fold increase in ceramide intensity normalized to background (imipramine) versus the density of ICAM-1 engagement for each particle size (see Methods, Section 3.8). (E) Percent uptake normalized to ceramide enrichment. Scale bars = 10 μm. Data represent mean  $\pm$  standard error of the mean. \* compares control versus imipramine for each size, # compares 200 nm to 1 μm, ! compares 200 nm to 4.5 μm, and & compares 1 μm to 4.5 μm ( $p < 0.05$  by Student's *t*-test).

As seen in Figure 8B, binding sites for anti-ICAM particles of all sizes were enriched in ceramide ( $\Delta > 1$ ), yet these levels were higher for both micron-sized particle groups compared to nanoparticles. In addition to this, all particle sizes exhibited specific

ceramide production, indicated by decreased enrichment in the presence of imipramine, an inhibitor of acid sphingomyelinase activity. The level of enrichment in the presence of imipramine was still substantial and similar for all sizes, suggesting that this lipid, which is an inherent resident of the plasma membrane, is present to a certain extent at particle binding sites even in the absence of enzymatic activity. Interestingly, the production of ceramide at sites of 200 nm particle binding was much lower (although significantly different from imipramine-treated) compared to micron-sized particles. This suggests that smaller particles have a lower requirement for ceramide production than micron-sized counterparts, because despite lower ceramide enrichment, they exhibited higher initial uptake rates (recall Figure 6).

Since  $\gamma 3$  particles had lower uptake than anti-ICAM particles, we also determined ceramide enrichment upon engagement of the ICAM-1 with  $\gamma 3$ -targeting. The particle sizes used for binding and uptake studies did not elicit detectable levels of ceramide at binding sites (data not shown). Thus, we also used  $\gamma 3$  4.5  $\mu\text{m}$  particles for this purpose. Detection of enrichment is typically more straightforward in this size of particles, and this size presented the highest density of  $\gamma 3$  on its surface (Table 2, page 33), which should elicit the highest ceramide response (refer to Figure 8D results below). Even this particle size failed to produce ceramide enrichment above the background levels seen in the presence of imipramine for anti-ICAM particles (Figure 8C). This lower level of ceramide may be due to lower binding avidity of  $\gamma 3$  particles than anti-ICAM counterparts, which could essentially elicit weaker signaling. However, this effect could also be due to differential epitope binding between the two types of particles (recall that anti-ICAM and  $\gamma 3$  particles bind distinct ICAM-1 epitopes), as binding of different

epitopes on the same molecule can differentially affect allosteric responses [214, 215]. Regardless of the reason behind this lower ceramide production, this fact could explain why  $\gamma 3$  particles exhibited a higher sensitivity to increasing particle size with respect to uptake efficiency compared to anti-ICAM particles. Lower production of ceramide to drive vesiculation and actin rearrangement, even for large particles, would generate this outcome. Nonetheless, it will be necessary to further explore the relationship between ceramide production, vesiculation, and actin rearrangement, as previous data show that despite no detectable levels of ceramide,  $\gamma 3$  particles engage ICAM-1 sufficiently to generate signaling for actin stress fiber formation [216]. Co-coating sphingomyelinases on the surface of  $\gamma 3$  drug carriers could enhance ceramide signaling and, hence, uptake, as in the case of carriers targeted to the M6PR (shown below in Section 4.2.5).

Our working model for CAM-mediated uptake proposes that binding of ICAM-1 triggers exocytosis of acid sphingomyelinase, leading to ceramide production [7]. Since the number of ICAM-1 molecules engaged could affect the degree of sphingomyelinase recruitment, we determined the relationship between ceramide production and potential ICAM-1 binding density for each particle (based on the number of antibodies per  $\mu\text{m}^2$  of particle; see Methods, Section 3.8). As seen in Figure 8D, the fold increase in ceramide enrichment was directly proportional to potential ICAM-1 binding density of each particle at the cell surface. This shows that although drug carriers of larger sizes could require higher ceramide production for uptake as suggested by our uptake data, their size may not inherently signal for this higher ceramide production. Instead, the density at which ligands engage ICAM-1 on the cell surface is likely to control this signaling output. Although not shown, the relationship between ceramide enrichment and density

of potential ICAM-1 engagement for  $\gamma 3$  particles was not linear. Instead, there was equal production of ceramide (close to imipramine levels) regardless of  $\gamma 3$  density on the particle surface. This suggests fundamental differences in the way which anti-ICAM particles engage ICAM-1 compared to  $\gamma 3$  particles, which may affect CAM-mediated signaling.

Due to the linear relationship between engagement density and ceramide enrichment for anti-ICAM particles, we also determined the internalization of each anti-ICAM particle size as a function of ceramide enrichment (Figure 8E). This revealed that nanoparticles exhibited higher percent uptake per unit of ceramide enrichment compared to micron-sized counterparts. Once again, this suggests that uptake through CAM-mediated endocytosis depends on ceramide production in a size-dependent manner.

Overall, for drug delivery purposes, nano-sized particles seem to have lower requirements for ceramide production to achieve earlier uptake, so nano-carriers would be beneficial when the main goal is high and quick intracellular drug delivery. However, an anti-ICAM drug carrier with larger surface area would exhibit more flexibility for controlling the density of ICAM-1 targeting molecules on its surface. This makes microparticles more suitable for manipulating ceramide enrichment and possibly control the efficiency of endocytosis, providing wider modulation of the therapeutic outcome that may not be achievable with nanocarriers.

#### 4.2.5. Role of particle size on the requirement for sphingomyelinase activity during endocytosis.

In order to verify the possible size dependency that connected ceramide production and uptake of anti-ICAM particles (recall Figure 8E), we used a system that allowed us to control the level of sphingomyelinase present. This consisted of 200 nm, 1  $\mu\text{m}$  or 4.5  $\mu\text{m}$  particles coated with antibodies to mannose 6-phosphate receptor (M6PR) along with varying levels of neutral sphingomyelinase (NSM; Table 4).

**Table 4. Particles used for the study of sphingomyelinase requirements in endocytosis.**

Size	Coat	Surface coverage
1 $\mu\text{m}$	Non-specific IgG	100%
1 $\mu\text{m}$	Anti-ICAM:IgG	50:50
1 $\mu\text{m}$	Anti-M6PR	100%
1 $\mu\text{m}$	Anti-M6PR:IgG	80:20
1 $\mu\text{m}$	Anti-M6PR:IgG	50:50
1 $\mu\text{m}$	Anti-M6PR:NSM	80:20
1 $\mu\text{m}$	Anti-M6PR:NSM	50:50

NSM = Neutral sphingomyelinase; Surface coverage = approximate fraction of particle surface that a molecule type occupies.

We selected M6PR because this receptor associates with clathrin-mediated endocytosis, does not associate with ceramide production and is independent of sphingomyelinase for internalization, and anti-M6PR carriers do not associate with CAM-mediated uptake [189]. We used neutral sphingomyelinase as a substitute for acid sphingomyelinase, because unlike engagement of ICAM-1, engagement of M6PR by antibody-coated particles does not recruit NHE1, thought to be necessary for acidification of the microenvironment to permit acid sphingomyelinase activity [7].

Anti-M6PR:NSM particles, at both concentrations of sphingomyelinase used, showed a substantial increase in internalization by cells compared to control anti-M6PR

particles lacking neutral sphingomyelinase (Figure 9A and B), also reflected when we calculated percent uptake (Figure 9C). When compared to CAM-mediated uptake of anti-ICAM particles (dashed line in Figure 9C), this NSM-enhanced uptake was less efficient, but substantial (approximately ~60-65% of putative CAM-mediated uptake).

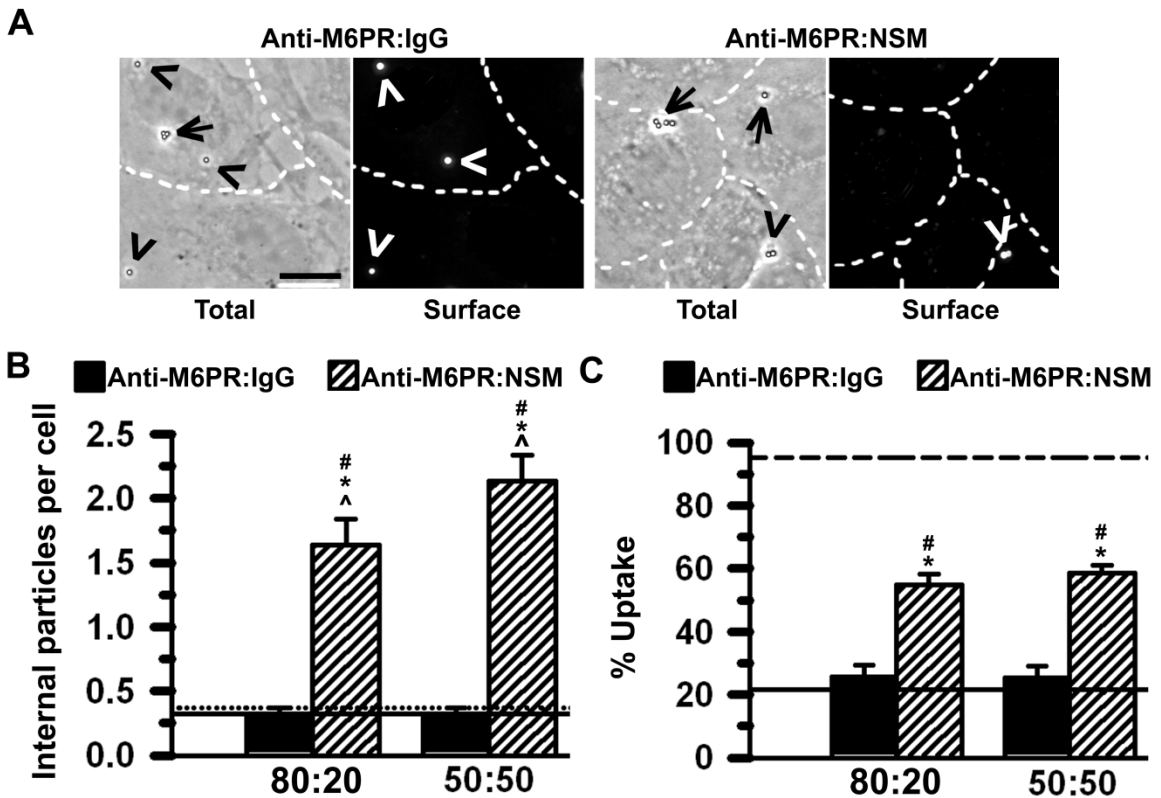


**Figure 9. Uptake of anti-M6PR particles coated with neutral sphingomyelinase.** Activated HUVECs were incubated with 1  $\mu$ m anti-ICAM:IgG, anti-M6PR:IgG or anti-M6PR:NSM (50:50 or 80:20 surface coverage), or anti-M6PR or non-specific IgG (100% surface coverage) particles for 3 hours at 37°C. Surface-bound, but not internalized, particles were immunostained to quantify percent uptake. A) Sample micrographs of anti-M6PR:IgG or anti-M6PR:NSM particles. Phase contrast shows total particles bound and internalized. Fluorescence images show surface-bound, non-internalized particles. Arrowheads indicate non-internalized particles and arrows indicate endocytosed ones. Scale bar = 10  $\mu$ m. (B) Total number of particles internalized per cell. Dotted line represents non-specific IgG particles. (C) Percent of particles internalized out of the total numbers of particles associated to cells (bound plus internalized). Dashed line represents anti-ICAM particles. Data represent mean  $\pm$  standard error of the mean. \* compares to 100% anti-M6PR particles (continuous line in both graphs); ^ compares to non-specific IgG particles; # compares to anti-M6PR:IgG particles ( $p < 0.05$  by Student's *t*-test).

In support of similar mechanisms of uptake, antiM6PR:NSM particles specifically (as opposed to anti-M6PR particles with no NSM) elicited enrichment of ceramide, as

well as rearrangement of actin into stress fibers, seen with anti-ICAM particles that undergo CAM-mediated endocytosis (Figure 10).

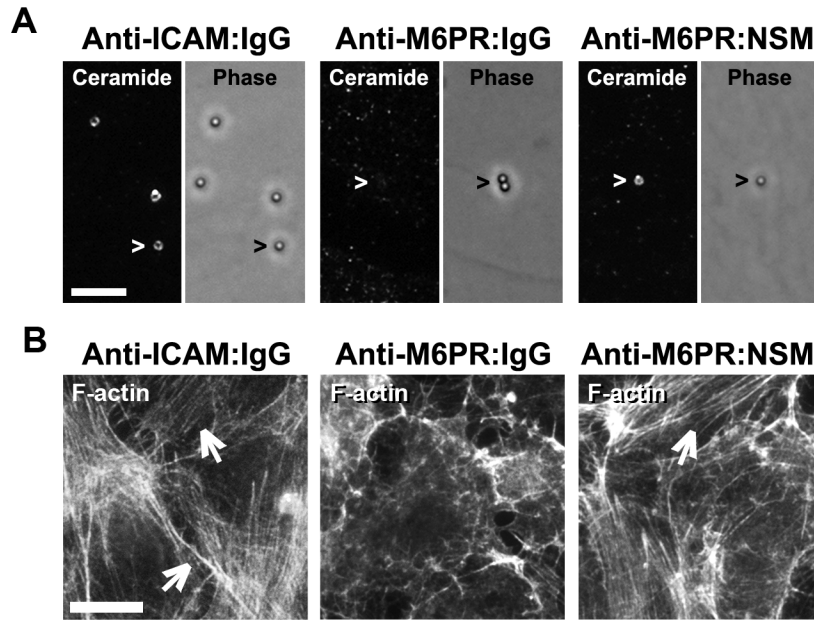


**Figure 10. Role of neutral sphingomyelinase on ceramide enrichment and actin for anti-M6PR particles.** Activated HUVECs were incubated with 1  $\mu\text{m}$  anti-ICAM:IgG, anti-M6PR:IgG or anti-M6PR:NSM particles (all 50:50 surface coverage) for 30 minutes at 37°C (A) Ceramide was immunostained for fluorescence microscopy. Particles (arrowheads) are shown in phase-contrast and ceramide is shown in the fluorescent channel. (B) F-actin was stained with fluorescent phalloidin. Arrows indicate stress fibers. Scale bars = 10  $\mu\text{m}$ .

Due to the size restrictions of clathrin-mediated uptake, internalization efficiency of anti-M6PR particles lacking neutral sphingomyelinase expectedly decreased with increasing particle size (Figure 11A). As predicted from the central role that ceramide has in creating an environment suitable for uptake in CAM-mediated endocytosis, the presence of sphingomyelinase increased the efficiency of anti-M6PR particle internalization for all sizes ( $\Delta > 1$ ; Figure 11B). More importantly, and supporting the notion that ceramide plays a role in the size-dependency of CAM-mediated uptake, the sphingomyelinase-dependent improvement in uptake was larger for micron-sized particles than for nanoparticles. Additionally, increasing sphingomyelinase from 20% to 50% of the particle surface did not change this improvement in the case of 200 nm or 1

$\mu\text{m}$  particles (~1-1.5-fold difference comparing 50% versus 20% sphingomyelinase; Figure 11C), but it did for 4.5  $\mu\text{m}$  particles (by 3-fold). Therefore, for larger particles there was a larger dependence for sphingomyelinase activity, likely to be reflected in the original CAM-mediated pathway, as our uptake and ceramide enrichment data suggested (recall Figures 6 and 8).

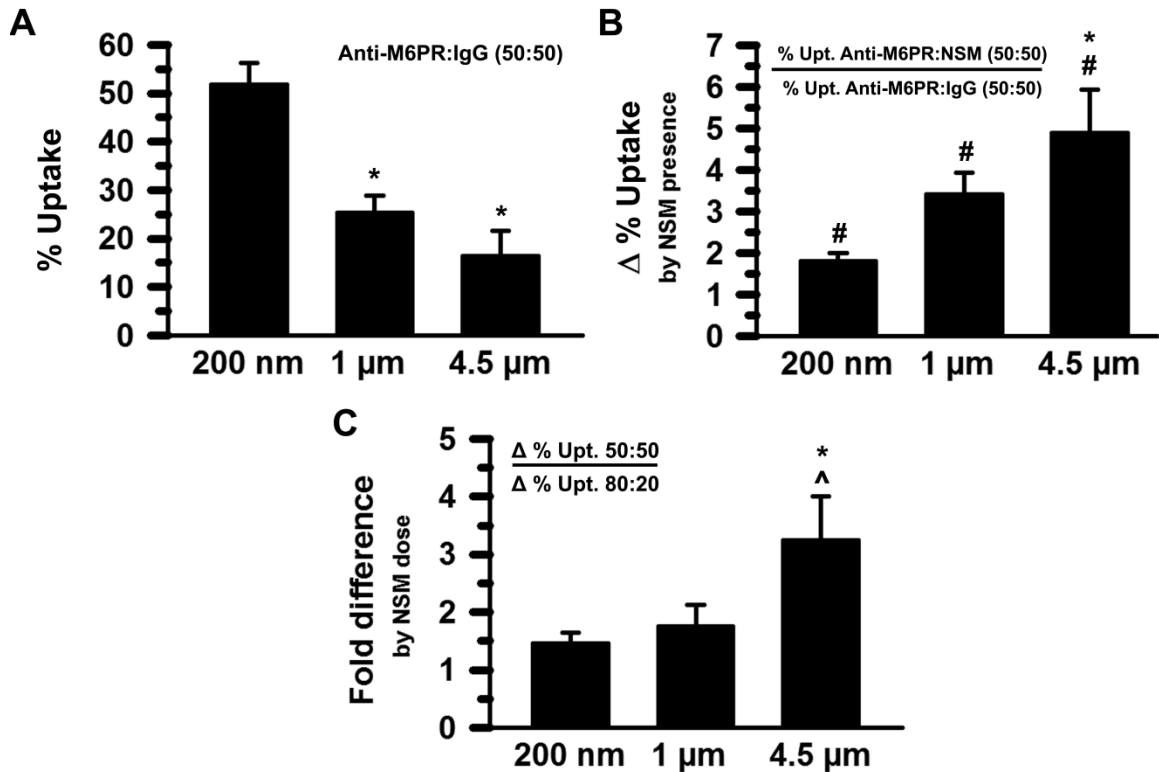


**Figure 11. Role of particle size on neutral sphingomyelinase dependency for uptake.** Activated HUVECs were incubated with 200 nm, 1  $\mu\text{m}$ , or 4.5  $\mu\text{m}$  anti-M6PR:IgG or anti-M6PR:NSM (either 50:50 or 80:20 surface coverage) for 3 hours at 37°C. (A) Percent of anti-M6PR:IgG (50:50) particles internalized out of the total number of particles associated to cells (bound plus internalized). (B) Fold increase ( $\Delta$ ) in the percent uptake of anti-M6PR:NSM particles over control anti-M6PR:IgG particles (both 50:50) for each particle size. (C) Comparative improvement in endocytosis ( $\Delta$  in B) for anti-M6PR:NSM particles bearing 50% NSM particle-surface coverage (50:50) over that of particles bearing 20% coverage (80:20). Data represent mean  $\pm$  standard error of the mean. \* compares microparticles to 200 nm particles; # compares anti-M6PR:NSM particles to anti-M6PR:IgG particles, ^ compares anti-M6PR:NSM/anti-M6PR:IgG of 50:50 surface-coverage to that of 80:20 particles for each given size ( $p < 0.05$  by Student's *t*-test).

Overall, these data support a role for ceramide in the particle size- and targeting moiety-dependent differences observed for CAM-mediated endocytosis. Namely, larger particles require higher (or more prolonged) sphingomyelinase activity (and, thus, ceramide

enrichment) for efficient internalization. Meanwhile, binding of  $\gamma 3$  particles elicits lower enrichment levels of ceramide compared to anti-ICAM particles (which may be a result of differential epitope binding or extent of ICAM-1 binding/engagement), leading to lower uptake levels of  $\gamma 3$  particles. The understanding of this mechanism opens our ability to further modulate CAM-mediated endocytosis of drug carriers. As said, particles of large sizes, or particles coated with  $\gamma 3$  instead of anti-ICAM, can be co-functionalized with sphingomyelinase as a means to aid their uptake efficiency, if desired. Furthermore, a collateral benefit of this study is that evidently uptake of drug carriers targeted to receptors that normally do not internalize micron-sized objects, such as M6PR, can be enhanced with the presence of sphingomyelinase in order to achieve intracellular uptake.

#### 4.2.6. Role of size and targeting moiety on intracellular trafficking of ICAM-1-targeted particles.

Next, in order to determine the role of size and targeting moiety on the intracellular fate of particles internalized by CAM-mediated endocytosis, we first explored their trafficking to lysosomes. To do this, we pre-incubated HUVECs with Texas Red-labeled dextran for 45 minutes, followed by a 45-minute chase. This allows for dextran to be endocytosed and fully transported to lysosomes, which has been confirmed using LAMP-1 staining [9, 193]. After pre-labeling of lysosomes, cells were incubated with 200 nm, 1  $\mu\text{m}$  or 4.5  $\mu\text{m}$  anti-ICAM or  $\gamma 3$  particles for 1 hour to allow binding, and 0, 2 or 4 hours (chase), to allow uptake and trafficking (Figure 12A). Surface-bound particles were immunostained and subtracted during analysis, such that percent colocalization with lysosomes only accounts for internalized particles. Analysis

after microscopy revealed, confirming historical data [77], that 200 nm anti-ICAM particles trafficked to lysosomes reaching a plateau of ~80% colocalization at 3 hours. Meanwhile, 1  $\mu\text{m}$  and 4.5  $\mu\text{m}$  particles reached a plateau of ~30% colocalization, indicative of less efficient trafficking to lysosomes for larger sizes (Figure 12B).

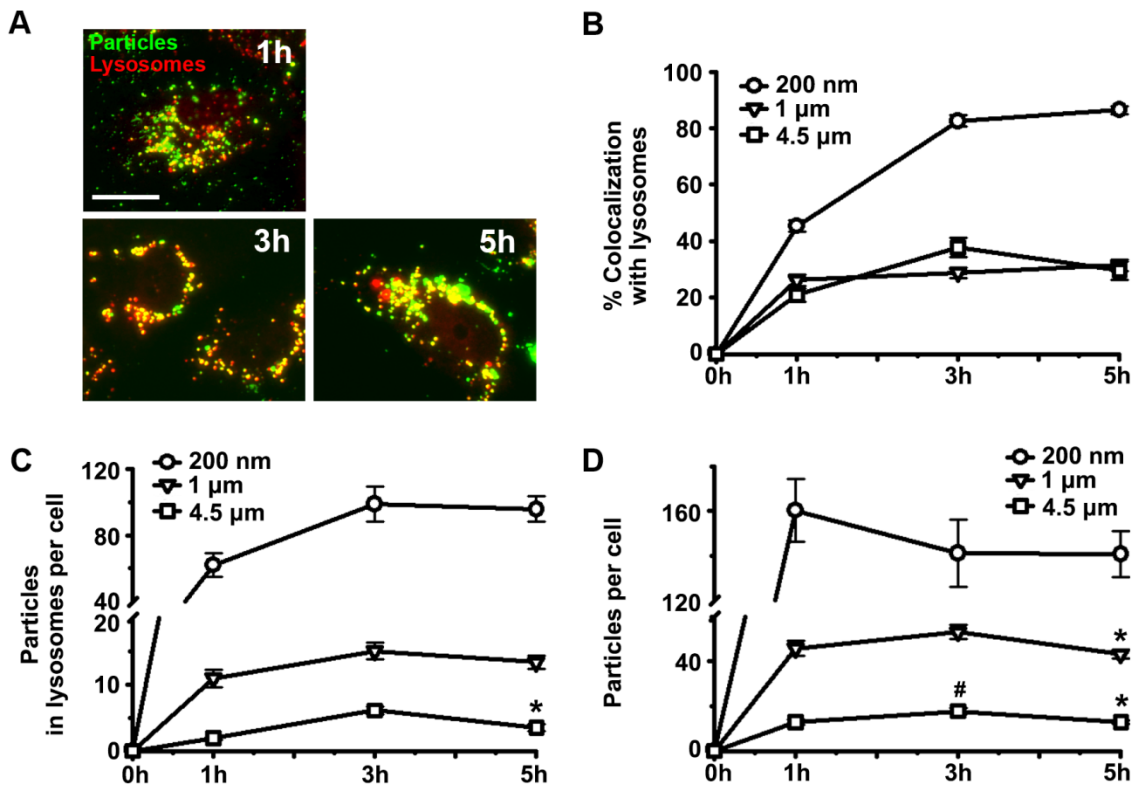


**Figure 12. Lysosome trafficking of anti-ICAM particles.** Activated HUVECs were pre-incubated for 45 minutes with Texas Red-labeled dextran, followed by a 45 minutes chase to label lysosomes. Then, cells were incubated with 200 nm, 1  $\mu\text{m}$ , or 4.5  $\mu\text{m}$  anti-ICAM particles for 1 hour, followed by washing and a chase of 0, 2 or 4 hours at 37°C. (A) Sample micrographs for each time-point for 200 nm green particles, which appear as yellow when colocalizing with red lysosomes. Scale bar = 20  $\mu\text{m}$ . (B) Quantification of the percent of internalized particles that colocalize with lysosomes per cell. (C) Quantification of the absolute number of particles that colocalize with lysosomes per cell. (D) Quantification of the absolute number of particles per cell. Data represent mean  $\pm$  standard error of the mean. \* compares 3 hours to 5 h; # compares 1 hour to 3 hours ( $p < 0.05$  by Student's *t*-test).

Curiously, the colocalization of 4.5  $\mu\text{m}$  particles decreased (although not significantly) between 3 and 5 hours (Figure 12B). This led us to examine the absolute values of lysosome-colocalized particles. Figure 12C shows that for 200 nm particles,

there was no change in the number of particles in lysosomes between 3 and 5 hours, similar to its percent values. Surprisingly, for both 1  $\mu\text{m}$  and 4.5  $\mu\text{m}$  particles, there was a decrease in the number of particles in lysosomes between these two time-points (only statistically significant for 4.5  $\mu\text{m}$  particles). Thus, it appeared that while lysosomes were the terminal compartment for nanometric particles, micron-sized objects not only traffic poorly here, but might divert from these compartments. This finding agrees with recent models that identify the lysosome as a dynamic organelle that does not necessarily serve as a terminal trafficking destination [217], and it points at a regulatory role for object size with respect to the dynamics of these trafficking events.

Since this suggested that post-endocytic trafficking, particularly for large particles, may not be terminal, we also determined the total number of particles associated with cells over time. As shown in Figure 12D, between 3 and 5 hours, there was no change in 200 nm cell-associated particles, as would be expected from a pulse/chase treatment. Meanwhile, both micron-sized particles showed a decrease in cell-associated particles between these time-points. Although these changes were small, they were significant and suggested a release of micron-sized particles from cells, which would coincide with a tendency of these particles to escape lysosomes or avoid lysosome trafficking altogether. Thus, overall, these data pointed at a role in particle size with respect to intracellular trafficking, suggesting that after CAM-mediated endocytosis and trafficking, large particles may be secreted from lysosomes and also from cells.

We also compared anti-ICAM and  $\gamma 3$  particle trafficking. We focused on 200 nm particles only in order to minimize issues with the slower binding and uptake, especially for larger particles, that could confound kinetics of lysosome colocalization (refer to our

binding and uptake data in Figures 3-7). As seen in Figure 13A,  $\gamma 3$  particles exhibited consistently lower levels of percent colocalization with lysosomes compared to anti-ICAM particles. Unlike micron-sized anti-ICAM particles which showed a similar behavior (recall Figure 12), however,  $\gamma 3$  particles did not appear to exit lysosomes or cells (Figure 13B and C).

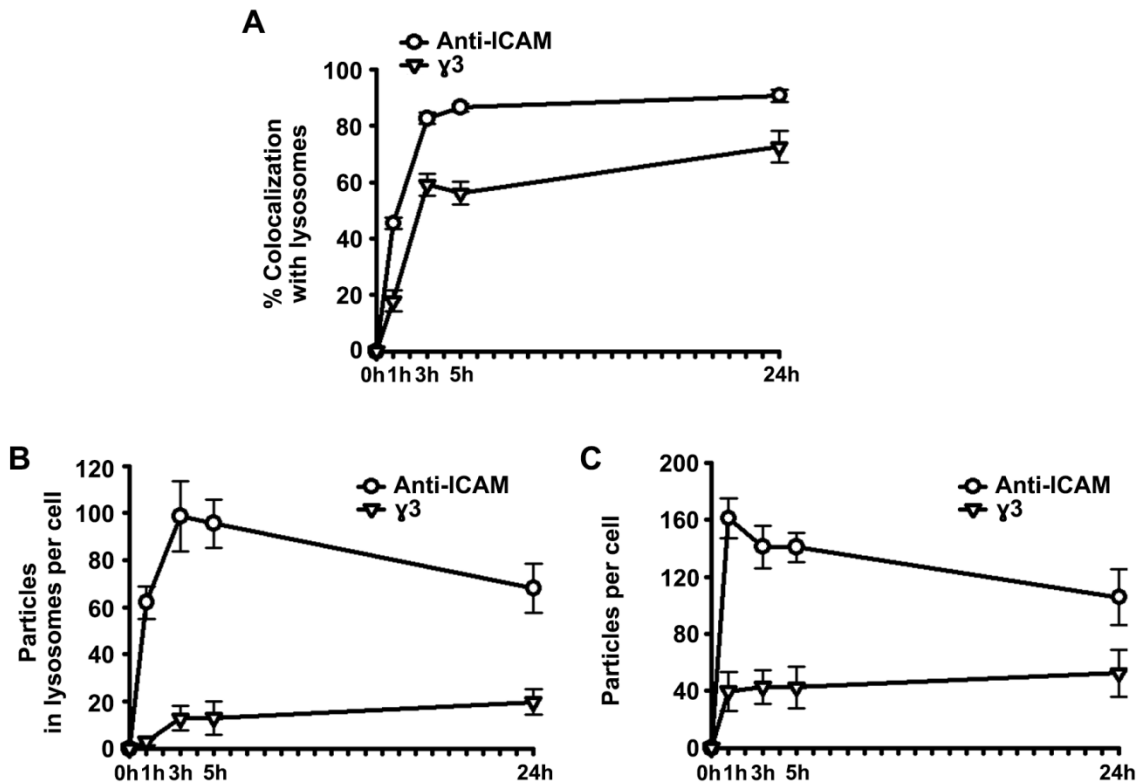


**Figure 13. Lysosome trafficking of anti-ICAM versus  $\gamma 3$  particles.** Activated HUVECs were pre-incubated for 45 minutes with Texas Red-labeled dextran, followed by a 45 minutes chase to label lysosomes. Then, cells were incubated with 200 nm anti-ICAM or  $\gamma 3$  particles for 1 hour, followed by washing and incubation (chase) for 0, 2, 4, or 23 hours at 37°C. (A) Quantification of the percent of internalized particles that colocalize with lysosomes per cell. (B) Quantification of the absolute number of particles that colocalize with lysosomes per cell. (C) Quantification of the absolute number of particles per cell. Data represent mean  $\pm$  standard error of the mean.

Since  $\gamma 3$  particles in general showed slower internalization kinetics compared to anti-ICAM particles, we extended the lysosome colocalization to 24 hours (where uptake was near 100% for both types). Even after this long period of time,  $\gamma 3$  particles still

exhibited lower percent colocalization than anti-ICAM counterparts ( $90.7 \pm 2.2\%$  and  $72.4 \pm 5.6\%$  for anti-ICAM and  $\gamma 3$  particles, respectively). This suggested that binding to ICAM-1 through the  $\gamma 3$ -associated epitope, or lower binding strengths, led to lower trafficking to lysosomes.

Since anti-ICAM nanocarriers exhibit high levels of lysosome trafficking, a major focus of CAM-mediated uptake strategies has been the delivery of drug carriers for treatment of lysosomal storage disorders. However, the discovery that changing anti-ICAM particle size can impede or delay lysosome trafficking has been explored to permit delivery of drugs to other intracellular compartments. The data presented here corroborate these ideas regarding size, and add a novel component in the use of  $\gamma 3$  to achieve lower rates of trafficking to lysosomes. This targeting moiety concept, which was already explored in PECAM-1-binding drug carriers, holds potential for the expansion of drug delivery techniques through CAM-mediated endocytosis.

#### 4.2.7. Size and targeting moiety of ICAM-1-targeted particles affect transport across endothelial cells.

Finally, with data suggesting differential intracellular trafficking after CAM-mediated endocytosis depending on size and targeting moiety, we examined particle transport across endothelial cells. We used human brain microvascular endothelial cell (HBMEC) monolayers plated on porous membranes, as the brain endothelium is an important target for transport of drug carriers, and we have previously shown similar patterns of binding and CAM-mediated uptake in HUVECs versus HBMECs [195]. Particles of 200 nm, 500 nm or 1  $\mu\text{m}$  diameter coated with  $^{125}\text{I}$ -anti-ICAM or  $\gamma 3$

(containing a small fraction of  $^{125}\text{I}$ -IgG, that does not affect binding, for tracing purposes; see Methods, Section 3.4) were added to HBMECs for 30 minutes to allow binding, followed by washing of both apical and basal fractions, and further incubation for 4.5 hours to allow for transport. After the assay, the basal and cell fractions were collected for quantification using a gamma counter. These readings consist of both intact proteins labeled with  $^{125}\text{I}$ , or free (non-protein-associated) iodine resulting from protein degradation. Thus, the free iodine content from each collected fraction was also determined and it was subtracted from the original readings to obtain numbers that only account for intact particles that associate with cells or cross from the apical to the basal chamber without being degraded. It is assumed that all intact radiolabeled proteins are retained on the particle surface, as historical data show [195] (see Methods, Section 3.4).

Similar to our microscopy studies, ICAM-1-targeted particle association with HBMECs grown on porous membranes was specific as compared to control non-specific IgG or  $\gamma$ 3S particles (Figure 14A, ICAM-1-targeted/Non-specific > 1, dashed line, in all cases). Free iodine for both targeted and non-specific formulations were similar and close to the background levels found in original particle formulations (~10%), which suggests that the readings obtained in the cell fraction are mostly representative of cell-bound particles (Figure 14B). Similar to our previous data, particle association with cells (after correcting for free iodine to only account for intact particles) was dependent on particle size and targeting moiety, with lower binding levels for anti-ICAM micron-sized particles and  $\gamma$ 3 nanoparticles, compared to anti-ICAM nanoparticles (Figure 14C).

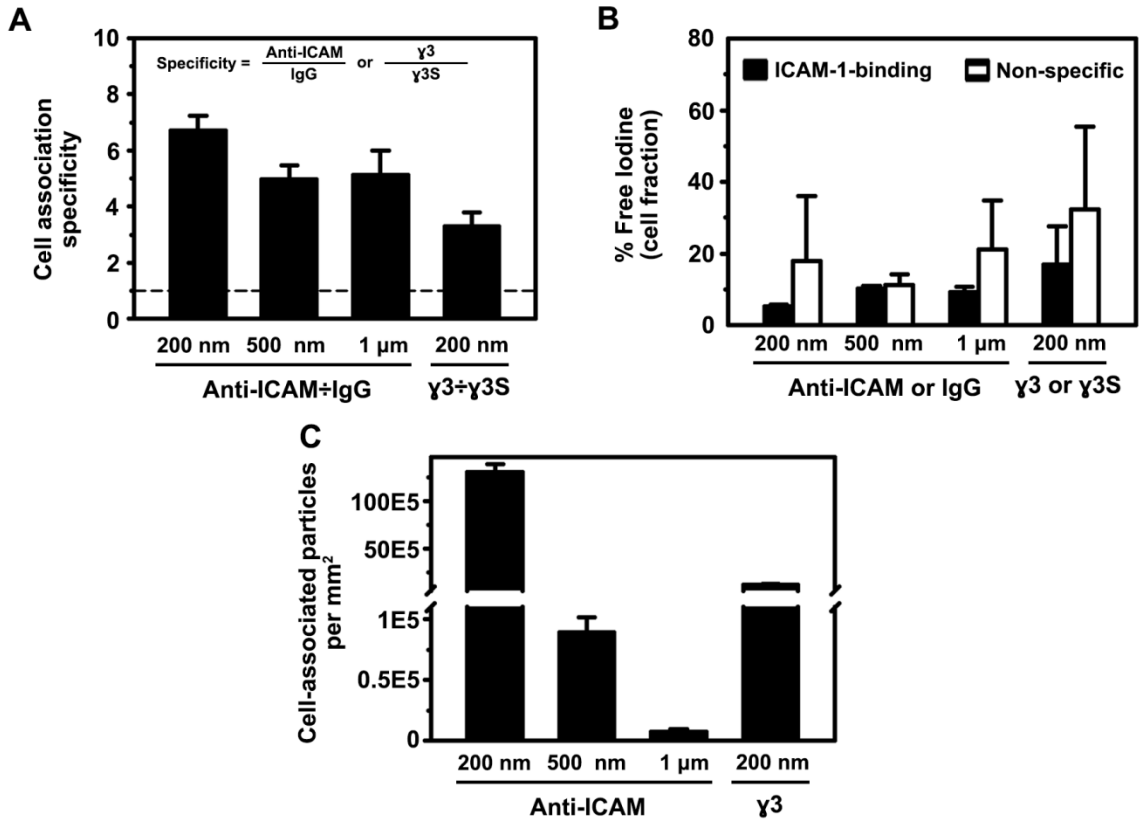


**Figure 14. Association of ICAM-1-targeted particles to endothelial cells on porous membranes.** Activated HBMECs grown on 3- $\mu$ m pore-size porous membranes were incubated in the presence of anti-ICAM, IgG,  $\gamma 3$ , or  $\gamma 3S$  200 nm, 500 nm, or 1  $\mu$ m particles (coated with radiolabeled proteins for tracing) for 30 minutes, followed by washing of both chambers and incubation (chase) for 4.5 hours at 37°C. Cell fraction and basal fraction were quantified with a gamma counter. (A) Quantification of cell-association specificity (cell fraction of anti-ICAM or  $\gamma 3$  particles divided by cell fraction of IgG or  $\gamma 3S$  particles). Dashed line = 1. (B) Quantification of the cell fraction free (non-protein-associated) iodine in each formulation. (C) Quantification of total cell-associated particles per mm<sup>2</sup> of cell surface after subtracting free iodine. Data represent mean  $\pm$  standard error of the mean.

Transport of ICAM-1-targeted particles was also specific compared to IgG and  $\gamma 3S$  (Figure 15A). Meanwhile, free iodine levels were above particle formulation backgrounds, indicating protein degradation (Figure 15B). However, the free iodine levels of ICAM-1-targeted particles were higher than those of non-specific counterparts. This shows that specific interaction with ICAM-1 elicits degradation of particle protein coats, and based on our microscopy data, this is likely due to intracellular trafficking of these particles, and particularly due to degradation in lysosomes.

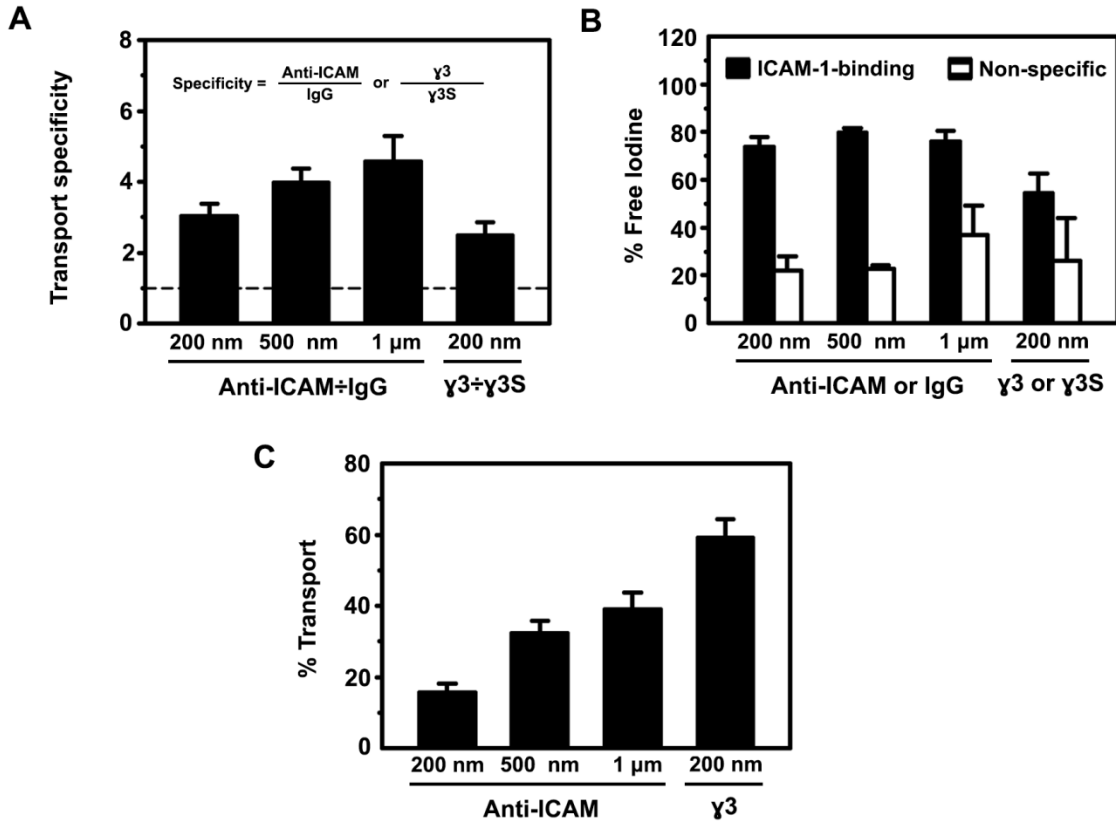


**Figure 15. Transport of ICAM-1-targeted particles across endothelial cells.** Activated HBMECs grown on 3- $\mu\text{m}$  pore-size porous membranes were incubated in the presence of anti-ICAM, IgG,  $\gamma3$ , or  $\gamma3S$  200 nm, 500 nm, or 1  $\mu\text{m}$  particles (coated with radiolabeled proteins for tracing) for 30 minutes, followed by washing of both chambers and incubation (chase) for 4.5 hours at 37°C. Cell fraction and basal fraction were quantified with a gamma counter. (A) Quantification of transport specificity (basal fraction of anti-ICAM or  $\gamma3$  particles divided by basal fraction of IgG or  $\gamma3S$  particles). Dashed line = 1. (B) Quantification of the basal free (non-protein-associated) iodine in each formulation. (C) Quantification of percent transport, calculated as (basal fraction)/(cell plus basal fraction)  $\times$  100. Data represent mean  $\pm$  standard error of the mean.

Finally, as shown in Figure 15C, the transport efficiency of ICAM-1-targeted particles was dependent on particle size and targeting moiety. For anti-ICAM particles, transport efficiency increased with increasing size. For the same size of particles (200 nm),  $\gamma3$  particles showed higher percent transport compared to anti-ICAM particles. These effects correlate with our lysosome colocalization data (recall Figures 12 and 13), supporting higher avoidance of terminal lysosome trafficking (as seen by microscopy), accompanied by higher rates of transcytosis with increasing object size after CAM-

mediated uptake. A similar conclusion can be made for particles binding via  $\gamma 3$  versus those binding via anti-ICAM.

Thus, these data show that CAM-mediated transport across barriers can be modulated by changing particle size and targeting moiety. Larger drug microcarriers versus nanometric counterparts may benefit the delivery of therapeutics into tissue as opposed to the vascular lining.  $\gamma 3$  carriers, as opposed to anti-ICAM carriers also hold to this notion.

#### 4.3. Conclusions

Using knowledge about the natural binding partners of ICAM-1, we selected two parameters to determine their effect on the outcomes of CAM-mediated endocytosis: particle size and ICAM-1-targeting moiety (which may affect binding epitope, avidity, etc.). Here, we present evidence showing that these parameters of ICAM-1-targeted particles affects the binding, uptake, ceramide enrichment and trafficking outcomes of CAM-mediated endocytosis, potentially guiding the future design of drug delivery carriers. As will be addressed later, these results may also shed light on the regulation of the physiological functions of the CAM-mediated pathway.

In summary, we have found that large ICAM-1-binding particles bind at faster initial rates than small counterparts, but in activated cells expressing high levels of ICAM-1, binding is saturated to similar values of cell surface occupancy over time. Furthermore, the role of ceramide production during CAM-mediated endocytosis makes this pathway sensitive to large objects, which require higher levels of sphingomyelinase activity for efficient uptake. In turn, ceramide enrichment appears to depend on the density of ICAM-1 engagement per individual particle. Despite a possible initial barrier

for uptake due to this ceramide dependence, objects even the size of a cell can be internalized by the endothelium through the CAM-mediated pathway. This may relate to the role of ICAM-1 on lymphocyte interaction and transmigration. Finally, after internalization, the size of particles affects their rate of trafficking to lysosomes, with larger particles avoiding lysosomal compartments, and possibly escaping these compartments and exiting the cell. This may be reflected in the higher rates of transendothelial transport observed for micron-sized particles versus nanometer-sized ones. Meanwhile, binding to ICAM-1 by  $\gamma 3$  particles, as opposed to anti-ICAM ones, leads to slower binding, lower ceramide production, lower internalization, and also lower trafficking to lysosomes, with higher transport across cells.

Thus, these data support the use of small high-affinity ICAM-1-targeted drug carriers for fast and efficient terminal delivery into cells (specifically lysosomes), while large carriers for transport across barriers. In addition, the inclusion of exogenous sphingomyelinase may increase internalization efficiencies, even for receptors other than ICAM-1.

# **Chapter 5: Contribution of Regulatory Elements of the CAM-Mediated Pathway to Lymphocyte Transmigration across Endothelial Cells**

## 5.1. Background

Crossing of endothelial cells by leukocytes (transmigration) is a process that requires an active role by both cell types involved. That is, despite the leukocyte being motile, it cannot by itself penetrate the endothelial layer. Instead, the endothelium must grant regulated access, which involves signaling and structural changes in both the membrane and the cytoskeleton of endothelial cells [109, 111]. For instance, when endothelial PECAM-1 is blocked by antibodies, leukocytes migrate laterally on the endothelial surface, but cannot transverse the endothelial cell layer [218]. More strikingly, when endothelial cells express an ICAM-1 mutant that lacks its cytosolic tail, leukocytes adhere to the endothelium but remain immobile and cannot migrate laterally or transversally [59], which also occurs if cells do not express ICAM-1 at all [219]. Leukocyte interaction with this ICAM-1 mutant, which is deficient in its ability to induce endothelial cytoskeleton rearrangement [220], also exhibits a deficiency in the ICAM-1- and actin-rich endothelial membrane docking structures that help drive transmigration [59]. This shows that endothelial membrane protrusions, ICAM-1-enriched microdomains, and cytoskeletal rearrangement are necessary for both lateral and transversal movement of the leukocyte.

Transmigration can occur through two pathways: the paracellular or the transcellular route [111]. Paracellular transmigration involves opening of endothelial junctions and crossing of the endothelium in between cells, while transcellular transmigration involves crossing of the endothelium across the body of a single endothelial cell [111]. Although endothelial signaling, cytoskeletal rearrangement, and ICAM-1-rich membrane protrusions are needed for both modes of transmigration, it is possible that ICAM-1 serves as a regulator between these two routes. For instance, the vesicles that form and fuse into the transcellular pore through which leukocytes cross the endothelium are enriched in ICAM-1 [121], and ICAM-1 undergoes transcytosis across the endothelial cell as leukocytes migrate through this transcellular pore [121]. Furthermore, transcellular migration increases upon overexpression of ICAM-1, and deletion of its cytoplasmic domain reduces specifically the transcellular route [127]. This evidence suggests that ICAM-1-dependent vesicular dynamics and cytoskeletal changes are key contributors specifically to transcellular migration.

Interestingly, the endothelial structures and signaling observed during leukocyte transmigration are also present upon ICAM-1-specific engagement by micron-sized inert beads coated with antibodies to ICAM-1. This includes the formation of docking-like structures [7, 124], Rho-dependent signaling [126], recruitment of tetraspanin domains [221], and development of transcellular pore-like invaginations [113]. In addition, these inert particles that specifically engage ICAM-1 elicit the pathway known as CAM-mediated endocytosis, which involves the  $\text{Na}^+/\text{H}^+$  exchanger activity of NHE1 and ceramide generation by acid sphingomyelinase [6, 7]. The signaling pathways necessary for CAM-mediated uptake are similar to those activated during leukocyte transmigration,

including the involvement of Rho, Rho-associated kinase, and Src kinase [6].

Downstream of these molecules actin rearranges into stress fibers (also seen during transmigration) and vesicles form, which allows endothelial cells to internalize objects as large as 10  $\mu\text{m}$  in diameter (within the dimensions of a leukocyte) [7, 77].

Due to this evidence, it is possible that interaction of leukocyte integrin  $\alpha_L\beta_2$  with endothelial ICAM-1 may elicit CAM-mediated endocytosis, which could contribute to transmigration, particularly through the transcellular route. The CAM-mediated pathway could provide signaling and membrane dynamics that result in formation of docking structures, and/or the vesicular events that result in formation of transcellular pores. Thus, in this chapter we explore the possible involvement of CAM-mediated endocytosis in leukocyte crossing of the endothelium, and regulation of the transmigration route.

## 5.2. Results

### 5.2.1. Contribution of CAM-mediated endocytosis to pre-transmigration interactions between lymphocytes and endothelial cells.

For our studies, the leukocytes used were lymphocytes collected from human blood by density-gradient centrifugation and activated with IL-2, and the endothelial cells were TNF- $\alpha$ -activated HUVECs. This is a widely used *in vitro* model of transmigration [192]. Previously, we have shown that during CAM-mediated endocytosis, endothelial cells form membrane protrusions around anti-ICAM particles that resemble the endothelial docking structures seen on leukocytes during transmigration [7]. The structures formed during CAM-mediated endocytosis are enriched in ICAM-1,

tetraspanin CD9, NHE1, acid sphingomyelinase, and ceramide [7, 113], which are key molecular players of CAM-mediated uptake. Although ICAM-1 and tetraspanin CD9 have been shown to be enriched at sites of leukocyte transmigration [221, 222], it is not known if NHE-1, acid sphingomyelinase, or ceramide are associated with transmigration events. Thus, we first tested whether these molecules are present at sites of interaction between lymphocytes and HUVECs. As shown in Figure 16, immunostaining of ICAM-1 (as a positive control), NHE-1, acid sphingomyelinase, and ceramide revealed the enrichment of these molecules at sites of lymphocyte interaction with endothelial cells after a 30-minute incubation. In some cases the enrichment was polarized to sites where the lymphocyte appeared to enter the endothelial cell, as estimated by phase-contrast (shown by arrows in Figure 16). Although this technique does not allow to distinguish if the enriched molecules were endothelial or on the lymphocyte, these results support the involvement of CAM-mediated pathway molecular elements in the process of leukocyte transmigration.

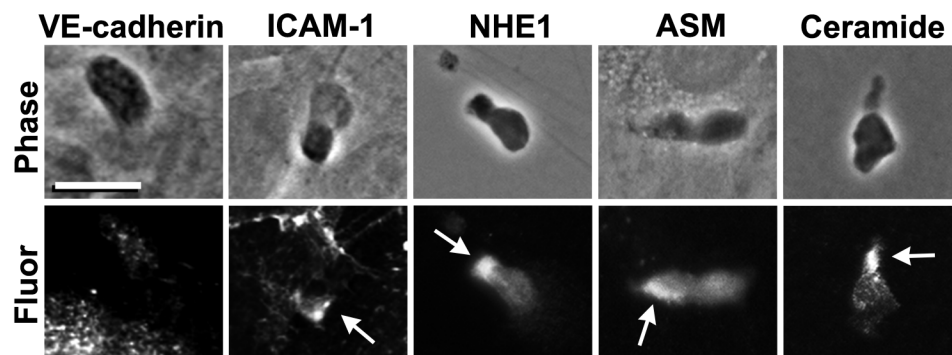


**Figure 16. Enrichment of plasma membrane molecules at sites of interaction between lymphocytes and endothelial cells.** Activated peripheral-blood lymphocytes were incubated with activated HUVECs grown on coverslips for 30 minutes at 37°C, followed by immunostaining (bottom panels) of VE-cadherin, ICAM-1, NHE1, acid sphingomyelinase (ASM), or ceramide. Top panels illustrate phase-contrast. Arrows indicate polarized enrichment. Scale bar = 10  $\mu$ m.

As illustrated by Figure 16 (phase-contrast panels), when lymphocytes interact with endothelial cells they can adopt irregular morphologies. Previous studies have

shown that leukocytes must change their rounded shape into these spread (also known as ‘polarized’) morphologies in order to perform sampling on the endothelial surface, which is required for transmigration [59, 223, 224]. It is also known that the endothelium plays an active role in this morphological change. For example, endothelium-specific inhibition of the signaling that regulates endothelial docking structures and invaginations results in rounded leukocytes that simply adhere to the endothelial cell and do not spread [59]. Thus, if CAM-mediated endocytosis were involved in the generation of pre-transmigratory cell membrane invaginations and docking structures, it could affect leukocyte sampling of the endothelium.

With this in mind, we first examined the interactions between lymphocytes and endothelial cells during the stage of sampling. Lymphocytes and HUVECs were incubated for 30 minutes, followed by thorough washing of non-bound lymphocytes. Scanning electron microscopy revealed that lymphocytes exhibiting flattened, irregular morphologies are associated with the podosomes and interdigitating endothelial membrane structures known to result in transmigration (Figure 17A, black arrowheads). Meanwhile, lymphocytes with a round morphology are simply (yet firmly) adhered to the endothelial cell (Figure 17A, white arrowhead). With this confirmation of historical data [59], we used a scoring system in which fluorescently labeled lymphocytes that exhibited a round morphology were scored as ‘adhered’, while spread lymphocytes (which may be sampling or already undergoing transmigration) were scored as ‘sampling’ to indicate a potential transmigratory event (Figure 17B). As shown in Figure 17C,  $69.3 \pm 2.3\%$  of lymphocytes were sampling the surface of HUVECs in this model, while  $30.7 \pm 2.3\%$  were simply adhered.

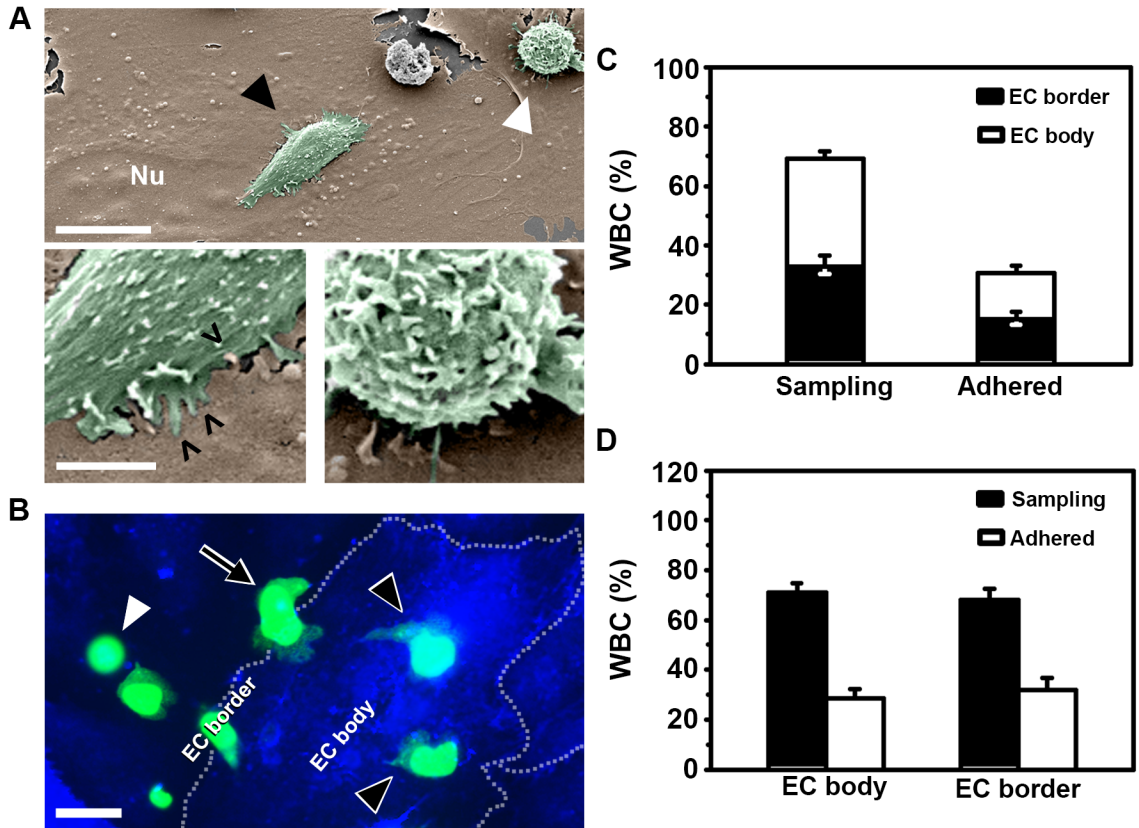


**Figure 17. Model to examine pre-transmigratory interactions between lymphocytes and endothelial cells.** Interaction of activated peripheral-blood lymphocytes (WBCs) with activated HUVECs grown on coverslips after incubation for 30 minutes at 37°C. (A) Scanning electron microscopy of WBCs interacting with HUVECs. Black closed arrowhead indicates a ‘sampling’ WBC. White arrowhead indicates a simply ‘adhered’ WBC. Open arrowheads show WBC podosomes and related sampling structures at the interface with HUVECs. Scale bars = 10 μm (top) and 2.5 μm (bottom). Nu = Nucleus. (B-D) Activated WBCs pre-stained with green fluorescent calcein AM and observed by fluorescence microscopy on activated HUVECs stained for ICAM-1 (blue). (B) The image shows an example of spread WBCs scored as ‘sampling’ (black arrowheads for endothelial cell (EC) body and black arrow for EC border), compared to rounded WBCs scored as simply ‘adhered’ (white arrowhead). Cell borders are indicated by dashed lines. Scale bar = 10 μm. (C) Percent of sampling WBCs on HUVECs with corresponding spatial distribution depending on the location of each sampling event (black for HUVEC border and white for HUVEC body). (D) Percent of ‘sampling’ WBCs (black bars) versus ‘adhered’ WBCs (white bars) out of only the population located on the HUVEC body (left) or the HUVEC border (right). Data represent mean ± standard error of the mean. In C, error bars correspond (from top to bottom) to Total sampling, Border sampling, and Body sampling, respectively.

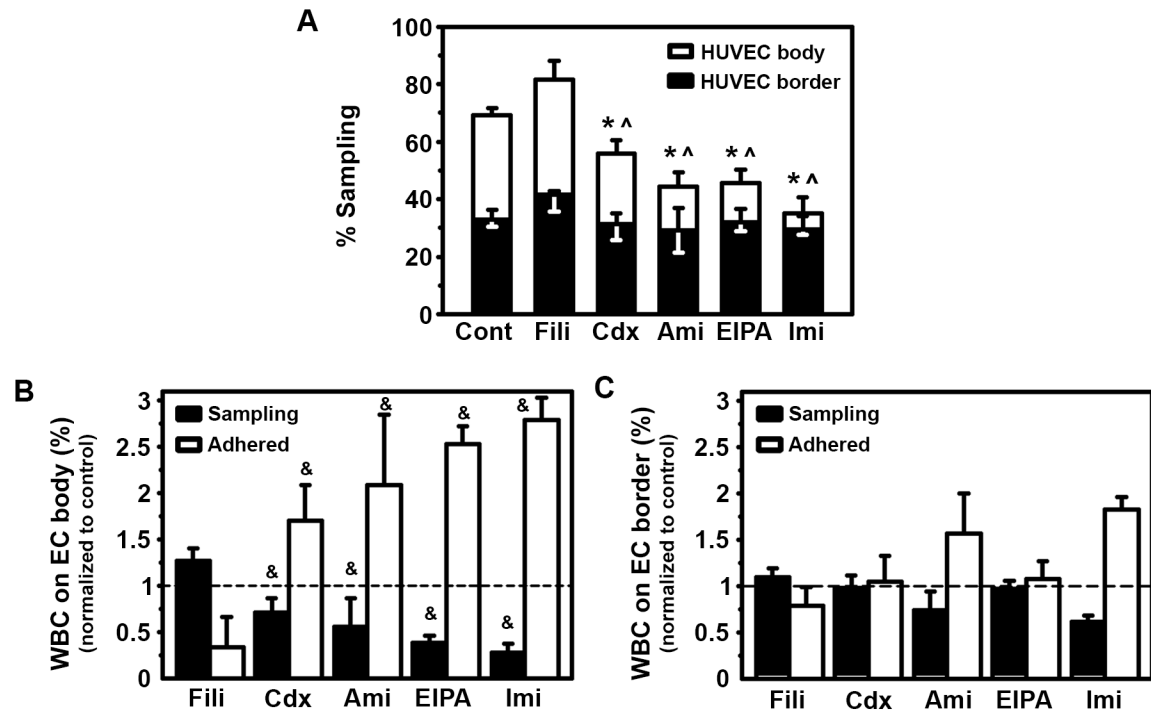
In order to also examine the potential route of transmigration that may follow these sampling interactions, we determined the lymphocyte spatial distribution on the endothelial cell surface, thereby scoring ‘sampling’ or ‘adhered’ lymphocytes as being directly on the ‘border’ of HUVECs or  $\geq 1 \mu\text{m}$  away from borders (referred to as ‘body’;

Figure 17B). This estimation of transcellular versus paracellular events has been used previously and is considered acceptable with the understanding that it might underestimate transcellular events because a fraction of transcellular transmigration occurs within 1  $\mu\text{m}$  of the closest endothelial border without disrupting cell-cell junctions [130].

This analysis revealed sampling events were equally distributed between the body and the border ( $53.4\pm 4.0\%$  on the body and  $46.6\pm 4.0\%$ , respectively; compare white and black regions in Figure 17D). Also, from within the population of lymphocytes only found on the HUVEC body,  $71.2\pm 3.5\%$  were involved in sampling interactions, and a similar percentage was observed for the population of lymphocytes only found on the HUVEC border ( $68.0\pm 4.7\%$ ; Figure 17D). Thus, these data suggested that under control conditions, the initiation of lymphocyte sampling did not exhibit a preference for the body or the border of HUVECs. Although sampling leukocytes do not necessarily represent those that fully migrate across endothelial cells, our percent sampling rates are in agreement with published percentages of leukocyte transmigration [127, 225, 226]. Thus, it is possible that most of these sampling interactions between lymphocytes and HUVECs may result in successful transmigration, half of which occurs at endothelial body locations where transcellular migration can occur.

With this model in place, we then tested the role of several molecular players of the CAM-mediated pathway on pre-transmigratory events using chemical inhibition. In addition, we tested the involvement of caveolae-related pathways as some studies suggest that caveolae are responsible for the vesicular events that occur during transcellular transmigration [138], yet this contribution is controversial [130]. As seen in Figure 18A,

methyl- $\beta$ -cyclodextrin (Cdx), a cholesterol-chelating agent that disrupts lipid raft domains, known to affect both CAM-mediated uptake and caveolae-mediated endocytosis, inhibited sampling by  $19.5 \pm 6.8\%$ . However, filipin, which affects caveolae-mediated endocytosis but not the CAM-mediated pathway [6], had no effect on sampling ( $17.5 \pm 9.7\%$  increase, non-significant). This suggested that the integrity of lipid domains in CAM-mediated endocytosis is important for the pre-transmigratory interaction between leukocytes and endothelial cells, but caveolae may have a less significant role.



**Figure 18. Effect of inhibitors on both lymphocytes and endothelial cells during pre-transmigratory interactions.** Activated HUVECs grown on cover slips were pre-incubated 30 minutes at 37°C in control medium or medium containing filipin (Fili), methyl- $\beta$ -cyclodextrin (Cdx), amiloride (Ami), EIPA, or imipramine (Imi), followed by incubation for 30 minutes with activated peripheral-blood lymphocytes (WBCs, pre-stained with green fluorescent calcein AM) in the presence of inhibitors. WBCs not firmly bound to HUVECs were washed followed by fixation, immunostaining of ICAM-1, and analysis by fluorescence microscopy. (A) Percent of sampling WBCs on HUVECs with corresponding spatial distribution (black for HUVEC border and white for HUVEC body). (B) Percent of sampling WBCs (black bars) versus simply ‘adhered’ WBCs (white bars) out of only the population located on the HUVEC body. (C) Percent of sampling WBCs (black bars) versus simply ‘adhered’ WBCs (white bars) out of only the population located on the HUVEC border. In B and C, data are normalized to control values (horizontal dashed line). Data represent mean  $\pm$  standard error of the mean. In A, error bars correspond (from top to bottom) to Total sampling, Border sampling, and Body sampling, respectively. \* compares total percent sampling to control; ^ compares percent body sampling to control, & compares each column to control ( $p < 0.05$  by Student’s *t*-test).

In support of this, inhibition with amiloride, which disrupts  $\text{Na}^+/\text{H}^+$  exchange among other cellular processes [227] associated with CAM-mediated uptake [6], led to  $36.2 \pm 7.3\%$  inhibition of sampling. Since amiloride can affect other endocytic pathways and cellular functions, we also used its analog 5-(N-Ethyl-N-isopropyl)amiloride (EIPA), which specifically inhibits NHE1, the exchanger involved CAM-mediated endocytosis [8, 228]. This more specific inhibition led to the same effect on lymphocyte sampling as amiloride ( $34.2 \pm 6.9\%$  inhibition). Finally, disruption of ceramide production through the inhibition of acid sphingomyelinase, a key enzyme that helps differentiate CAM-mediated uptake from other pathways, inhibited lymphocyte sampling by  $49.6 \pm 8.2\%$  (Figure 18A imipramine).

More interestingly, in all cases this decrease in sampling was due to a reduction of events occurring on the cell body, as opposed to the cell border. As seen in Figure 18A, the proportion of sampling occurring on cell borders (black) remained the same in the presence of CAM-mediated uptake inhibitors, while the proportion occurring on the endothelial cell body (white) decreased ( $67.5 \pm 15.2\%$ ,  $41.6 \pm 20.8\%$ ,  $37.1 \pm 8.6\%$ , and  $15.1 \pm 4.7\%$  of control for Cdx, amiloride, EIPA, and imipramine, respectively). Confirming this, when we focused only on the population of lymphocytes on the HUVEC body, the inhibitors of CAM-mediated endocytosis, but not filipin, decreased percent sampling and increased the proportion of ‘adhered’ lymphocytes with respect to control (Figure 18B). Meanwhile, when we focused only on the population of lymphocytes on the HUVEC body, none of the inhibitors had an effect on ‘sampling’ or ‘adhered’ events (Figure 18C).

Since in the assay described above the inhibitors were present during the interaction of lymphocytes with endothelial cells, the effects observed could be due to an effect on lymphocytes and not necessarily on HUVECs. In order to clarify our results, we repeated the sampling assays by pre-incubating HUVECs with inhibitors, followed by washing prior to the addition of lymphocytes. As shown in Figure 19A, inhibitors of the CAM-mediated pathway, but not filipin, had a negative effect on total lymphocyte sampling ( $6.9 \pm 9.5\%$ ,  $27.9 \pm 9.0\%$ ,  $25.9 \pm 12.35\%$ ,  $24.3 \pm 7.7\%$ , and  $20.9 \pm 7.3\%$  inhibition for filipin, Cdx, amiloride, EIPA, and imipramine, respectively). The effect of imipramine, however, was not statistically significant. This pattern of inhibition was similar to our previous assay and suggested endothelium-specific CAM-mediated endocytosis contributed to the initiation of lymphocyte sampling events. However, a lack of sampling inhibition by imipramine suggested that the role of endothelial acid sphingomyelinase in this process might not be as important as other molecular elements of CAM-mediated uptake, or that acid sphingomyelinase contribution from the lymphocyte might be sufficient to induce sampling morphologies.

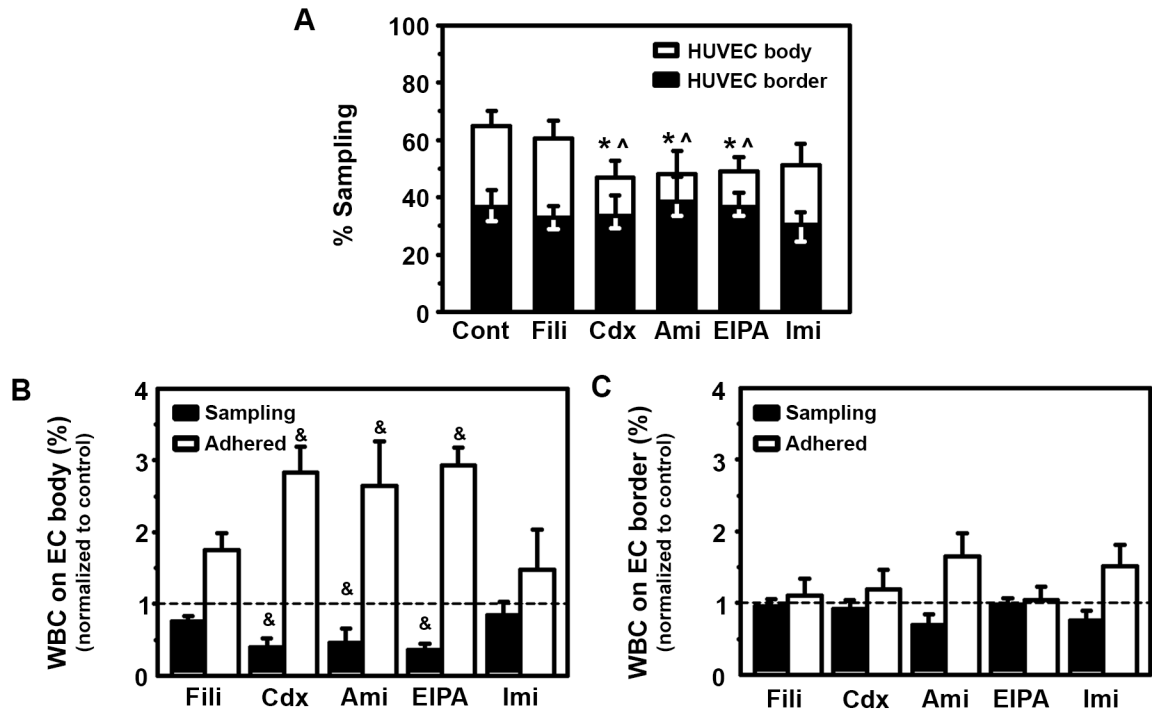


**Figure 19. Effect of inhibitors only on endothelial cells during pre-transmigratory interactions with lymphocytes.** Activated HUVECs grown on cover slips were pre-incubated 30 minutes at 37°C in control medium or medium containing filipin (Fili), methyl- $\beta$ -cyclodextrin (Cdx), amiloride (Ami), EIPA, or imipramine (Imi), followed by washing of inhibitors, and then incubation for 30 minutes with activated peripheral-blood lymphocytes (WBCs, pre-stained with green fluorescent calcein AM) in the absence of inhibitors. WBCs not firmly bound to HUVECs were washed followed by fixation, immunostaining of ICAM-1, and analysis by fluorescence microscopy. (A) Percent of sampling WBCs on HUVECs with corresponding spatial distribution (black for HUVEC border and white for HUVEC body). (B) Percent of ‘sampling’ WBCs (black bars) versus simply ‘adhered’ WBCs (white bars) out of only the population located on the HUVEC body. (C) Percent of ‘sampling’ WBCs (black bars) versus simply ‘adhered’ WBCs (white bars) out of only the population located on the HUVEC border. In B and C, data are normalized to control values (horizontal dashed line). Data represent mean  $\pm$  standard error of the mean. In C, error bars correspond (from top to bottom) to Total sampling, Border sampling, and Body sampling, respectively. \* compares total percent sampling to control; ^ compares percent body sampling to control, & compares each column to control ( $p < 0.05$  by Student’s *t*-test).

In addition to the absolute inhibitory effect on sampling, inhibitors of the CAM-mediated pathway decreased the percent of sampling events occurring on the HUVEC body compared to control without affecting sampling on the HUVEC borders, as seen before (compare black and white bars within Figure 19A). The exception to this again was imipramine, which did not significantly affect sampling on the endothelial cell body. Similarly, when considering only lymphocytes located on the HUVEC body, the

inhibitors of CAM-mediated endocytosis except imipramine decreased ‘sampling’ and increased ‘adhered’ lymphocytes, as seen in our previous assay (Figure 19B). Also as seen in our previous assay, when we focused only on the lymphocyte population on the HUVEC border, none of the inhibitors affected ‘sampling’ or ‘adhered’ events (Figure 19C).

Curiously, imipramine affected sampling (specifically on the HUVEC body) in Figure 18, when the inhibitor was pre-incubated and also present during lymphocyte interaction with HUVECs, but this effect was not observed in Figure 19, when the inhibitor was only pre-incubated with HUVECs. This could suggest that the activity of leukocyte acid sphingomyelinase might be required for sampling, specifically on the endothelial cell body. Previous studies indicate that leukocyte-specific sphingomyelinase activity contributes to binding to and/or transmigration across the endothelium [229-231]. Explaining the location-specific requirement, it is possible that sampling at the endothelial cell body has more stringent requirements compared to the endothelial cell border. For instance, sampling and probing at the endothelial border could be facilitated by the disruption of cell-cell junctions, while the deformability and vesiculation of the endothelial membrane on the endothelial cell body might require ceramide production.

Overall, these data support a role for key players of CAM-mediated endocytosis in the generation of morphologies that are indicative of transmigration at the interface between leukocytes and endothelial cells, predominantly in areas away from the endothelial cell border. Specifically, it appeared that the contribution by this pathway was mainly endothelial and not by leukocytes since the inhibitory effects were similar regardless of whether HUVECs and lymphocytes versus only HUVECs were exposed to

the inhibitors. This suggests that endothelial CAM-mediated endocytosis might have a regulatory role in the process of transmigration, specifically through the transcellular route.

### 5.2.2. Contribution of CAM-mediated endocytosis to lymphocyte transmigration across endothelial cells.

Next, we tested a functional role for elements of CAM-mediated uptake in leukocyte transmigration. We used a model consisting of a confluent monolayer of TNF- $\alpha$ -activated HUVECs grown on porous membranes, through which IL-2-activated lymphocytes can transmigrate driven by the presence of the chemoattractant SDF-1 $\alpha$  in the basal chamber [232]. Under control conditions 72.3 $\pm$ 3.7% of lymphocytes underwent transmigration after 30 minutes, as opposed to 0% transmigration by K562 cells, a non-migratory erythroid leukemia cell line used as a negative control (Figure 20A). As expected, disrupting the interaction between leukocyte integrins and endothelial cell surface molecules inhibited transmigration. For instance, blocking antibodies to leukocyte integrin  $\alpha_L\beta_2$  (LFA-1), which interacts with endothelial ICAM-1, resulted in 56.2 $\pm$ 12.8% inhibition, and blocking antibodies to leukocyte integrin  $\alpha_4\beta_1$  (VLA-4), which interacts with endothelial VCAM-1, resulted in 36.8 $\pm$ 6.4% inhibition (Figure 20B). These levels of inhibition were not absolute due to the functional redundancy of integrins during leukocyte transmigration [233]. In both cases, blocking antibodies had no effect on the ability of leukocytes to move across the porous membrane in the absence of a HUVEC monolayer, showing that the effect on transmigration seen with these antibodies was due to a disruption of lymphocyte-HUVEC interactions.

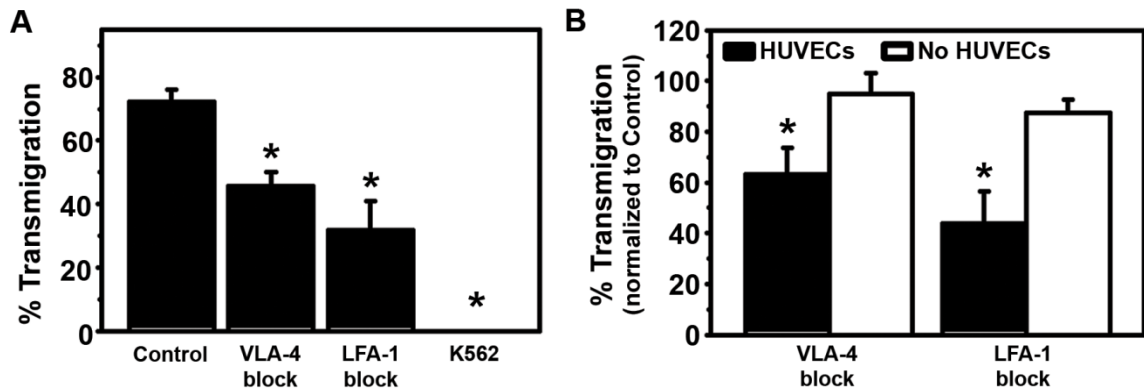


**Figure 20. Model to examine transmigration of lymphocytes across endothelial monolayers.** Activated peripheral-blood lymphocytes or K562 cells were added on top of HUVECs grown on 8- $\mu$ m pore size porous membranes (or porous membranes without HUVECs, when indicated), followed by a 30-minute incubation at 37°C in the absence (control) or presence of antibodies to block integrins VLA-4 or LFA-1. Lymphocytes in the basal chamber were collected and counted. (A) Percent transmigration, calculated as the number of lymphocytes collected in the basal chamber out of the total lymphocytes initially added the top chamber. (B) Percent transmigration of antibody-blocked lymphocytes in the presence (black) or absence (white) of a HUVEC monolayer (normalized to non-blocked controls). Data represent mean  $\pm$  standard error of the mean. \* compares each column to its respective control ( $P < 0.05$  by Student's *t*-test).

With this model which showed data consistent with the literature [225, 226], we used the series of inhibitors from our microscopy assays to determine the role of elements of the CAM-mediated pathway in transmigration. We retained the use of filipin as a negative control, shown previously to have no effect on transmigration across porous membranes under conditions similar to our model [234], and no role on lymphocyte sampling in our previous assays (recall Figures 18 and 19). As seen in Figure 21A, Cdx decreased lymphocyte transmigration by  $51.9 \pm 4.8\%$ . However, filipin had no effect on transmigration ( $12.0 \pm 7.7\%$  inhibition, non-significant), supporting previous evidence and suggesting that the integrity of lipid domains in CAM-mediated endocytosis is required for transmigration, but caveolae may not be crucial to this event. Furthermore, inhibition of  $\text{Na}^+/\text{H}^+$  exchange with amiloride and EIPA led to  $61.4 \pm 3.7\%$  and  $80.3 \pm 1.8\%$  inhibition of lymphocyte transmigration, while imipramine inhibited transmigration by  $52.1 \pm 7.2\%$ .

Not only does this pattern of inhibition coincide with that observed in the CAM-mediated uptake of anti-ICAM-1-coated particles [6, 7], but it also supports our data on leukocyte pre-transmigration sampling (recall Figure 18).

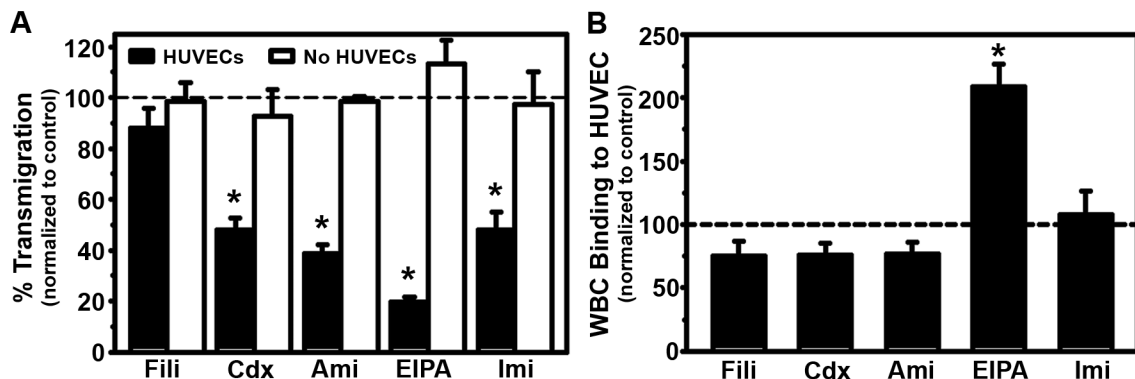


**Figure 21. Effect of inhibitors on both lymphocytes and endothelial cells during binding and transmigration.** (A) Activated peripheral-blood lymphocytes (WBC) were added on top of HUVECs grown on 8- $\mu$ m porous membranes (or porous membranes without HUVECs, when indicated), followed by a 30-minute incubation at 37°C in the absence (control) or presence of filipin (Fili), methyl- $\beta$ -cyclodextrin (Cdx), amiloride (Ami), EIPA, or imipramine (Imi). Lymphocytes in the basal chamber were collected and counted. Percent transmigration was calculated as the number of lymphocytes collected in the basal chamber out of the total lymphocytes initially added to the top chamber. (B) Lymphocytes (pre-stained with green fluorescent calcein AM) were added on top of HUVECs grown on coverslips and incubated with inhibitors as done in A. Microscopy was used to count total lymphocytes bound per HUVEC. Data represent mean  $\pm$  standard error of the mean. \* compares each column to control ( $P < 0.05$  by Student's *t*-test).

As addressed in our microscopy sampling assays, the effect of inhibitors in Figure 21 may have been on either the endothelium, or the lymphocytes, or both cell types. In order to clarify the possible role of inhibitors on lymphocytes versus endothelial cells, we first tested whether the migratory ability of lymphocytes across a porous membrane was affected in presence of inhibitors but the absence of a HUVEC barrier. As shown in Figure 21A (white columns), none of the inhibitors used appeared to affect the migratory ability of lymphocytes towards a chemokine. In addition, as seen by microscopy, the inhibitors used did not affect the levels of lymphocyte binding to HUVECs (Figure 21B), with the exception of EIPA, which increased binding by  $\sim$ 2-fold. This ruled out indirect

effects by these inhibitors on the lower percent transmigration rates observed compared to control.

To corroborate this, we tested the transmigration of leukocytes by pre-incubating HUVECs with each respective inhibitor, followed by washing prior to the transmigration assay so that lymphocytes were not directly exposed to the inhibitor. As seen in Figure 22A, this resulted in similar inhibitory patterns as compared to the presence of inhibitors during transmigration (recall Figure 21A), and did not affect leukocyte binding to HUVECs (Figure 22B). Thus, it is likely that the effects observed in these assays were endothelium-specific, supporting the role of endothelial CAM-mediated uptake in leukocyte transmigration. It was interesting to see that the effect of imipramine on transmigration was retained even when the inhibitor was only pre-incubated, because this was not the case for lymphocyte sampling. This suggests that although endothelial acid sphingomyelinase activity might not be necessary for lymphocyte sampling, it is indeed required for the downstream event of crossing of the endothelial cell layer.

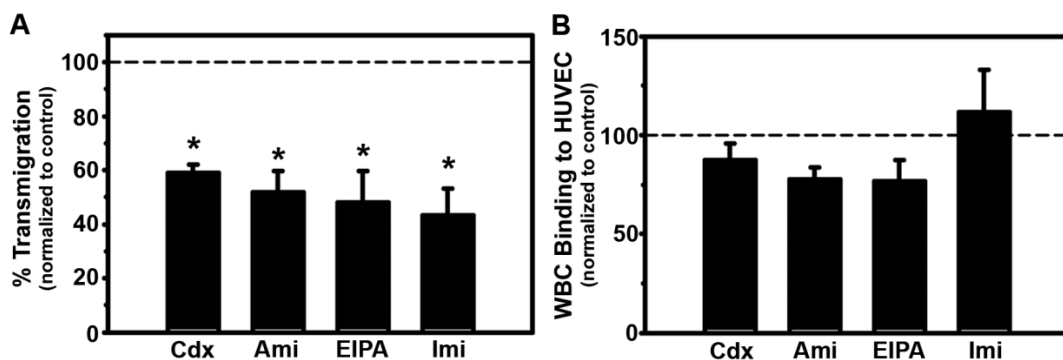


**Figure 22. Effect of inhibitors only on endothelial cells during lymphocyte binding and transmigration.** (A) Activated HUVECs grown on 8- $\mu$ m porous membranes were pre-incubated for 30 minutes in the absence (control) or presence of filipin (Fili), methyl- $\beta$ -cyclodextrin (Cdx), amiloride (Ami), EIPA, or imipramine (Imi). Cells were washed prior to adding activated peripheral-blood lymphocytes (WBC) on top of HUVECs, followed by a 30-minute incubation at 37°C. Lymphocytes in the basal chamber were collected and counted. Percent transmigration was calculated as the number of lymphocytes collected in the basal chamber out of the total lymphocytes initially added the top chamber. (B) Lymphocytes (pre-stained with green fluorescent calcein AM) were added on top of HUVECs grown on coverslips and pre-incubated with inhibitors as done in A. Microscopy was used to count total lymphocytes bound per HUVEC. Data represent mean  $\pm$  standard error of the mean. \* compares each column to control ( $p < 0.05$  by Student's  $t$ -test).

Interestingly, the NHE1-specific inhibitor EIPA resulted in a ~2-fold higher inhibition of transmigration when it was present during transmigration as opposed to only pre-incubated (compare the EIPA bar in Figures 21A versus 22A). In addition to this, EIPA increased binding to HUVECs by 2-fold but only when it was present during transmigration (instead of simply pre-incubated; Figures 21B versus 22B). However, EIPA did not show different inhibitory effects on lymphocyte sampling when it was present during transmigration or simply pre-incubated (recall Figures 18 and 19). Thus, this suggested that the activity of lymphocyte NHE1 may be involved in transmigration but is not sufficient to maintain this function. Also, the role of leukocyte NHE1 in this process may be associated with binding-related mechanisms. For example, NHE1 is known to interact with and regulate the actin cytoskeleton [235], which is crucial in the regulation of integrin adhesion to endothelial CAMs [236]. Thus, it is possible that EIPA caused dysregulation of lymphocyte adhesion to endothelial cells, increasing binding strength such that even though a fraction of lymphocytes might have been able sample and go across the endothelial cell, they were not able to detach into the basal chamber. Indeed, this exchanger protein, which is expressed by leukocytes, has been associated with post-transmigratory cell motility [237].

Overall, these results agree with previous studies suggesting a role for lipid raft domains in leukocyte transmigration, as seen through the inhibition by Cdx [128, 138, 221]. In addition, an effect due to inhibition of NHE1 and acid sphingomyelinase, but not caveolae-related pathways corresponds well with the pattern observed for endocytosis of anti-ICAM particles by HUVECs [6], which agrees with a potential role for CAM-mediated endocytosis in the crossing of endothelial barriers by leukocytes.

### 5.2.3. Contribution of CAM-mediated endocytosis lymphocyte transcellular transmigration across endothelial cells.

Finally, in order to confirm the effect of these inhibitors on transmigration, but also explore whether the CAM-mediated pathway has a role determining the routes of transmigration, we used established methodologies that allow for the differentiation between transcellular versus paracellular transmigration using confocal microscopy [192]. This procedure involves staining of actin (Figure 23A, middle panel) in order to localize leukocytes and observe their position in the z-axis with respect to the top and bottom of the endothelial cell. In addition, staining of VE-cadherin (Figure 23A, bottom panel) to observe the integrity of endothelial junctions allows for determination of the transmigration route without relying on the distance between the leukocyte and the HUVEC border.

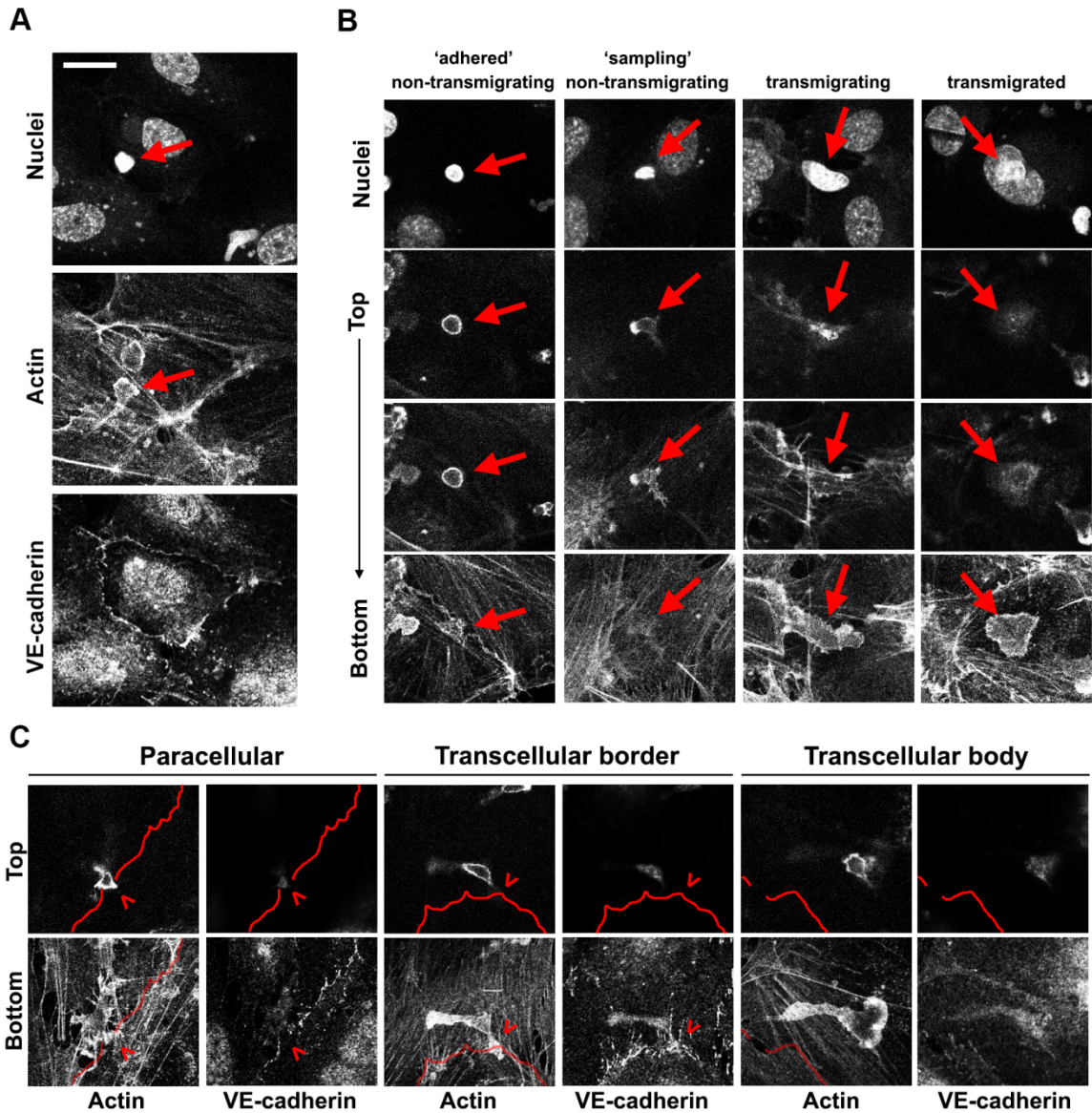


**Figure 23. Confocal microscopy of the route of lymphocyte transmigration across endothelial cells.** HUVECs growing on glass cover slips were incubated with activated peripheral-blood lymphocytes for 15 minutes at 37°C in control medium. Lymphocytes not firmly adhered to HUVECs were washed, followed by fixation, staining of actin with red phalloidin, nuclei in blue, and immunostaining of VE-cadherin in green. Cells were analyzed by confocal microscopy. (A) Example micrograph of a lymphocyte (red arrow) interacting with HUVECs. Scale bar = 20  $\mu$ m. (B) Sample micrographs of non-transmigrating (either round or deformed, to illustrate the simply 'adhered' and 'sampling' morphologies from previous assays), transmigrating, or already transmigrated lymphocytes (red arrows). Top panels show nuclei and bottom bottom three panels show z-stack sections from the top of the sample, where only lymphocyte actin is detected, to the bottom of the HUVEC monolayer in contact with the cover slip. Transmigration is occurring when lymphocyte actin can be observed both on top of and underneath the HUVEC monolayer. (C) Sample of three modes of transmigration. Paracellular transmigration occurs on cell borders and disrupts VE-cadherin staining. Transcellular transmigration can occur close to cell borders without disrupting VE-cadherin staining, or away from cell borders ('body'). Red lines delineate VE-cadherin staining. Arrowheads indicate the site at which lymphocytes overlap with cell borders.

Figure 23B illustrates that actin staining allows to determine if lymphocytes are in the process of transmigration, as the staining can be detected both on the top and the bottom of the HUVEC layer. This also allows to observe lymphocytes that are only on top of an endothelial cell (not transmigrating), or those that are at the bottom of the endothelial layer (already transmigrated). As revealed by this imaging technique, a fraction of lymphocytes that exhibit deformed morphologies (i.e.: those scored as ‘sampling’ in our previous assay) may not be in the act of transmigration. Thus, although our previous microscopy assays reveal important information about the pre-transmigratory interactions between leukocytes and endothelial cells, they do not directly reflect transmigration events. Figure 23C also reveals that those leukocytes that are transmigrating near the endothelial border can be scored as using the transcellular or paracellular route depending on whether or not they disrupt VE-cadherin staining.

Using this scoring system, we found that under control conditions,  $68.1 \pm 2.9\%$  of leukocytes were undergoing transmigration, and within these transmigratory events  $53.1 \pm 2.4\%$  were paracellular, while  $46.9 \pm 2.4\%$  were transcellular (Figure 24A). These route preferences were similar to the percent of lymphocyte sampling on the border versus the cell body in our previous assay (recall Figure 17), highlighting the close link between sampling and transmigration. In order to only account for inhibition of endothelial function, we performed pre-incubation of HUVECs with filipin, Cdx, amiloride, EIPA and imipramine, followed by washing of inhibitors before adding lymphocytes for the transmigration assay. Supported by our previous assays, inhibition of all elements of the CAM-mediated pathway, but not with filipin, decreased the percent of transmigrating lymphocytes (Figure 24A). Since imipramine inhibited transmigration in

this assay and also in our porous membrane study, but not sampling (recall Figure 19), it appears that endothelial ceramide is important in steps downstream of leukocyte sampling, possibly in the aperture of transcellular pores, which would pair well with the known role of ceramide in vesicular fusion [86, 238].

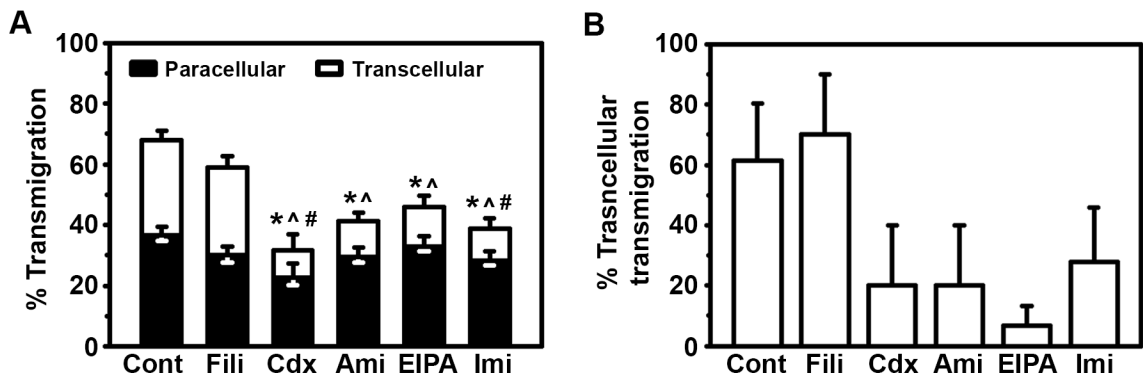


**Figure 24. Effect of inhibitors on the route of lymphocyte transmigration across endothelial cells.** HUVECs growing on glass cover slips were pre-incubated 30 minutes at 37°C with filipin (Fili), methyl- $\beta$ -cyclodextrin (Cdx) amiloride (Ami), EIPA, or imipramine (Imi), followed by washing and incubation with activated peripheral-blood lymphocytes for 15 minutes in control medium. Lymphocytes not firmly adhered to HUVECs were washed, followed by fixation, staining of actin with red phalloidin, nuclei in blue, and immunostaining of VE-cadherin in green. Cells were analyzed by confocal microscopy. (A) Quantification of percent transmigration, including route of transmigration (black for paracellular and white for transcellular). (B) Assay was performed as A, but using non-confluent HUVECs to only observe transcellular events. Bars show quantification of percent transmigration. Data represent mean  $\pm$  standard error of the mean. In A, error bars correspond (from top to bottom) to Total transmigration, Paracellular transmigration, and Transcellular transmigration, respectively. \* compares percent transmigration, ^ compares percent transcellular transmigration, # compares percent paracellular transmigration, each compared to respective control ( $p < 0.05$  by Student's *t*-test).

More importantly, as seen in Figure 24A, this decrease in transmigration by inhibiting CAM-mediated endocytosis was due to an inhibition specifically of transcellular events, but not paracellular events. The exception to this were Cdx and imipramine, both of which affected transcellular and paracellular migration alike, albeit the effect on paracellular transmigration was lower (~40-50% inhibition for transcellular versus ~8-30% inhibition for paracellular). Recall that Cdx and imipramine had no effect on lymphocyte sampling on cell borders in our previous assay, which means that cholesterol-dependent lipid domains and acid sphingomyelinase may be important for

paracellular transmigration even though lymphocytes can still properly engage by probing/sampling at cell borders. This is a significant finding because, to the best of our knowledge, it identifies for the first time two endothelial molecular elements that differentially regulate the stage of lymphocyte sampling versus the stage of actual transmigration. This finding also opens the possibility that CAM-mediated endocytosis could be involved in both transcellular and paracellular transmigration, although possibly to different extents, reflected by the fact that inhibition of NHE1 exchange only affected transcellular transmigration, while inhibition with Cdx and imipramine inhibited both routes. Otherwise, it is possible that both routes share similar molecular elements, even if they do not share an underlying endocytic mechanism.

Finally, we also performed transmigration assays using sub-confluent endothelial cell cultures in order to exclusively observe transcellular transmigration events, and we found similar results as those observed with confluent monolayers. Under control conditions and in the presence of filipin, percent transmigration (all transcellular) was  $61.3 \pm 19\%$  and  $70 \pm 20\%$ , respectively, while in the presence of Cdx, amiloride, EIPA, and imipramine, it was  $20 \pm 20\%$ ,  $20 \pm 20\%$ ,  $6.67 \pm 6.67\%$ , and  $27.8 \pm 18.1\%$ , respectively. Thus, these data implicate CAM-mediated endocytosis not only in the process of transmigration, as seen using a different technique (Figures 21 and 22), but specifically contributing to the transcellular pathway.

### 5.3. Conclusion

Leukocyte transmigration depends on membrane and vesicular dynamics downstream of ICAM-1 signaling. This includes the formation of endothelial docking

structures and invaginations that support leukocyte sampling of the endothelial cell, and also endocytic vesicle fusion to form the transcellular pore [121]. Overall, the studies presented here expand our current knowledge by supporting a contribution by regulatory elements of the CAM-mediated pathway to these events.

Key molecular elements of the CAM-mediated pathway, NHE1, acid sphingomyelinase, and ceramide, are enriched at sites of leukocyte interaction with endothelial cells. These molecules as well as cholesterol, in an endothelium-specific manner, contribute to the generation of leukocyte sampling events, known to be a preliminary step crucial to transmigration. Importantly, this contribution specifically occurs at sites away from the endothelial border. Meanwhile, caveolae-mediated pathways appear to have a less significant role in sampling. In addition to this, inhibition of CAM-mediated endocytosis, but not caveolae-mediated pathways, in the endothelium disrupts crossing of leukocytes across endothelial layers, and this inhibition is specifically through an effect on the transcellular route of transmigration.

Since our data showed that CAM-mediated endocytosis is involved in promoting lymphocyte sampling, which temporally precedes actual crossing of the endothelial cell, we cannot fully determine whether CAM-mediated endocytosis is involved only in promoting the sampling of lymphocytes (which in turn affects transmigration) or also contributes to opening of the transcellular pore. Such studies prove difficult, as it is still unclear whether these two events are discrete in the first place [122]. However, the fact that inhibition of endothelial acid sphingomyelinase alone did not disrupt lymphocyte sampling but affected transmigration itself, suggests that indeed the CAM-mediated pathway may mediate events that occur downstream of lymphocyte sampling, such as

opening of the transcellular pore. Thus, the role of ceramide in transmigration may be an important clue regarding the intricacies behind this phenomenon.

Based on our data from Chapter 4, we have found that CAM-mediated endocytosis is capable of mediating transport of micron-sized particles across cells. This corresponds well with the apparent physiological function of this pathway in leukocyte transmigration across the endothelium, suggesting that the CAM-mediated pathway may contribute to the generation of transcellular pores through the formation of vesicles that fuse into larger structures through which leukocytes can cross. In addition, our studies using particles reveal a potential relationship between ICAM-1 engagement density and ceramide enrichment, which in turn can regulate the efficiency of CAM-mediated uptake. This may have ramifications in the context of leukocyte transmigration, as is possible that leukocytes could potentially modulate the LFA-1 density in their membranes to engage ICAM-1 at different extents, ultimately affecting the extent of transmigration, or even the preference for CAM-mediated transcellular migration versus using the paracellular route.

## **Chapter 6: Contribution by the CAM-Mediated Pathway to Endothelial Uptake and Degradation of Fibrin Polymers.**

### *6.1. Background*

Coagulation and fibrinolysis are crucial to the maintenance of blood flow within the vascular system. The former prevents leakage of blood out of vessels upon injury through the formation of a clot, while the latter ensures the fluid state of blood is preserved via clot degradation [156]. Proper functioning of this balance requires several activators and inhibitors, and involves regulation at the macromolecular and cellular levels [239]. For instance, the architecture of a fibrin clot (e.g.: size and polymerization density) is affected by its interaction with endothelial cells and can have a significant effect on fibrinolysis [182, 196]. In addition, the small peptides produced by fibrinolysis can serve as signaling agents upon interaction with cell surface molecules, affecting the resolution of a clot [178].

Interestingly, these small peptides, which have been well studied, account for only a small fraction of the products of fibrinolysis [180]. It is known that dissolution of a blood clot depends only on 25% of its degradation, such that fibrinolysis produces many large fibrin polymers that become circulating materials [182, 183]. This also means that fibrinolysis fragments remain bound to the surface of the endothelium after clot dissolution [240]. Since these blood clot fragments (in circulation) and remnants (on the endothelial surface) have potential to sustain inflammation and to re-ignite fibrin deposition, there must be systems in place to discard these materials in order to prevent

the coagulation cascade from being reinitiated. Abnormalities in this clearance might be associated with pathological states such as atherosclerosis and thrombosis.

It is known that macrophages can internalize fibrin and degrade it in their lysosomes [241], and hepatic macrophages accumulate fibrin after clot resolution [242]. Meanwhile, endothelial cells might use similar mechanisms as phagocytes for removal of fibrin blood clot remnants (i.e.: clearance via endocytosis). Indeed, the endothelium is adapted to clear particulate materials found in capillaries, including apoptotic cells, sickle and parasite-infected erythrocytes, foreign particles, such as asbestos, and pathogens [243-245]. Such capabilities for uptake are reflected by endothelial cell display of several types of endocytic pathways [246, 247], which could contribute to the uptake of blood clot remnants and other forms of fibrin. In fact, recent reports show that endothelial cells are capable of engulfing blood clots using membrane protrusions, which leads to their removal from the vasculature, yet the mechanism behind this phenomenon remains unexplored [22].

It is known that fibrinogen and fibrin can interact directly with several molecules on the surface of endothelial cells, including VE-cadherin, integrin  $\alpha_v\beta_3$ , and ICAM-1 [145, 147, 149], which could in turn serve as signaling agents to stimulate this uptake and transport. Fibrin(ogen) can also indirectly interact with tPA receptor, uPA receptor, and thrombomodulin [150, 151], known to mediate endocytosis through clathrin- and caveolae-mediated pathways [248]. Although the extent to which these interactions contribute to physical retention or potentially uptake of a forming, completed, or partially degraded blood clot are not characterized, certain signaling events are known to be elicited from these interactions. The majority of these responses are in the context of

angiogenesis and cell survival, but in the case of ICAM-1, binding by fibrin can also elicit rearrangement the actin cytoskeleton [249], possibly through Rho signaling [250]. This outcome is similar to that observed when anti-ICAM particles undergo CAM-mediated endocytosis, which is not surprising since both anti-ICAM particles and fibrin polymers can engage multiple copies of ICAM-1. The endothelial protrusions shown to form around blood clots also resemble those observed during the CAM-mediated uptake of micron-sized anti-ICAM particles [7, 22]. Furthermore, these signaling events, and subsequent CAM-mediated endocytosis also occur when particles are coated with a peptide sequence ( $\gamma 3$ ) corresponding to the ICAM-1-binding region of fibrin(ogen) (recall Chapter 4) [216]. Thus, it is possible that this endocytic pathway occurs upon interaction of fibrin polymers (such as blood clot remnants) with the endothelium, and this may be a mechanism for their clearance. This chapter elaborates on our efforts to study the possible link between CAM-mediated endocytosis and endothelial internalization of fibrin polymers.

## 6.2. Results

### 6.2.1. Initial interaction between fibrin meshes and endothelial cells.

In order to mimic the interaction between the blood clot remnants and endothelial cells, we used a model consisting of activated HUVEC cultures incubated for 30 minutes with purified fluorescently labeled fibrinogen and thrombin to generate artificial fibrin meshes. This model is used for studying the interaction between clots and the endothelium both cell culture [196] and *in vivo* [22]. Under the conditions used, fibrin meshes of a mean diameter of  $1.9 \pm 0.6 \mu\text{m}$  formed on the surface of endothelial cells, with

9.4±0.7 objects bound per cell (Figure 25A and B). The thrombin-dependent formation of these meshes was confirmed by a reduction in total meshes bound per cell, as well as mesh size, in the presence of thrombin inhibitor hirudin (3.7±0.3 objects/cell with 0.88±0.04 μm mean diameter; Figure 25B and C). In addition, the polymeric nature of these meshes was confirmed by a reduction in binding and size in the presence of the glycine-proline-arginine-proline (GPRP) peptide, an inhibitor of fibrin polymerization (2.2±0.3 objects/cell with 0.9±0.1 μm mean diameter).

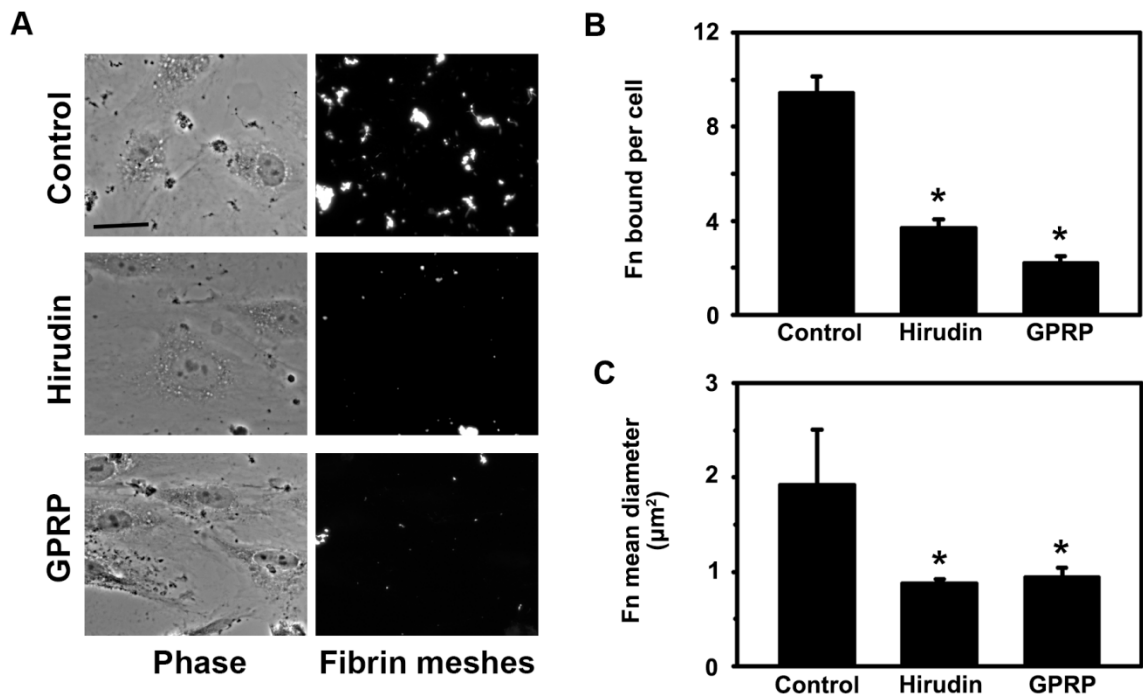


**Figure 25. Formation of fibrin meshes on the surface of endothelial cells.** Activated HUVECs growing on coverslips were incubated in the presence of fluorescently labeled fibrinogen with thrombin in the absence (control) or presence of hirudin or GPRP for 30 minutes at 37°C. (A) Sample micrographs of each treatment. Left panels are phase-contrast and right panels are fluorescence. Scale bar = 20 μm. (B) Quantification of total number of fluorescent fibrin (Fn) meshes bound to HUVECs by microscopy. (C) Quantification of fibrin mesh size. Data represent mean ± standard error of the mean. \* compares hirudin or GPRP to control ( $p < 0.05$  by Student's *t*-test).

As a preliminary characterization of this model, we determined the kinetics of interaction between these micron-sized fibrin meshes and HUVECs to see if we could detect evidence their transport across the endothelium, as has been observed previously

with injected fibrin emboli in mouse brains *in vivo* [22]. We tested this by forming fibrin meshes on HUVECs monolayers grown on a porous membrane for 30 minutes, followed by washing and a chase of different time-points (Figure 26). Confocal analysis showed that at initial time-points (1 hour chase), fibrin meshes appeared to be on top of HUVECs, as they were detected on planes above cells where nuclei were not detectable. Also, at this time-point, some meshes may have been internalized by cells, as they could not be seen on top of HUVECs, but only on the same plane as cell nuclei. Meanwhile, no fibrin meshes could be detected at the plane of the porous membrane underneath HUVECs. At 3 and 5 hours, fibrin meshes could not be detected on top of HUVECs, but were abundant on the same plane of nuclei, suggesting possible internalization by cells. Meanwhile, at 5 hours there was an increase in detected fibrin meshes beneath HUVECs, which would be consistent with transendothelial transport. Although these transport-specific results will require more scrupulous validation, it appeared this model is suitable for studying the mechanisms behind the previously described endothelial transport of blood clots and their remnants.

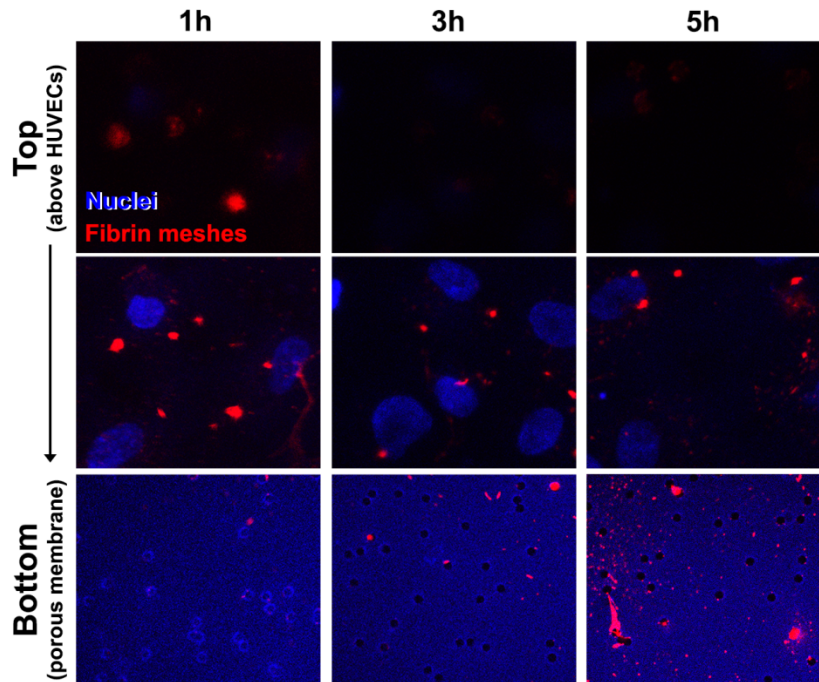


**Figure 26. Kinetics of fibrin mesh interaction with endothelial cells grown on porous membranes.** Activated HUVECs grown on 3 $\mu$ m-pore size porous membranes were incubated in the presence of fluorescently labeled fibrinogen with thrombin for 30 minutes at 37°C. Apical and basal chambers were washed and cells were incubated (chase) for 1, 3 or 5 hours. Confocal micrographs at three planes on the z-axis are shown. Top panels show a plane above the HUVEC layer, where nuclei cannot be identified. Middle panels are at the level of the nuclei plane. Bottom panels show the porous membrane beneath HUVECs. Nuclei are blue and fibrin meshes are red. Scale bar = 20  $\mu$ m.

Using this model, we first characterized the involvement of endothelial cell surface molecules on the formation and binding of fibrin meshes using blocking antibodies to known binding partners of fibrin(ogen). As seen in Figure 27A, blocking antibodies to integrin  $\alpha_v\beta_3$  led to a reduction in the total number of fibrin meshes bound to endothelial cells, suggesting that this integrin may be important in the initial deposition of fibrin on the activated endothelium. Conversely, antibodies to ICAM-1, VE-cadherin, tPA receptor, uPA receptor and thrombomodulin did not significantly affect the total number bound fibrin meshes compared to control. However, mesh size was reduced in the presence of ICAM-1-blocking antibodies (Figure 27B), suggesting an interaction between ICAM-1 and fibrin in this model. Since ICAM-1 blocking did not change the

total number of meshes bound, but decreased their size, it is possible that binding to ICAM-1 could serve as a mechanism to support fibrin polymerization on the surface of the endothelial cell.

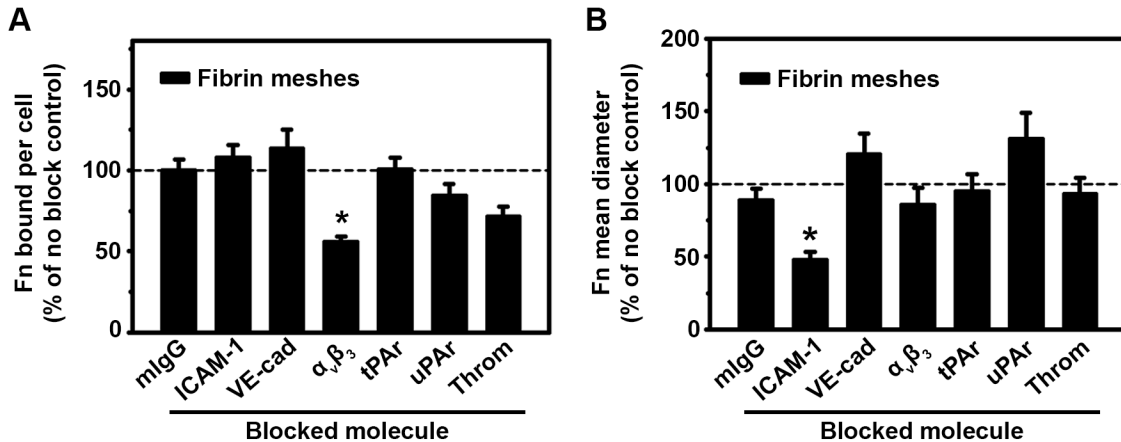


**Figure 27. Effect of blocking antibodies on the binding of fibrin meshes to endothelial cells.** Activated HUVECs were incubated in the presence of fluorescently labeled fibrinogen with thrombin for 30 minutes at 37°C in the absence (control) or presence of non-specific mouse IgG or blocking antibodies to ICAM-1, VE-cadherin (VE-cad), integrin  $\alpha_v\beta_3$ , tPA receptor (tPA), uPA receptor (uPA), or thrombomodulin (Throm). After fixing, cells were analyzed by epifluorescence microscopy. (A) Quantification of fibrin (Fn) mesh binding per cell. (B) Quantification of fibrin mesh mean diameter. Data are normalized to non-blocking control and represent mean  $\pm$  standard error of the mean. \* compares each condition to non-blocking control ( $p < 0.05$  by Student's *t*-test).

With this evidence supporting an interaction between ICAM-1 and fibrin meshes, we tested the presence of this molecule at sites of fibrin mesh binding to HUVECs. Figure 28A illustrates that immunostaining of ICAM-1 followed by microscopy revealed ICAM-1 enrichment at these sites. Quantification of the overlap between fluorescent fibrin meshes and ICAM-1 immunostaining (calculated as the percent of fibrin mesh fluorescent area that overlapped with ICAM-1 fluorescent area above an intensity threshold; see Methods, Section 3.14) showed  $86.3 \pm 2.6\%$  colocalization (Figure 28B). This enrichment and substantial percent overlap suggested engagement of multiple copies of ICAM-1 by fibrin meshes, which may lead to signaling events observed when anti-ICAM or  $\gamma_3$  particles that undergo CAM-mediated uptake. Thus, we also tested for the

enrichment of molecules associated with CAM-mediated endocytosis. Both NHE1 and acid sphingomyelinase were enriched at sites of fibrin mesh binding and showed  $88.5 \pm 2.8\%$  and  $83.3 \pm 4.5\%$  colocalization, respectively (Figure 28B). This, however, was not the case for VCAM-1 ( $30.5 \pm 3.9\%$  colocalization), an Ig superfamily endothelial surface molecule similar in structure to ICAM-1, but not associated with CAM-mediated endocytosis [251], serving as a negative control. Thus, these data supported the specific recruitment of elements of the CAM-mediated pathway at sites of interaction between fibrin polymers and endothelial cells.

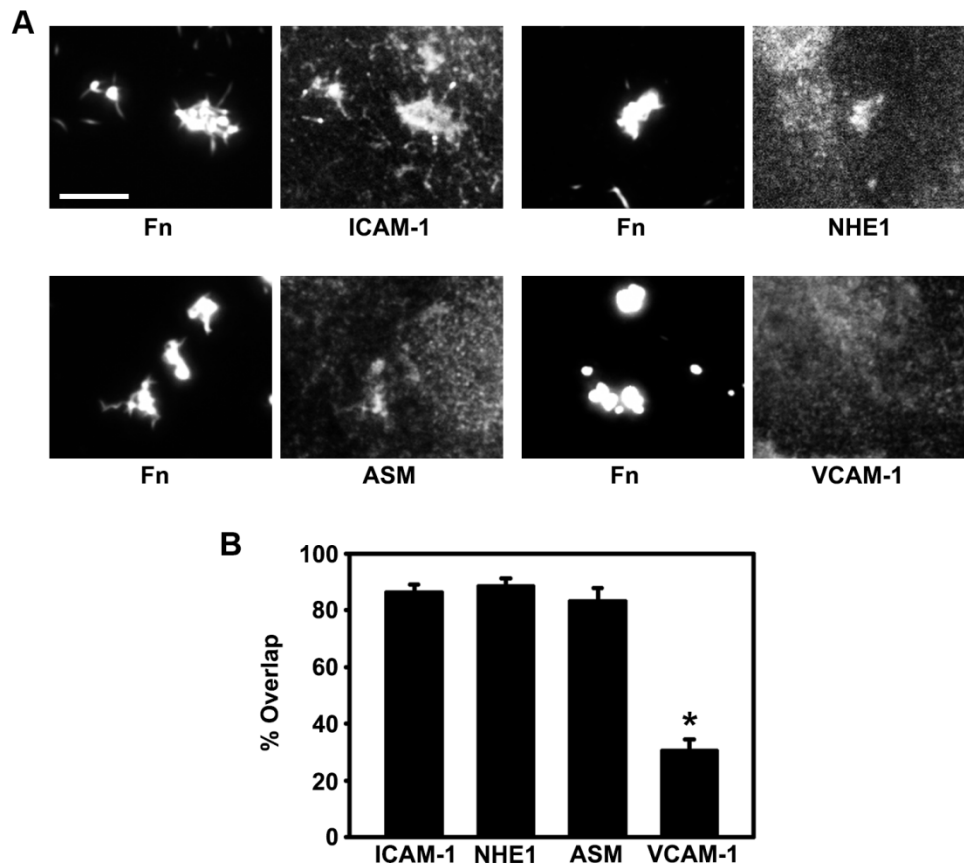


**Figure 28. Enrichment of endothelial molecules at sites of fibrin mesh binding to endothelial cells.** Activated HUVECs were incubated in the presence of fluorescently labeled fibrinogen with thrombin for 30 minutes at 37°C, followed by fixation and immunostaining of ICAM-1, NHE1, acid sphingomyelinase (ASM) or VCAM-1. (A) Sample micrographs showing fibrin (Fn) meshes (left panels) or each immunostained molecule (right panels). Scale bar = 10  $\mu$ m. (B) Quantification of percent overlap between fibrin meshes and each immunostained molecule. Data represent mean  $\pm$  standard error of the mean. \* compares each molecule to ICAM-1 ( $p < 0.05$  by Student's *t*-test).

### 6.2.2. Internalization of fibrin meshes by endothelial cells with contribution by the CAM-mediated pathway.

With data supporting an interaction between fibrin meshes and ICAM-1, as well as the presence of key molecular players of CAM-mediated uptake at binding sites, we tested if these binding interactions are followed by endocytosis. We first determined the kinetics of interaction between fluorescent fibrin meshes and HUVECs by incubating fibrin mesh mixture for 30 minutes (pulse), followed by washing and a chase of several time-points. Following fixation, we immunostained surface-bound, non-internalized fibrin to differentiate surface meshes from those inside of cells, which are inaccessible to antibodies (Figure 29A). Figure 29B shows that fibrin meshes were internalized by endothelial cells, reaching a plateau of ~80% uptake at 3 hours. Note that since this treatment had a 30-minute pulse to allow for mesh formation, the 0-minute chase time-point already showed a degree of internalization.

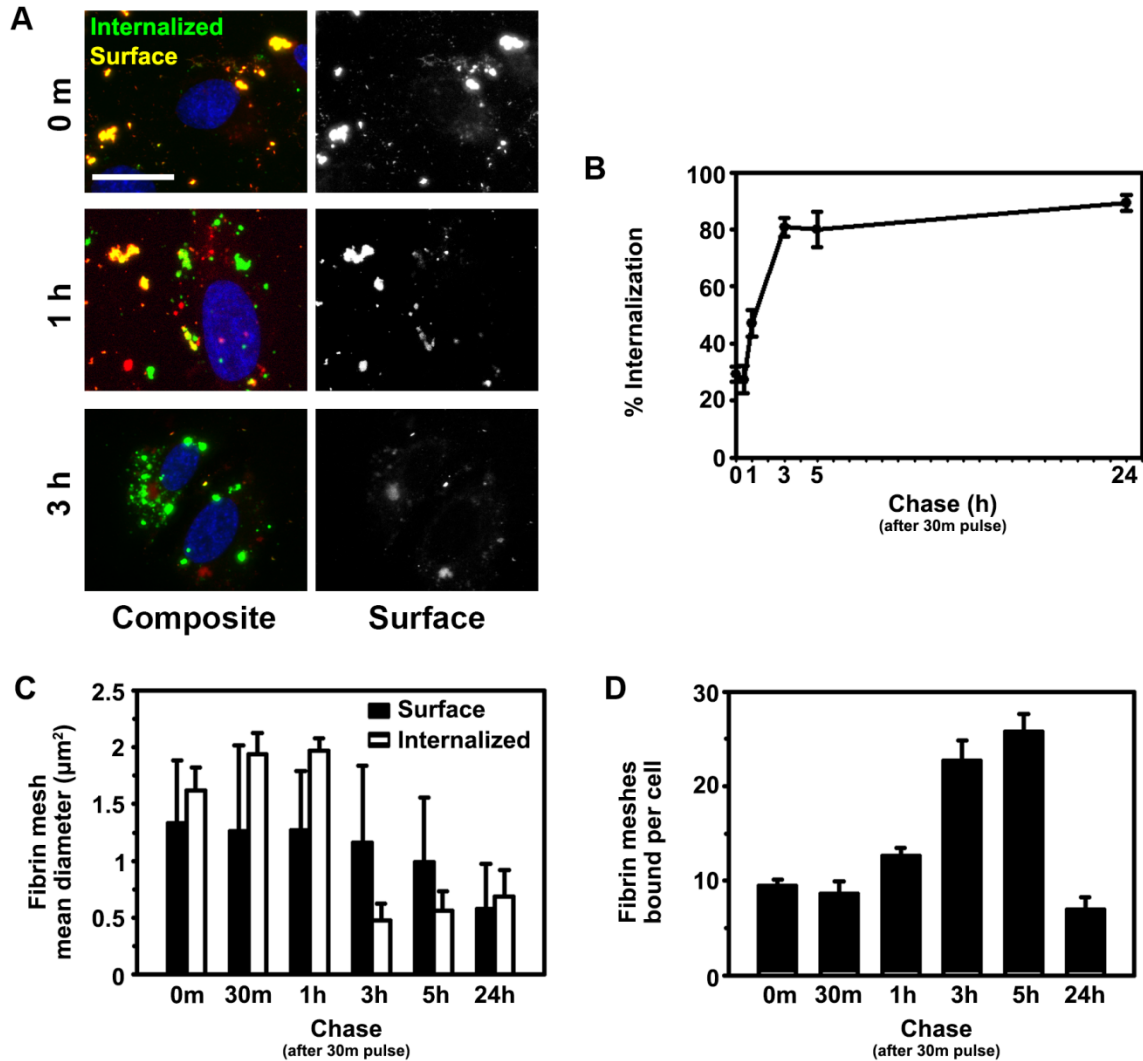


**Figure 29. Kinetics of fibrin mesh internalization by endothelial cells.** Activated HUVECs were incubated in the presence of green fluorescently labeled fibrinogen with thrombin for 30 minutes at 37°C, followed by washing and incubation (chase) for 0, 30 minutes, 1, 3, 5 or 24 hours at 37°C. After fixation, cells were immunostained with anti-fibrin, followed by a red fluorescent secondary antibody. (A) Sample micrographs showing fibrin mesh internalization at representative time-points. Green is internalized meshes, yellow (red + green) is surface-bound, non-internalized meshes, blue is nuclei (DAPI). Right panels show only red fluorescence (surface fibrin meshes). Scale bar = 20 µm. (B) Quantification of percent internalization, calculated as  $\text{internalized}/(\text{internalized}+\text{surface})\times 100$ . (C) Quantification of the mean diameter of the surface or the internalized populations of fibrin meshes. (D) Quantification of total (both internalized and surface) fibrin meshes bound per cell. Data represent mean  $\pm$  standard error of the mean.

In order to examine the properties of these internalized fibrin meshes, we calculated the mean diameter of both non-internalized (surface-bound) and internalized meshes separately (Figure 29C). This revealed that the size of internalized fibrin meshes at earlier time-points (white bars between 0 and 1 hour chase), was equal to the original

non-internalized mesh size (~1.5-2  $\mu\text{m}$  diameter), which supports the internalization of micron-sized fibrin polymers by HUVECs. Furthermore, the size of these internalized fibrin meshes decreased between 1 and 3 hours, suggesting distribution of fibrin into smaller vesicular compartments and/or intracellular degradation. Indeed, when we determined the number of fibrin meshes associated with cells, we observed an increase in the number of fibrin meshes over time until 5 hours, likely due to distribution into smaller compartments, followed by a dramatic decrease by 24 hours (Figure 29D), possibly due to degradation. This increase in number of fibrin meshes accompanied by a decrease in mesh size revealed a dynamic internalization and intracellular trafficking of fibrin polymers by endothelial cells.

It was interesting to note that these rates of endocytosis for fibrin meshes over time were slower and less efficient compared to those of CAM-mediated endocytosis of spherical anti-ICAM particles (Figure 4) [77]. However, they were more similar to the CAM-mediated uptake kinetics curve of disk-shaped objects and of  $\gamma 3$  particles (Figure 7) [77]. Due to the irregular (non-spherical) shape of fibrin meshes, which were mostly in the 1-2  $\mu\text{m}$  diameter range, this could be expected if they are internalized by cells using this pathway. Indeed, it is a feature of CAM-mediated uptake that it becomes more sensitive to irregularities in object shape as object size increases (Muro, unpublished data).

It is known that cultured endothelial cells can produce tPA and uPA, as well as proteases, which could drive fibrinolysis and/or non-specific degradation of fibrin meshes prior to internalization. This opens the possibility that these extracellular degradation events might have a role in the uptake of fibrin meshes. Thus, we determined

internalization in the presence of aprotinin and plasminogen activator inhibitor 1 (PAI-1), which inhibit endothelium-derived serine proteases and tPA/uPA (thus preventing extracellular degradation of fibrin meshes during incubation), respectively. Using these inhibitors in an internalization assay had no effect on the endothelial uptake of fibrin meshes ( $102.5 \pm 0.3\%$  of control, Figure 30A).

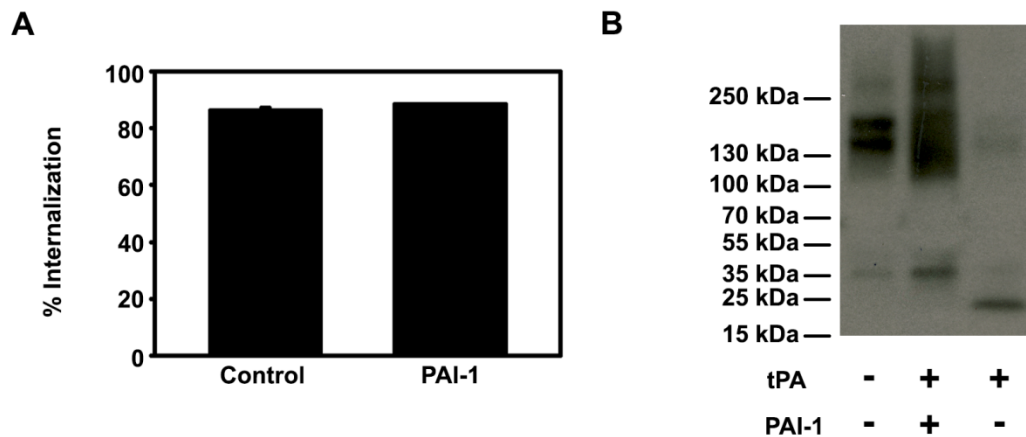


**Figure 30. Role of fibrinolysis in the internalization of fibrin meshes by endothelial cells.** (A) Activated HUVECs were incubated in the presence of green fluorescently labeled fibrinogen with thrombin for 30 minutes at 37°C, followed by washing and incubation (chase) for 3 hours at 37°C in the absence (control) or presence of PAI-1 plus aprotinin. After fixation, cells were immunostained with anti-fibrin, followed by a red fluorescent secondary antibody to differentiate non-internalized versus internalized fibrin meshes. Graph shows quantification of percent internalization. (B) Green fluorescently labeled fibrinogen was incubated with thrombin for 8 hours in control conditions or in the presence of tPA along with PAI-1 and aprotinin, or tPA alone. Image shows Western blot with an antibody to fibrin, after SDS PAGE. Data represent mean  $\pm$  standard error of the mean.

This confirmed that endothelial cells are equipped to internalize fibrin polymers as large as  $\sim 2 \mu\text{m}$  in diameter without depending on fibrinolytic activity. Since the inhibitors had no effect on uptake, we confirmed they were active using a test-tube assay followed by Western blotting with an antibody to fibrin (see Methods, Section 3.17 for details). As Figure 30B shows, under control conditions (left lane) we observed two major bands above 130 kDa, while the presence of tPA to induce fibrinolysis (right lane) led to a reduction of these bands and appearance of a smaller band below 25 kDa. In the

presence of PAI-1 plus aprotinin, tPA lost this effect (middle lane), revealing the inhibitory activity.

In order to further test if endothelial cells internalized full fibrin meshes instead of extracellular degradation products, we performed an internalization assay as done previously (recall Figure 28) but prior to immunostaining, we permeabilized cells. This allows for anti-fibrin to access both the surface and the inside of cells, and thus immunodetection does not discriminate between internalized or surface-bound fibrin. As shown in Figure 31A (top panels), in the absence of permeabilization, there was a decrease over time in the number of immunodetectable fibrin meshes, as expected from their internalization by HUVECs. At 0 and 1 hours, when cells were permeabilized, there was an increase in immunodetection of fibrin compared to non-permeabilized cells (Figure 31B). This indicates that when antibodies could access the inside of cells, they were able to recognize fibrin, supporting the idea that HUVECs are able to internalize non-degraded fibrin meshes.

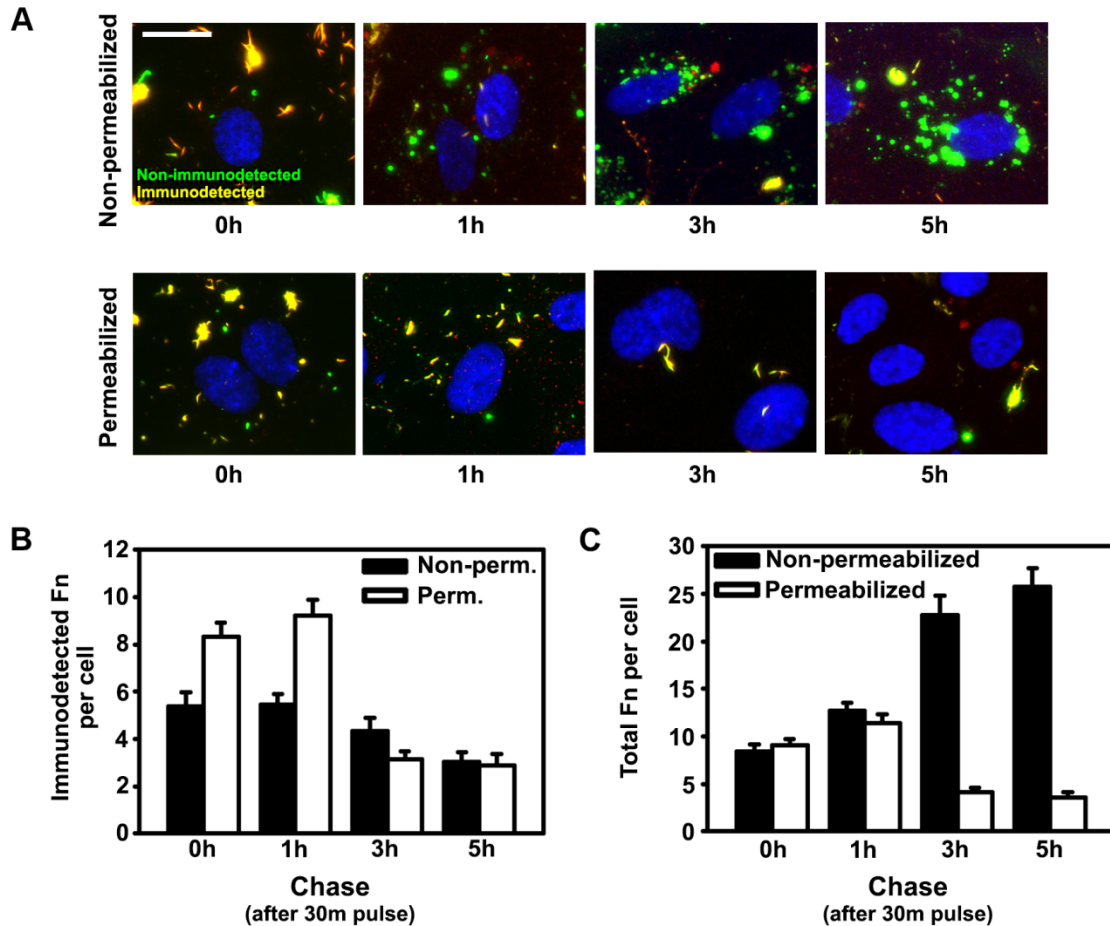


**Figure 31. Immunodetectability of endothelium-internalized fibrin meshes after permeabilization.** Activated HUVECs were incubated in the presence of green fluorescently labeled fibrinogen with thrombin for 30 minutes at 37°C, followed by washing and incubation (chase) for 0, 1, 3 or 5 hours at 37°C. After fixation, cells were either permeabilized or not prior to immunostaining with anti-fibrin, followed by a red fluorescent secondary antibody. (A) Sample micrographs showing fibrin (Fn) mesh immunostaining in the absence (top panels) or presence (bottom panels) of permeabilization. Green is non-immunodetectable Fn, yellow (red + green) is immunodetectable Fn, blue is nuclei (DAPI). Scale bar = 20  $\mu$ m. (B) Quantification of immunodetected (yellow) fibrin meshes per cell. (C). Quantification of total (includes green-only and yellow) fibrin meshes per cell. Data represent mean  $\pm$  standard error of the mean.

Interestingly, after 3 and 5 hours, permeabilization did not increase the level of immunodetected fibrin. Instead, it drastically reduced the detected green (non-immunodetectable) fluorescence at these two time-points (compare top to bottom 3- and 5-hour panels in Figure 31A; Figure 31C). This suggests that at these time-points permeabilization led to washing off of non-immunostained objects. Thus, as our size data suggested previously (recall Figure 29C showing a reduction of internalized fibrin mesh

size), it is possible that that between 1 and 5 hours after internalization, fibrin meshes were intracellularly degraded into molecular species small enough to diffuse out of the cell upon permeabilization.

In order to determine the possible uptake mechanism used by endothelial cells, we incubated fibrin meshes and HUVECs in the presence of a series of chemical inhibitors, including those disrupt CAM-mediated endocytosis. As seen in Figure 32, inhibition with filipin, which affects caveolae-mediated endocytosis, had no effect on the internalization of fibrin meshes ( $97.1 \pm 3.0\%$  of control). Meanwhile, all other inhibitors used had a significant negative effect on fibrin mesh uptake. Monodansylcadaverine and wortmannin, which affect clathrin-mediated uptake and PI3K-dependent macropinocytosis/phagocytosis, respectively, had a mild effect on endocytosis ( $84.4 \pm 5.4\%$  and  $85.0 \pm 4.4\%$  of control, respectively). Amiloride and imipramine, which affect CAM-mediated uptake through their inhibition of  $\text{Na}^+/\text{H}^+$  exchange and acid sphingomyelinase, respectively, had a more drastic effect on the uptake fibrin meshes ( $45.3 \pm 3.5\%$  and  $67.4 \pm 6.3\%$  of control, respectively).

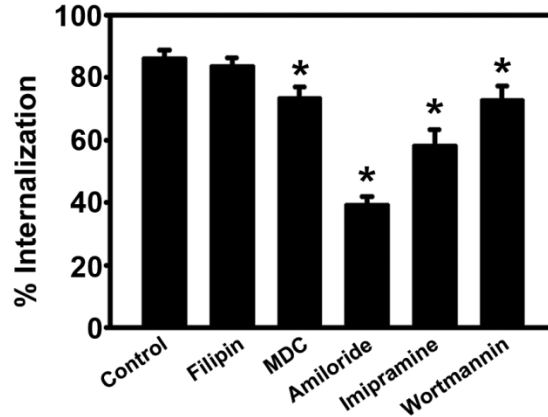


**Figure 32. Mechanism of fibrin mesh internalization by endothelial cells.** Activated HUVECs were incubated in the presence of green fluorescently labeled fibrinogen with thrombin for 30 minutes at 37°C, followed by washing and incubation (chase) for 3 hours at 37°C in the absence (control) or presence of filipin, monodansylcadaverine (MDC), amiloride, imipramine, or wortmannin. After fixation, cells were immunostained with anti-fibrin, followed by a red fluorescent secondary antibody to distinguish between non-internalized and internalized fibrin meshes. Microscopy was used to quantify percent internalization, shown in the graph. Data represent mean ± standard error of the mean. \* compares each inhibitor to control ( $p < 0.05$  by Student's *t*-test).

The effect by inhibitors of different pathways is suggestive of overlapping mechanisms of uptake. This is feasible due to the variety of potential binding partners for fibrin on the surface of endothelial cells, including VE-cadherin, known to be associated with clathrin-mediated endocytosis [252], and  $\alpha_v\beta_3$ , which regulates actin-dependent uptake of fibrinogen in epithelial cells [253]. However, it appears from these inhibition data that ICAM-1-dependent CAM-mediated endocytosis is a major contributor to this uptake in activated endothelial cells. This is supported by the role of ICAM-1 we observed in our binding studies, and also the enrichment of this molecule, NHE1 and acid sphingomyelinase, at mesh binding sites.

6.2.3. Intracellular trafficking of fibrin meshes and contribution of lysosomes to fibrin mesh degradation.

We next examined the kinetics of fibrin mesh intracellular trafficking using microscopy. Analysis of the spatial distribution of fibrin meshes interacting with HUVECs revealed a tendency of migration toward the perinuclear region over time (percent perinuclear localization rose from  $15.6 \pm 6.4\%$  to  $70.6 \pm 4.2\%$  between 0 minutes and 3 hours; Figure 33A and B), suggesting trafficking to lysosomes, as seen with anti-ICAM and  $\gamma 3$  particles targeted to CAM-mediated endocytosis (recall Figures 12 and 13).

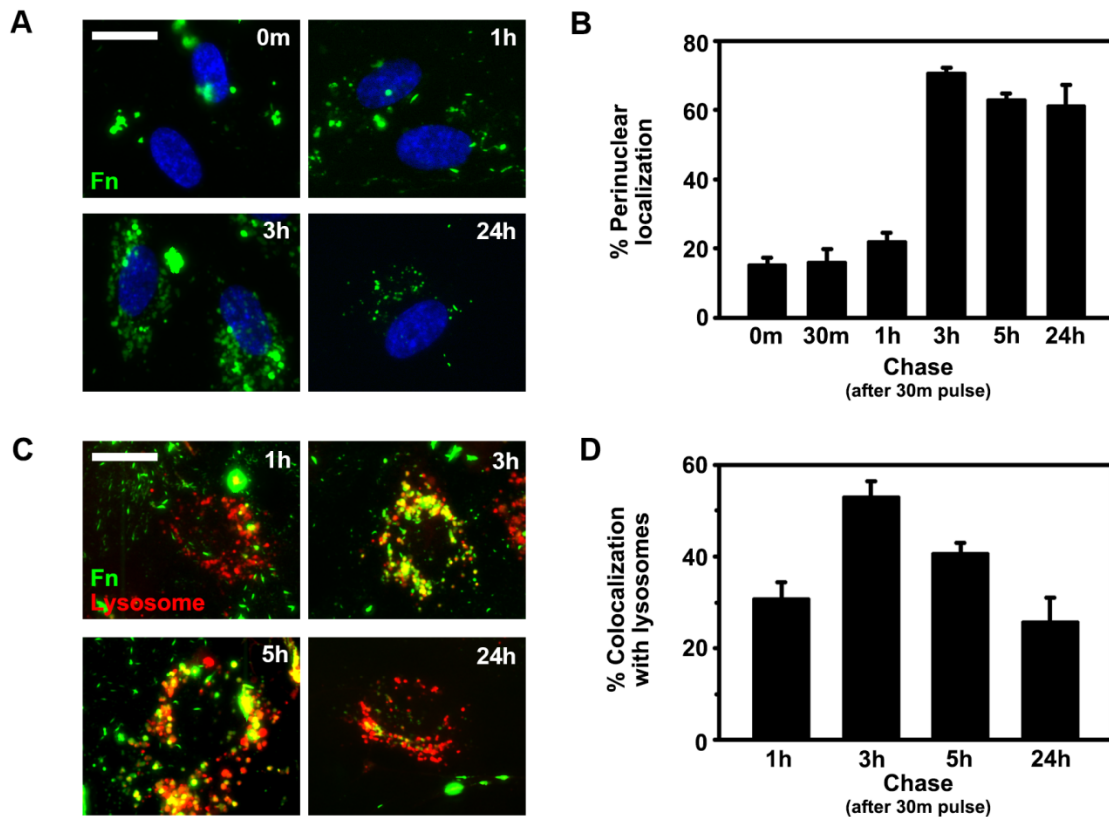


**Figure 33. Intracellular trafficking of fibrin meshes in endothelial cells.** Activated HUVECs were incubated in the presence of green fluorescently labeled fibrinogen with thrombin for 30 minutes at  $37^{\circ}\text{C}$ , followed by washing and incubation (chase) for 0, 30 minutes, 1, 3, 5 or 24 hours at  $37^{\circ}\text{C}$ . For C and D, HUVECs were pre-incubated for 45 minutes with Texas Red-labeled dextran, followed by a 45 minutes chase to label lysosomes. (A) Sample micrographs showing green fibrin (Fn) meshes and nuclei (blue). (B) Quantification of percent perinuclear localization, defined as a region  $\sim 5 \mu\text{m}$  surrounding the nucleus. (C). Sample micrographs showing green Fn meshes and red lysosomes. Colocalization is yellow. (D) Quantification of percent colocalization between Fn meshes and lysosomes. Scale bars =  $20 \mu\text{m}$ . Data represent mean  $\pm$  standard error of the mean.

To validate this, we pre-incubated HUVECs with Texas Red-labeled dextran for 45 minutes, followed by a 45-minute chase. This ensures that dextran has fully trafficked to and labels lysosomes, a technique shown to be a suitable alternative to immunostaining of LAMP-1 [9, 193]. Then, we determined the colocalization between these compartments and internalized fibrin meshes over time (Figure 33C). This revealed that the percent of fibrin mesh objects internalized by endothelial cells colocalizing with Texas Red-labeled lysosomes increased until 3 hours, indicating trafficking to these compartments. The percent colocalization then declined after 5 and 24 hours, suggesting that at later time-points, lysosome-resident fibrin meshes were degraded. This is supported by our previous observation that between 5 and 24 hours, the number of fibrin meshes detected on HUVECs was greatly reduced (recall Figure 29D; also see Figure 32A and C, bottom right panels).

In order to examine the role of lysosomes in this later decrease of colocalization, we determined colocalization in the presence of chloroquine, a lysosomotropic base that inhibits lysosome hydrolases [254]. As seen in Figure 34, at 5 hours the presence of chloroquine did not affect fibrin mesh colocalization with lysosomes compared to control. However, at 24 hours chloroquine elicited an increase in colocalization. Also, in the presence of chloroquine, the percent colocalization between fibrin and lysosomes increased over time (while it decreased in control conditions), possibly due to continued trafficking and accumulation of fibrin in lysosomes in the absence of degradation. This suggests that inhibition with chloroquine prevented degradation of fibrin, supporting a role for lysosomes in fibrin mesh degradation.

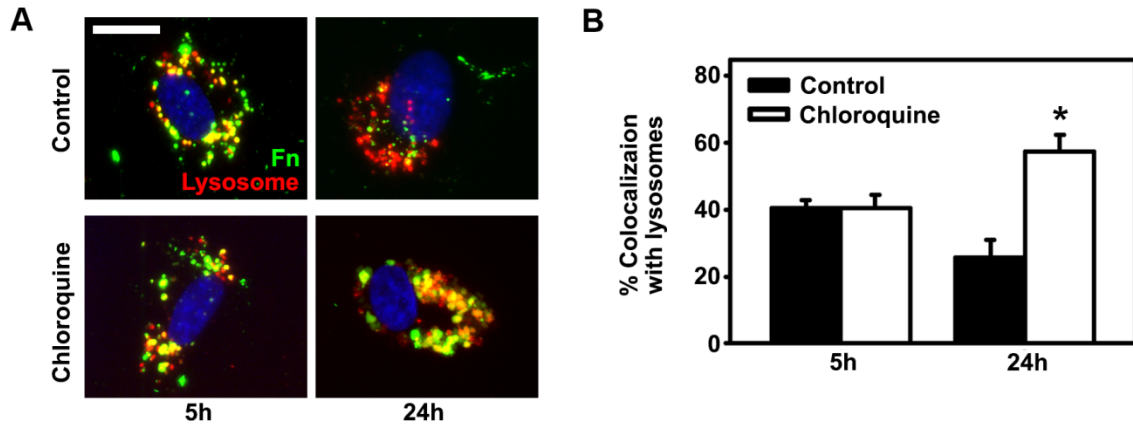


**Figure 34. Effect of chloroquine on fibrin mesh colocalization with lysosomes in endothelial cells.**

Activated HUVECs were pre-incubated for 45 minutes with Texas Red-labeled dextran, followed by a 45-minute chase to label lysosomes. Cells were incubated in the presence of green fluorescently labeled fibrinogen with thrombin for 30 minutes at 37°C, followed by washing and incubation (chase) for 5 or 24 hours at 37°C in the absence (control) or presence of chloroquine (A) Sample micrographs for each condition. Fibrin (Fn) meshes are green and lysosomes are red. Colocalization is yellow. Scale bar = 20 μm. (B) Quantification of percent colocalization between fibrin meshes and lysosomes. Data represent mean ± standard error of the mean. \* compares chloroquine to control within each time-point (p<0.05 by Student's *t*-test).

Despite our inability to detect chloroquine-sensitive degradation at 5 hours with this colocalization assay, our previous permeabilization assay showed that even at this time-point, internalized fibrin meshes appeared to be degraded (recall that for the 5-hour time-point, after permeabilization internalized green fluorescent objects diffused out of cells in Figure 31). Thus, it is possible that although we did not see a change in colocalization due to the presence of chloroquine at 5 hours, the composition of lysosome-resident fibrin was different between control and chloroquine conditions. To test this, we compared the immunodetectability of internalized fibrin meshes in the presence or absence of chloroquine, using cell permeabilization prior to staining with antibodies to fibrin (Figure 35A). This assay uses the same concept as seen in Figure 31: Total fluorescent objects are either fibrin meshes or fibrin derivatives that still retain the green fluorophore. Objects that are green and red (yellow) are those immunodetected by anti-fibrin, and thus must consist of protein intact enough to retain the antibody-binding

epitope. Finally, non-immunodetectable objects (those that are only green), still retain the fluorophore, but must consist of degraded fibrin derivatives that do not have the anti-fibrin epitope.

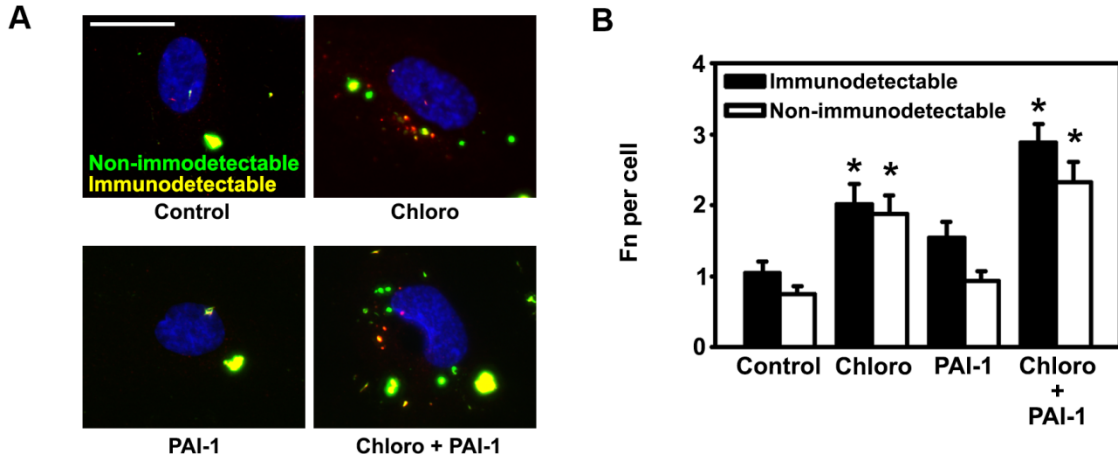


**Figure 35. Role of lysosomes in fibrin mesh degradation by endothelial cells.** Activated HUVECs were incubated in the presence of green fluorescently labeled fibrinogen with thrombin for 30 minutes at 37°C, followed by washing and incubation (chase) for 5 hours at 37°C in the absence (control) or presence of chloroquine (Chloro), PAI-1 plus aprotinin, or Chloro plus PAI-1 plus aprotinin. After fixation, cells were permeabilized prior to immunostaining with anti-fibrin, followed by a red fluorescent secondary antibody. (A) Sample micrographs showing non-immunodetectable (green only) or immunodetectable (yellow) fibrin. (B) Columns show quantification of immunostained (yellow) or non-immunostained (green only) fibrin. Data represent mean  $\pm$  standard error of the mean. \* compares each column to its respective control ( $p < 0.05$  by Student's *t*-test).

As shown in Figure 35B, the presence of chloroquine increased the number of both immunodetectable and non-immunodetectable fibrin (by 2- and 2.5-fold, respectively). This suggests that lysosomes contribute to the degradation of both intact fibrin, and also fibrin derivatives. Although we already observed that endothelial uptake of fibrin meshes did not depend on fibrinolysis, it was possible that fibrinolytic activity could affect their degradation. Suggesting otherwise, the presence of PAI-1 and aprotinin did not significantly increase immunodetectable or non-immunodetectable fibrin. However, since there was a slight increase in the presence of these inhibitors, we tested the effect of inhibiting both lysosomes and fibrinolysis concomitantly. As illustrated by

Figure 35B, co-incubation with chloroquine and PAI-1 plus aprotinin increased the number of immunodetectable and non-immunodetectable fibrin to a greater extent than chloroquine alone (2.7-fold and 3.1-fold, respectively). Due to this additive effect, it seems that fibrinolysis of fibrin meshes occurred upstream of, and could facilitate, their subsequent degradation in lysosomes.

In order to corroborate these results, we used protein gel electrophoresis. We repeated the incubation of fluorescent fibrin mesh mixture with HUVECs for 30 minutes, followed by a 5-hour chase in the presence of degradation inhibitors. Then, we characterized HUVEC lysates using SDS-PAGE followed by Western blotting with an antibody to the  $\beta$  chain of fibrin. As shown in Figure 36A, immunodetection of cell lysates allowed us to distinguish a major band corresponding to the intact  $\beta$  chain of fibrin (~55 kDa). We were also able to detect a smaller band of ~22 kDa, which is the same size as the band observed upon tPA-stimulated degradation seen previously (recall Figure 30). Densitometry analysis showed that the ratio between the 22 kDa and the 55 kDa bands was larger for cells incubated for 5 hours versus those incubated for 0 hours after fibrin mesh binding (Figure 36A). This suggested that the lower band was a product of degradation over time. Although we detected several bands between 55 and 22 kDa, also suggestive of degradation, these were difficult to quantify. Thus, we used the 22/55 band ratio as an estimation of the effect of inhibitors on fibrin degradation.

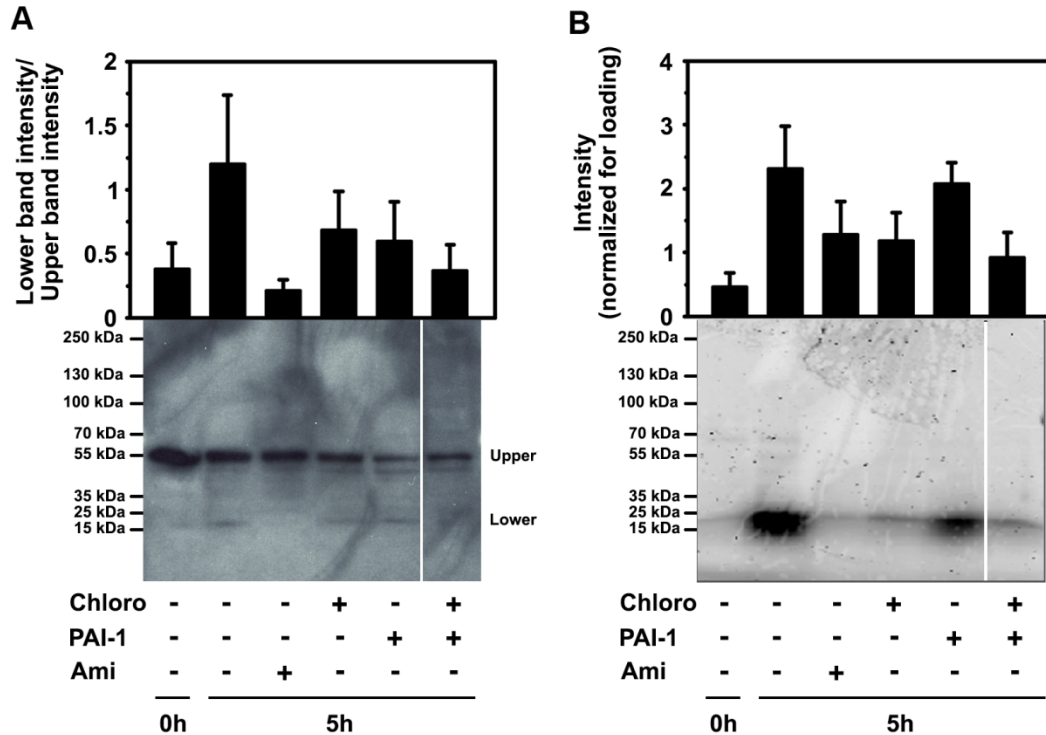


**Figure 36. SDS-PAGE and Western blot characterization of fibrin mesh interaction with endothelial cells.** Activated HUVECs were incubated in the presence of red fluorescently labeled fibrinogen with thrombin for 30 minutes at 37°C, followed by washing and incubation (chase) for 0 or 5 hours at 37°C in the absence (control) or presence of chloroquine (Chloro), PAI-1 plus aprotinin, amiloride (Ami), or different combinations, as detailed in each panel. Cell lysates were processed for SDS-PAGE (A) Western blotting with an antibody to fibrin (bottom) and analysis by densitometry (top). Columns represent the ratio of intensities between the lower (~22 kDa) band and the upper (~55 kDa) band. (B) Direct fluorescence imaging after SDS-PAGE (bottom) and analysis by densitometry (top). Columns represent the intensity of the ~22 kDa band after normalization to a non-specific protein from Ponceau staining. Data represent mean  $\pm$  standard error of the mean.

As seen in Figure 36A, the presence of amiloride, which disrupts internalization of fibrin meshes (recall Figure 32), appeared to fully inhibit degradation, suggesting that the detected fibrin degradation was intracellular and associated with the CAM-mediated pathway. Incubation with chloroquine also inhibited degradation, suggesting a role by lysosomes in this intracellular degradation, and validating our microscopy data. However, this inhibition was lower than that of amiloride, suggesting that other factors contributed to intracellular degradation of fibrin meshes or that degradation products (of fibrinolysis) were also internalized. Indeed, incubation with PAI-1 plus aprotinin, to inhibit

fibrinolysis, also inhibited degradation. Finally, similar to our microscopy data, co-incubation with chloroquine and PAI-1 appeared to have an additive effect on this inhibition.

Alternatively, we directly imaged gels by fluorescence in order to detect fibrin regardless of its immunodetectability by anti-fibrin. This revealed one main band at ~22 kDa (Figure 36B). Although we observed a 55 kDa band using this technique, its signal was much weaker compared to the 22 kDa band and, thus, it cannot be observed in Figure 36B. Densitometry analysis of the 22 kDa band revealed that this band appeared to be a degradation product, as its intensity increased between 0 and 5 h. The presence of amiloride inhibited this degradation (suggesting intracellular degradation), as also occurred with chloroquine (suggesting lysosomal degradation). Contrary to our observation with Western blotting, chloroquine was sufficient to inhibit degradation to the same level as amiloride, while PAI-1 had very low (if any) effect on degradation. Thus, it seems that this band was the product of non-specific proteolysis in lysosomes, instead of the site-specific cleavage by plasmin, which retains antibody-binding sites on the fibrin chains. However, co-incubation with chloroquine and PAI-1 appeared to have an additive effect on this inhibition, as we previously observed by microscopy.

Thus, overall, these data support a contribution by lysosomes in the degradation of internalized fibrin meshes. Meanwhile, fibrinolysis may help this degradation, possibly by cleaving fibrin meshes into smaller fragments upstream of their arrival to lysosomes. While these assays do not reveal whether fibrinolysis occurred prior to fibrin mesh uptake or inside of cells, our internalization data showing that endothelial cells internalize full-sized fibrin meshes that are immunodetectable by anti-fibrin, suggest that at least a

fraction of this fibrinolysis activity occurs within cells. It is likely that in a physiological setting, fibrinolysis inside and outside of endothelial cells helps to make lysosomal degradation of blood clot remnants more efficient.

#### 6.2.4. Characterization of model fibrin microemboli for *in vivo* studies.

After describing the internalization of fibrin meshes by endothelial cells, followed by degradation in lysosomes, we next studied these interactions *in vivo*. To do this, we aimed at injecting pre-formed fibrin meshes in mice intravenously, a model previously used for studying blood clot interaction with the endothelium [22, 255]. Since injected pre-formed fibrin meshes (hereby referred to as fibrin microemboli) bind to the endothelium instead of forming directly on it, we first characterized their binding and endocytosis in cell culture. As seen in Figure 37A, fibrin microemboli showed similar dimensions as those seen with fibrin meshes ( $1.56 \pm 0.7 \mu\text{m}$  diameter, compared to  $1.9 \pm 0.6 \mu\text{m}$  for fibrin meshes), although they bound at lower numbers ( $2.36 \pm 0.1$  fibrin microemboli per cell, compared to  $9.4 \pm 0.7$  fibrin meshes per cell).

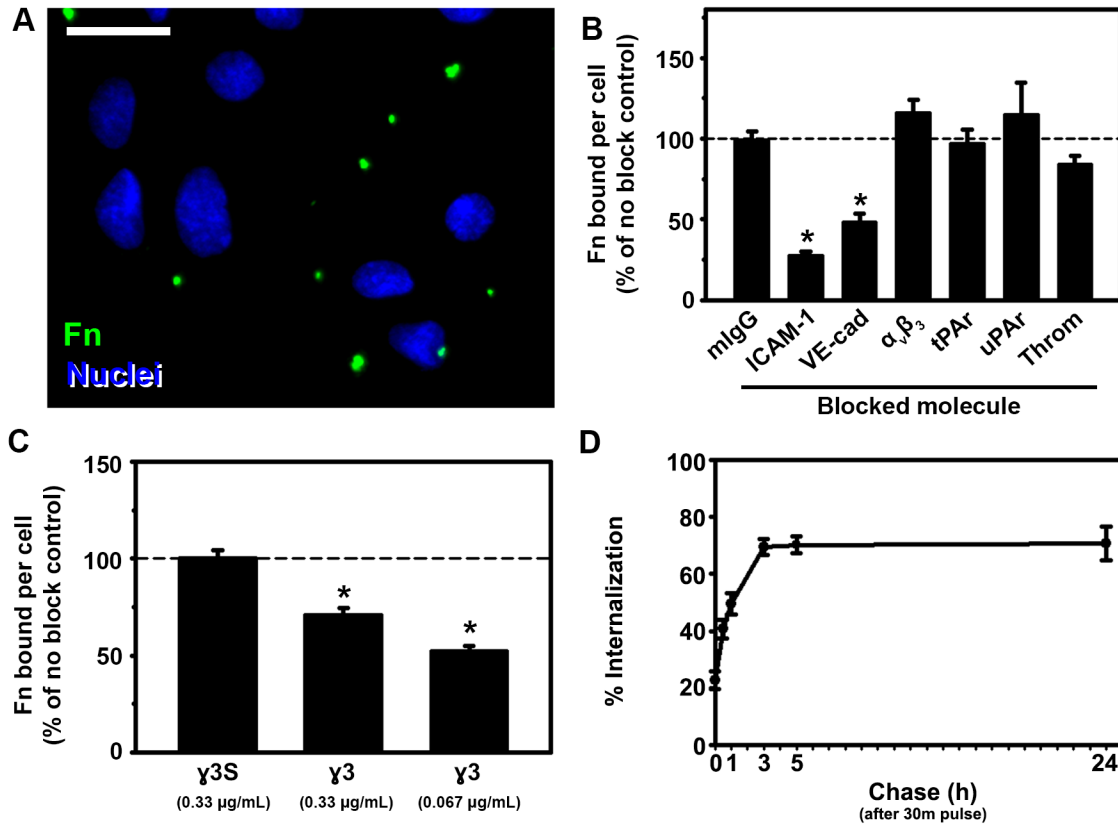


**Figure 37. Binding and internalization of fibrin microemboli by endothelial cells.** Activated HUVECs were incubated in the presence pre-formed fluorescent fibrin microemboli pre-formed in test tubes and then added to cells for 30 minutes at 37°C in the absence (control) or presence of non-specific mouse IgG or blocking antibodies to ICAM-1, VE-cadherin (VE-cad), integrin  $\alpha_v\beta_3$ , tPA receptor (tPAr), uPA receptor (uPAr), or thrombomodulin (Throm), or different concentrations of  $\gamma 3$  peptide or scrambled  $\gamma 3$  ( $\gamma 3S$ ). (A) Sample micrograph of fibrin microemboli (green) bound to endothelial cells (blue nuclei). Scale bar = 20  $\mu m$  (B) Quantification of fibrin microemboli binding per cell by microscopy, expressed as a percent of binding in the absence of antibodies (B) Quantification of fibrin microemboli binding per cell by microscopy, expressed as a percent of binding in the absence of peptides. (D) After the 30-minute binding period, HUVECs were incubated (chase) for 0, 30 minutes, 1, 3, 5 or 24 hours at 37°C. After fixation, cells were immunostained with anti-fibrin, followed by a red fluorescent secondary antibody to differentiate non-internalized fibrin microemboli from internalized counterparts. Graph shows quantification of percent internalization by microscopy. In B and C, data are normalized to non-blocking control. Data represent mean  $\pm$  standard error of the mean. \* compares each condition to non-blocking control ( $p < 0.05$  by Student's *t*-test).

We determined the contribution of cell surface molecules to binding of fibrin microemboli to endothelial cells, as done with fibrin meshes (recall Figure 27). As shown in Figure 37B, blocking antibodies to ICAM-1 and VE-cadherin led to a reduction in binding of fibrin microemboli, while antibodies to the other molecules had no effect. The role of ICAM-1 in binding of fibrin microemboli was confirmed by a similar inhibitory

effect in the presence of  $\gamma 3$ , the peptide derived from the fibrin(ogen) ICAM-1-binding region, in a concentration-dependent manner and also compared to compared to a scrambled  $\gamma 3$  ( $\gamma 3S$ ) control (Figure 37C). While VE-cadherin is highly localized to cell-cell junctions, these results are in agreement with previous data that show a contribution by VE-cadherin to fibrin binding to endothelial monolayers [147]. Meanwhile, these data support the idea that ICAM-1 could also be a key molecule during the interaction of clot microemboli with the endothelium, possibly inducing CAM-mediated uptake as seen with fibrin meshes. Indeed, internalization assays with fibrin microemboli by HUVECs revealed similar kinetics compared to fibrin meshes (recall Figure 29B), with a slightly lower plateau at  $\sim 75\%$  internalization around 3 hours (Figure 37D).

#### 6.2.5. Contribution by the CAM-mediated pathway to endothelial uptake of fibrin microemboli *in vivo*.

Our results show a contribution by ICAM-1 to binding of both fibrin meshes formed on the endothelial cell surface and fibrin microemboli added to endothelial cells, followed by uptake and intracellular degradation. The endocytosis of fibrin polymers by the endothelium may be a mechanism to remove clot fragments from the endothelial surface, preventing sustained inflammation and reocclusion after fibrinolysis. To test this, we proceeded with *in vivo* studies. In order to examine possible uptake of fibrin microemboli in the context of CAM-mediated endocytosis, we compared wild-type mice to ICAM-1 or acid sphingomyelinase (ASM) knockout strains, both of which are deficient in this endocytic pathway [7]. We injected green fluorescent fibrin microemboli into mice and allowed sufficient time for internalization (1.5 hours), based on uptake

kinetics from our microscopy studies. Since we observed that the highest accumulation occurred in lung tissue, we performed confocal microscopy of lung capillaries to facilitate imaging. Here, we observed that in wild-type mice, injected fluorescent fibrin microemboli appeared to be surrounding the perinuclear region of cells, and they were found to be in the same z-plane as cell nuclei (Figure 38A). Meanwhile, in ICAM-1 and ASM knockout strains, fibrin microemboli remained on z-planes on top nuclei, suggesting that they were possibly found on the surface of the cell, and thus, not internalized in these CAM-mediated endocytosis deficient mice.

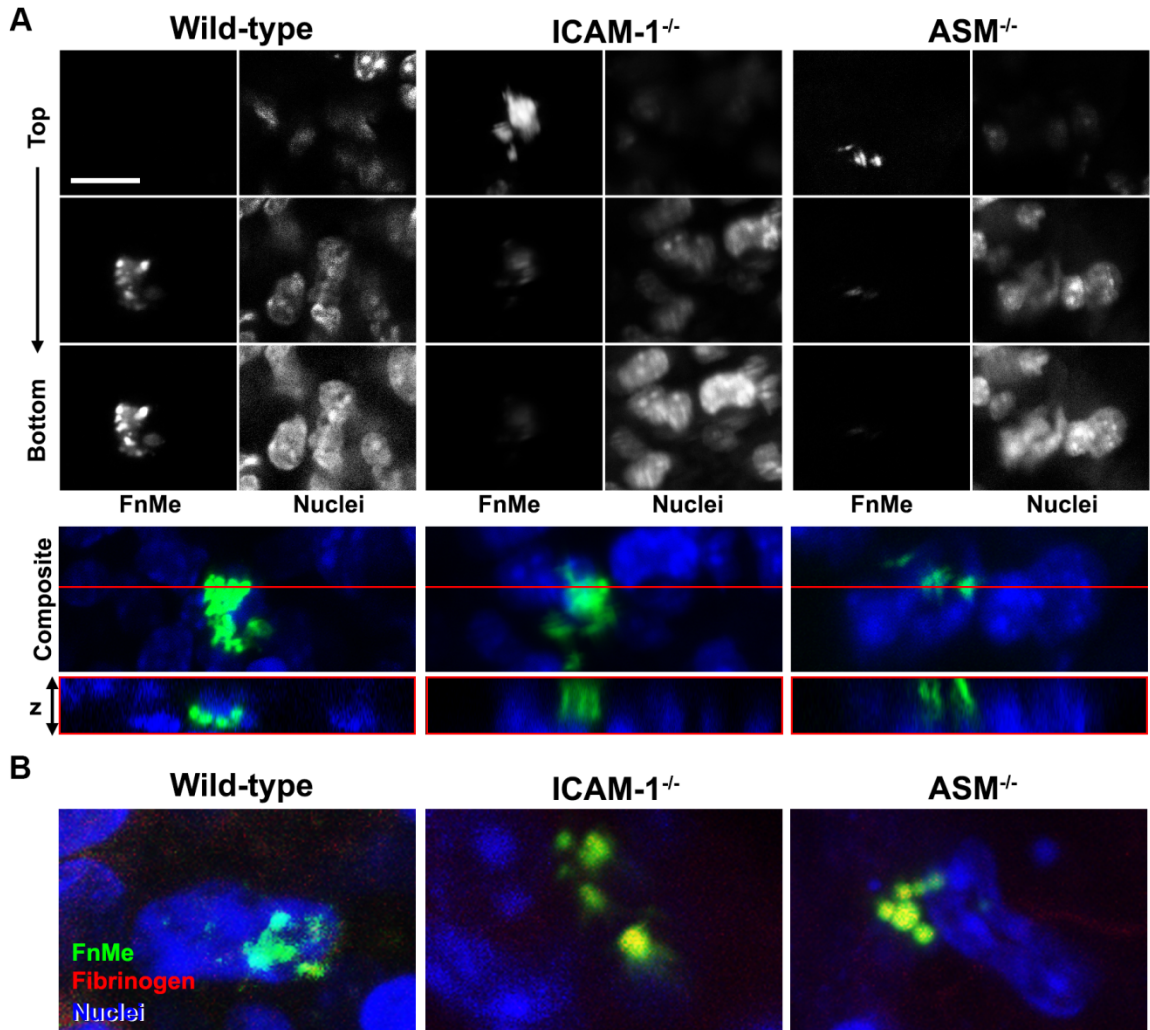


**Figure 38. Confocal analysis of fibrin microemboli interaction with cells in mouse lungs.** Wild-type, ICAM-1 knockout (-/-), or ASM knockout mice were injected with AF488 (green fluorescently labeled) fibrin microemboli (FnMe), followed by a 1.5-hour incubation. In (B) mice were then injected with AF594 (red fluorescently labeled) fibrinogen. (A) Z-sections of FnMe associated with alveolar cells from the top of cells, where nuclei are not visible, to the plane where nuclei are visible. Bottom panels show a maximum-intensity composite and a reconstruction of the z-axis at the site indicated by a red horizontal line. Scale bar = 30  $\mu$ m. (B) Maximum-intensity composite showing green FnMe and red fibrinogen (which appear as yellow when colocalizing).

To corroborate this, we injected green fibrin microemboli for 1.5 hours, followed by injection of red fibrinogen. This circulating red fibrinogen could potentially be incorporated into green microemboli adhered to the endothelial surface. As seen in Figure 38B, in wild-type mice, green microemboli did not overlap with red, suggesting that

microemboli were internalized and not accessible to circulating fibrinogen. Meanwhile, in both knockout strains there was colocalization of green microemboli and injected red fibrin(ogen). This supported the lack of internalization of these materials ICAM-1 and ASM knockout mice, which may possibly reignite fibrin formation from the injected fibrinogen.

Although this technique does not provide sufficient resolution to confirm a deficiency in fibrin microemboli internalization for CAM-mediated pathway-deficient mice, other members of our group have validated these results using electron microscopy. These data show that in wild-type mice endothelial cells exhibit fibrous structures on their surface 30 minutes after injection with fibrin microemboli. These structures disappear from the endothelial surface at 3 hours, while electron dense vesicles appear inside the endothelium. In contrast, in ICAM-1 knockout mice, fibrin microemboli remain as fibrous structures on the surface of the cell even at 3 hours. (Muro, unpublished data).

With this evidence that CAM-mediated uptake of fibrin microemboli may occur *in vivo*, we explored a possible physiological function of this endocytosis. As mentioned previously, it is possible that endothelial uptake of blood clot fragments/remnants on the endothelial surface could serve to prevent re-initiation of clotting. Not only would this be relevant in the natural resolution of clotting after wound healing, but could also have implications in the context of vessel re-occlusion following induced thrombolysis in a clinical context [256]. Thus, we tested this in mouse brains because clot-related pathologies in this organ have high clinical significance (e.g.: a major cause of stroke is brain embolism). We injected mice with different formulations as will be described

below, and used two-photon microscopy to image and quantify the number of fibrin microemboli found in  $400 \times 400 \mu\text{m}^2$  regions of post-mortem brain tissue (see Methods, Section 3.18 for details).

To test for re-initiation of clotting after induced thrombolysis, we designed the following treatment consisting of three injections: First, inject non-fluorescent fibrin microemboli, such that they would accumulate in mouse brain tissue. Then, inject tPA in order to induce fibrinolysis, which, as speculated, still leaves fibrin remnants on the endothelial surface that could re-initiate clotting if not internalized by the endothelium. Finally, inject fluorescent fibrinogen, which would serve as a detectable circulating pool of monomer for new clotting if this occurs.

Prior to this experiment, we confirmed its feasibility by characterizing our model in wild-type mice. As shown in Figure 39, injection of (red) fluorescent fibrin microemboli led to accumulation of  $28.9 \pm 4.0$  microemboli per field ( $2.3 \pm 0.1 \mu\text{m}$  in diameter, similar to dimensions observed in cell culture). Furthermore, injection of non-fluorescent microemboli followed by (red) fluorescent fibrinogen led to the detection of  $23.7 \pm 3.5$  microemboli. This showed that injected microemboli can accumulate in mouse brains, and also that injected circulating fibrinogen could interact with endothelium-adhered fibrin materials.

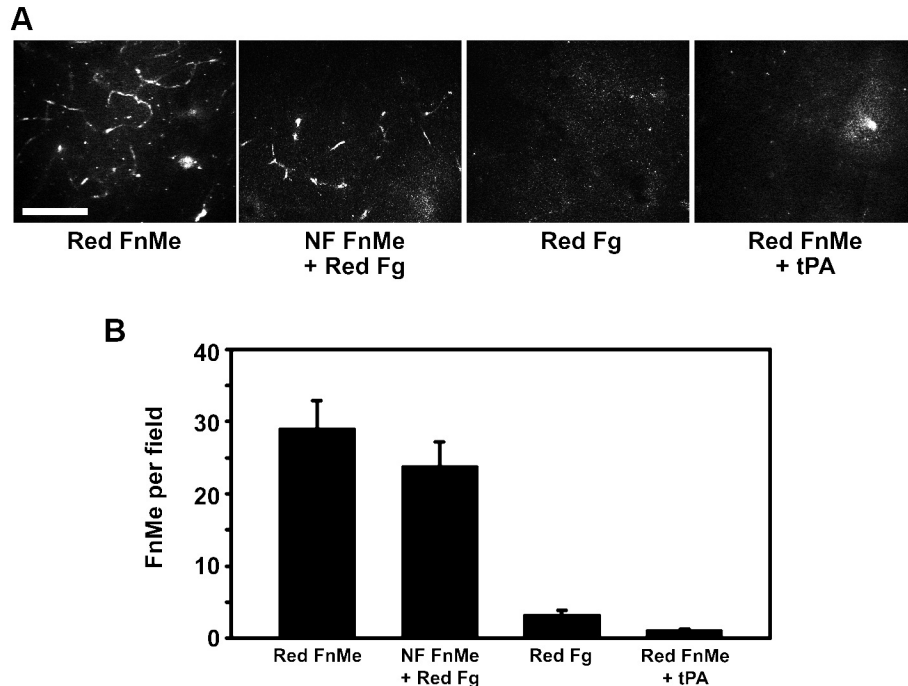


**Figure 39. Model to study fibrin microemboli in the brain *in vivo*.** Two-photon microscopy was used to observe mouse brain tissue after injection of several formulations of fibrin microemboli (FnMe). Formulations are detailed in Methods, Section 3.18. In short, from left to right: AF594 fluorescent (red) FnMe; non-fluorescent (NF) FnMe followed by red fibrinogen (Fg); red fibrinogen; red FnMe followed by tPA. (A) Sample micrographs for each treatment. Scale bar = 100  $\mu\text{m}$  (B) Quantification of FnMe per field for each treatment. Data represent mean  $\pm$  standard error of the mean.

Meanwhile, injection of only fluorescent fibrinogen into wild-type mice resulted in detection of  $3.14 \pm 2.1$  microemboli, which possibly corresponds to background levels of fibrinogen deposition on the endothelium, or background coagulation. This shows that in this model, mice were not prone to accumulate injected fibrinogen or form clots unless previously injected with microemboli. Finally, injection of fluorescent microemboli followed by tPA injection revealed  $0.94 \pm 0.3$  microemboli, showing that tPA injection could induce microemboli fibrinolysis. Although we were not able to directly detect the presence of remnants after tPA-induced fibrinolysis using this technique, other members of our group have shown evidence of this in mice after similar injection regimes (Muro, unpublished data).

We next tested our model in ICAM-1 knockout or ASM knockout mice. First, we compared fibrin microemboli accumulation in wild-type versus ICAM-1 knockout brains because our cell culture experiments showed that ICAM-1 was important in fibrin microemboli binding (Figure 40A). However, our *in vivo* data showed no difference in fibrin microemboli accumulation in mouse brains ( $26.9 \pm 2.5$  microemboli in ICAM-1 knockout brains versus  $28.9 \pm 4.0$  in wild-type). Since we did not induce inflammation to overexpress ICAM-1 in our mouse model and other endothelial molecules could contribute to binding, this result is reasonable. Also, mechanical entrapment could be contributing to fibrin microemboli accumulation, which would be independent of ICAM-1 expression.

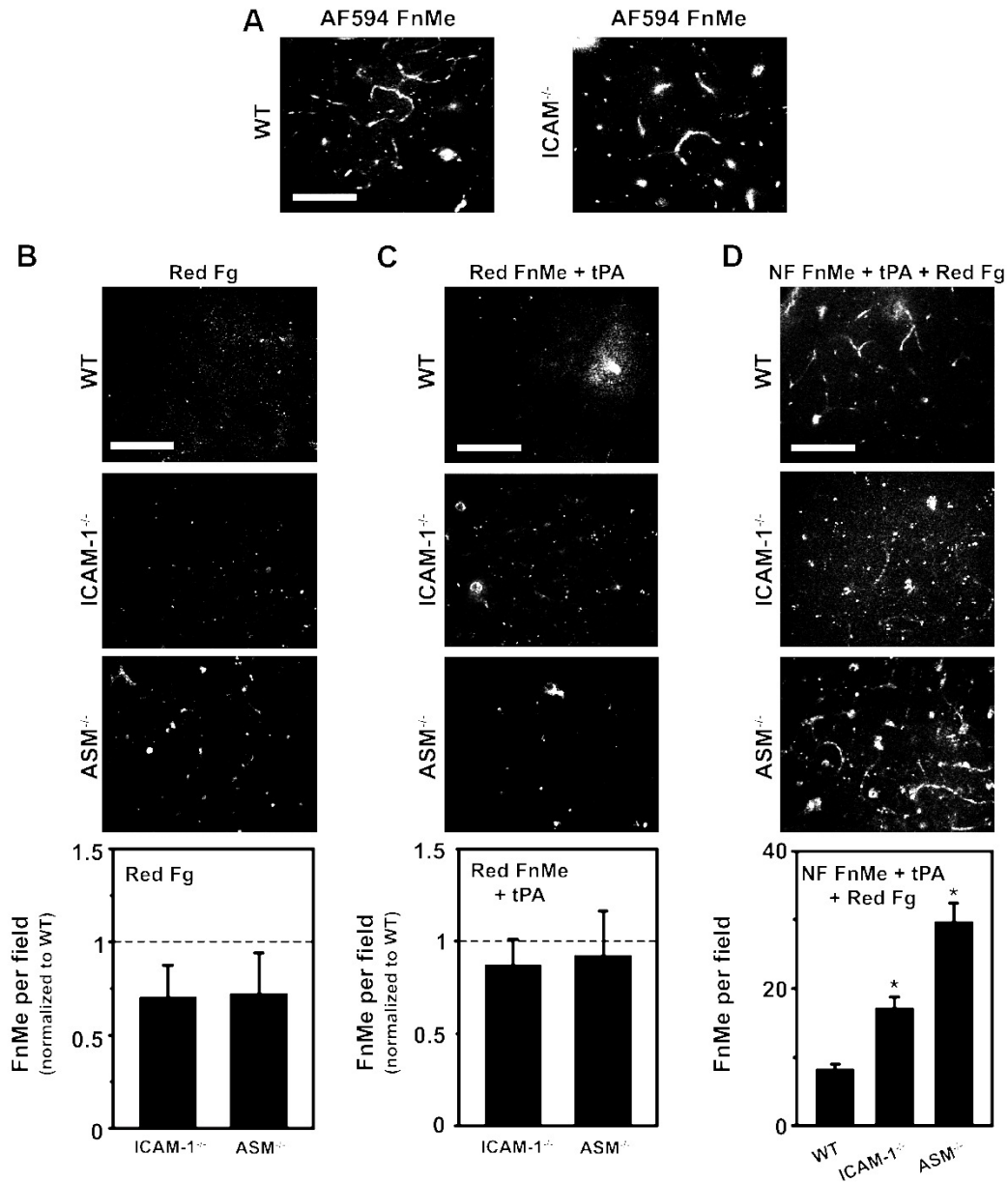


**Figure 40. Role of CAM-mediated endocytosis in fibrin microemboli clearance *in vivo*.** Two-photon microscopy was used to observe mouse brain tissue after injection of several formulations of fibrin microemboli (FfMe; as detailed in Methods, Section 3.18) in wild-type, ICAM-1 knockout (-/-), or ASM knockout mice. (A) Micrographs after injection of AF594 fluorescent (red) FfMe. (B-D) Micrographs and quantification of FfMe per field after injection of red fibrinogen (Fg; B), red FfMe followed by tPA (C), or non-fluorescent (NF) FfMe followed by tPA, followed by red fibrinogen (D). Scale bars = 100  $\mu$ m Data represent mean  $\pm$  standard error of the mean, and are normalized to wild-type in B and C. \* compares each value to wild-type ( $p < 0.05$  by Student's *t*-test).

Next, we compared injection of (red) fluorescent fibrinogen, to determine the basal levels of fibrinogen accumulation on the endothelium or background clotting in

knockout mice. As shown in Figure 40B, both knockout mouse strains showed similar basal levels of detected fibrin microemboli to wild-type, suggesting that the knockout strains did not have a predisposition for fibrin(ogen) deposition/clotting compared to wild-type. Then, we injected of (red) fluorescent fibrin microemboli followed by tPA in both knockout strains to determine the levels of fibrinolysis in these strains. This revealed low accumulation of microemboli similar to wild-type background (Figure 40C), indicating tPA-induced fibrinolysis was successful in both knockout strains.

With these controls in place, we injected non-fluorescent fibrin microemboli (which would accumulate in brain tissue, as seen with fluorescent microemboli), followed by tPA (to induce fibrinolysis), and finally (red) fluorescent fibrinogen (which could potentially be incorporated into new clots, and allow for their detection). As shown in Figure 40D, after this treatment, wild-type mice showed  $8.0 \pm 0.9$  microemboli per field, while ICAM-1 knockout and ASM knockout mice showed  $17.0 \pm 1.7$  and  $29.6 \pm 2.7$  microemboli, respectively. With our compounded data, this result suggests that in the absence of ICAM-1 and key elements of CAM-mediated endocytosis (acid sphingomyelinase), there was no endothelial uptake of tPA-induced fibrin microemboli remnants, leading to re-clotting, which could be detected upon injection of fluorescent fibrinogen. Thus, these *in vivo* data support a role for CAM-mediated endocytosis in the internalization of fibrin remnants by endothelial cells, effectively clearing from the vasculature post-fibrinolytic materials that could re-initiate coagulation.

### 6.3. Conclusion

The interaction between blood clots and endothelial cells evidently involves more than mechanical adherence, as several signaling mechanisms are activated once fibrinogen or fibrin materials interact with the endothelium [20, 72, 174, 257]. Beyond induction of angiogenesis and endothelial cytoskeleton rearrangement, previous studies show that this interaction can also prompt endothelial cells to engulf and transport clots out of the vasculature [22]. Expanding this current knowledge, our studies presented here show that endothelial cells can use the ICAM-1-dependent CAM-mediated pathway for internalization and intracellular degradation of fibrin polymers.

We show that fibrin meshes and microemboli, a model for blood clot remnants/fragments, interact with endothelial cells in an ICAM-1-dependent manner, leading to enrichment of this molecule at binding sites, and also accompanied by enrichment of molecular players of CAM-mediated endocytosis, NHE1 and acid sphingomyelinase. Following binding, these fibrin materials are internalized by endothelial cells in a manner consistent with CAM-mediated endocytosis, both through its kinetics and its sensitivity to chemical inhibitors. After internalization, fibrin meshes follow a trafficking itinerary similar to that observed after CAM-mediated uptake of polystyrene-latex particles. This involves trafficking to lysosomes, where fibrin meshes are degraded. These results are supported by *in vivo* data that suggest uptake of injected fibrin microemboli occurs in wild-type mice, but not in ICAM-1 and ASM knockout mice, both of which are deficient in CAM-mediated uptake. Importantly, this endocytic pathway appears to be involved in maintaining the effective clearance of clots or clot remnants after fibrinolysis.

Based on our findings from Chapter 4, it might be possible that CAM-mediated endocytosis is also used for the transcellular transport of internalized fibrin materials. Indeed, colocalization of  $\gamma 3$  particles (which bind using the same peptide sequence as fibrin) with lysosomes is only partial (~70% colocalization) and these particles exhibit transport across endothelial monolayers. The similarly partial colocalization percentages found with our fibrin mesh model (~60% at maximum levels), may be an indication that a fraction of internalized fibrin polymers are also transported across cells. Thus, it is plausible that physiologically, a certain fraction of clot remnants are degraded in lysosomes, while another fraction undergo transcytosis and are degraded outside of the vasculature possibly by resident macrophages [241]. Our data from Chapter 4 suggesting that micron-sized objects are transported more efficiently than nanometer-sized counterparts may hold a key to understanding this potential divergent trafficking. Indeed, the extravasation observed in previous reports was observed for large clot fragments several microns in diameter [22].

## Chapter 7: Overall Conclusions

### *7.1. Summary of Results, Significance, and Novelty*

CAM-mediated endocytosis is a pathway elicited when drug carriers bind multiple copies of ICAM-1 on the cell surface. Signaling events associated with this binding culminate in the uptake of drug carriers of a wide range of sizes [6, 77], which can be used as a strategy for delivery of therapeutics into cells. Despite significant efforts at characterizing ICAM-1-dependent CAM-mediated endocytosis for drug delivery [6-9, 77, 101, 258-260], some of the regulatory mechanisms behind this pathway have not been fully elucidated. Furthermore, the possible physiological role of this endocytic pathway in endothelial cells remains unexplored. Motivated by these gaps in knowledge, the studies presented in this dissertation provide insight into the regulation of CAM-mediated drug delivery and the possible biological significance of this endocytic pathway. In short, this work expands our ability to optimize the design of drug carriers targeted to CAM-mediated endocytosis by changing ICAM-1-targeted particle size and targeting moiety. In addition, this work provides significant evidence to assign a link between CAM-mediated endocytosis and the process of leukocyte transmigration, as well as endothelial uptake of fibrin materials.

### 7.1.1. Role of drug carrier size and targeting moiety on the outcomes of ICAM-1-mediated endocytosis.

First, we show through the use of ICAM-1-targeted particles of different sizes and coated with different targeting moieties (anti-ICAM versus  $\gamma 3$  peptide), that these two parameters can significantly affect the outcomes of CAM-mediated endocytosis. Anti-ICAM particles bind to ICAM-1 on cells with higher efficiency than  $\gamma 3$  counterparts, although concomitant endocytosis can mitigate this difference. Increasing the size of ICAM-1-targeted particles lowers the initial efficiency of their uptake, yet after sufficient time, endothelial cells can endocytose particles of a wide range of sizes. Although this holds true for both anti-ICAM and  $\gamma 3$  particles, it appears that internalization of  $\gamma 3$  particles is less efficient as particle size increases. Helping explain this, we provide data suggesting that higher ceramide production during CAM-mediated endocytosis is required as particle size increases. This is in agreement with other studies showing that ceramide is particularly suited to generate large membrane compartments and vesicular fusion [83, 86, 238]. Since  $\gamma 3$  particles appear to elicit low ceramide levels regardless of their size, they show consistently lower rates of CAM-mediated uptake. After internalization, micron-sized particles have a tendency to avoid lysosomes and be transported across cells more readily compared to nanoparticles. Meanwhile,  $\gamma 3$  nanoparticles elicit lower lysosome trafficking and higher transport across cells compared to anti-ICAM particles of the same size.

Overall, these results confirm previous reports by showing that the size and coating of ICAM-1-targeted particles can be manipulated to modulate the behavior of CAM-mediated endocytosis [77, 101]. However, the data presented here provide new

knowledge regarding the involvement of ceramide during this regulation, information about the use of  $\gamma 3$  particles specifically, and novel findings regarding transport across cell barriers. This knowledge will prove useful to preferentially regulate CAM-mediated drug carrier uptake rates, trafficking to lysosomes, and transport across cells.

Furthermore, it is possible that these findings can have implications in the physiological function of CAM-mediated endocytosis, or other endocytic pathways. For example, although the concept of endocytosis and trafficking regulation due to ligand geometry has been considered in the past [96, 261-263], this is, to our knowledge, the first study to suggest a relationship between particle size, internalization, and the level of sphingomyelinase-driven ceramide enrichment. Since ceramide is gaining recognition as an important modulator of endocytosis, our results could have implications in this context. Indeed, the variety of materials internalized in a ceramide-dependent manner present a considerably wide range of sizes (from micron-sized *Trypanosoma cruzi* [264] to nanometer-sized viruses [13]).

#### 7.1.2. Role of ICAM-1-mediated endocytosis in leukocyte transmigration.

Next, we show that the processes that precede lymphocyte transmigration as well as transmigration itself are dependent on key molecules of the CAM-mediated pathway. Using chemical inhibition, we see that NHE1 and acid sphingomyelinase, but not caveolae, are needed for the development of lymphocyte sampling. Furthermore, these molecules are required for transmigration of lymphocytes across HUVECs on porous membranes. Finally, inhibition of these molecules specifically disrupts the transcellular route of transmigration without affecting paracellular events.

These findings are supported by the fact that inhibition of NHE1 prevents accumulation of leukocytes at inflammatory sites in mice [265], while NHE1 null mice are protected from inflammation-related injuries [266]. Our results also highlight for the first time a mechanistic link between ceramide production by endothelial acid sphingomyelinase and transmigration, which helps explain previous findings that link ceramide to the inflammatory response. This includes events such as decreased leukocyte influx into alveolar space in acid sphingomyelinase knockout mice [229], and higher levels of leukocytes in tissue under metabolic imbalances that cause high levels of ceramide [267].

It is believed that although paracellular transmigration is tightly regulated, it might be used under scenarios in which the integrity of the endothelium is not of prime importance or is already compromised, such as pathological states and inflammation. Conversely, transcellular migration is thought to be more prevalent for surveillance functions, and also at specific sites such as the blood-brain barrier and lymph nodes [17]. Our findings presented here open new avenues of study to examine whether CAM-mediated endocytosis is preferentially activated in these conditions or by these specific cell types, and if so, what drives this preferential activation. In turn, this knowledge will be useful in the development of clinical interventions during situations where the regulation between paracellular and transcellular transmigration might be disrupted, causing excessive opening of the endothelial monolayer [268, 269].

In addition to ICAM-1, when antibody-coated drug carriers bind multiple copies of PECAM-1, CAM-mediated uptake is activated. Since PECAM-1 is also a major contributor to leukocyte transmigration, it is possible that the mechanisms through which

this molecule contributes to transmigration also relate to CAM-mediated endocytosis. Most recent data on leukocyte transmigration show that vesicular dynamics associated with PECAM-1 are involved in transcellular transmigration, supporting this idea [130, 131]. This opens the possibility that other CAMs may be associated with CAM-mediated endocytosis and help regulated leukocyte transmigration. Indeed, activated leukocyte cell adhesion molecule (ALCAM), CD47 and ICAM-2 have been implicated in specialized forms of transmigration [270-272]. Whether the engagement of these molecules by leukocytes directly elicits the signaling responses and morphological changes seen with ICAM-1 remains to be determined. However, our data encourage study of the involvement of other CAMs in transmigration within the context of CAM-mediated uptake.

#### 7.1.3. Role of ICAM-1-mediated endocytosis in clearance of blood clot fragments/remnants.

Finally, our data also show that fibrin polymers (mimicking the remnants/fragments or clot fibrinolysis) bind to endothelial cells at sites enriched in ICAM-1, NHE1 and acid sphingomyelinase. After binding of fibrin meshes/microemboli, endothelial cells can internalize these micron-sized fibrin polymers without requiring their extracellular degradation. This uptake is dependent on regulatory elements of the CAM-mediated pathway, although other internalization mechanisms may also contribute to uptake. Finally, after internalization, fibrin meshes traffic to lysosomes, where fibrin is degraded. In mice, this endocytosis appears to protect the endothelium from re-initiation of clot growth.

Our studies shed light on the possible mechanism used for the recently described novel endothelial function of clot extravasation [22], which here we show may correspond to CAM-mediated endocytosis. Indeed, using porous membranes, we show that these clot-fragment mimicking fibrin meshes appear to be transported across cells. In our case, we also identify that a fraction of internalized fibrin meshes colocalizes with lysosomes, which is followed by lysosomal degradation of internalized fibrin objects. However, this colocalization is partial, and may be affected by factors such as fibrin mesh size and the fact that our studies were done on coverslips. Thus, it is possible that endothelial cells are equipped to both transport clots into tissue, and also degrade them in lysosomes. This clearance by the endothelium might be a mechanism for prevention of recurrent formation of clots after fibrinolysis, or housekeeping maintenance of the basal liquid state of blood. Abnormalities in ICAM-1-dependent uptake may be a cause for clot-related pathologies, bringing important clinical significance to our results. Indeed, thrombosis and vessel re-occlusion represent one of the most common causes of disability and mortality in certain countries such as the USA, associated to acute and chronic vascular pathologies [161]. Our findings could serve for development of interventions for thrombosis-associated conditions, such as ischemic stroke, deep vein thrombosis, atherosclerosis, hypertension, and diabetes.

Overall, the findings explored in this dissertation contribute to the field of carrier-assisted drug delivery through a better understanding of how endothelial cells respond to objects with different physical properties. Furthermore, they shed light on the function of the endothelium, promoting further study and opening avenues for clinical intervention.

## 7.2. Future Directions

Beyond the contributions of this work to the understanding of CAM-mediated endocytosis and endothelial function, a variety of potential studies emerge from our data and interpretations.

In the context of drug delivery, future studies should be performed in order to more systematically understand the role of particle size and valency on the outcomes of CAM-mediated endocytosis. This could be done by using particles of different sizes as done in these studies, but also coated with different densities of anti-ICAM or  $\gamma 3$  on their surface. Antibody coating densities on the surface of particles could be matched for different sizes in order to determine the extent of binding, ceramide enrichment, internalization, lysosome trafficking, and transport. In this context, it will be important to determine the avidity of each particle formulation and relate this parameter to the outcomes of the CAM-mediated pathway. Our experimental design did not compare the trafficking and transport rates of  $\gamma 3$  particles of different sizes. However, as seen with anti-ICAM particles, size is an important parameter defining the outcomes of CAM-mediated uptake. Future work should aim at studying this size relationship by coating particles of different sizes with  $\gamma 3$  and comparing their trafficking to lysosomes and transport across cells. Not only would this be significant in the context of drug delivery, but it could also serve as a preliminary model to understand how binding of ICAM-1 by fibrin polymers (such as clot fragments) of different sizes can affect binding, internalization and intracellular trafficking of these physiologically relevant materials.

Finally, it is known that anti-ICAM clone R6.5 used in our studies and  $\gamma 3$  bind to different epitopes of ICAM-1. However, any epitope-related effects that may have been

manifested in our studies were potentially confounded by other differences between anti-ICAM and  $\gamma 3$ . For instance, since anti-ICAM is a full antibody, it contains an Fc region that may bind to Fc receptors on endothelial cells and elicit additional responses. Previous data suggest that this is unlikely since the interaction between IgG-coated particles and endothelial cells does not involve significant binding or induce substantial endocytosis [189, 190]. However, this may be addressed by coating particles only with the F(ab')<sub>2</sub> region of anti-ICAM. Furthermore, anti-ICAM and  $\gamma 3$  have different affinities to ICAM-1. Thus, it will be interesting, thus, to coat particles with targeting moieties that bind different epitopes of ICAM-1 with similar affinity (including a variety of available antibodies to ICAM-1) and determine if and how this affects the outcomes of CAM-mediated uptake.

In the context of leukocyte transmigration, it will be important to perform similar sampling and transmigration assays using genetic models in order to validate the role of CAM-mediated endocytosis. For example, transmigration assays should be repeated using wild-type leukocytes incubated with ICAM-1, NHE1 and acid sphingomyelinase knockout or knockdown endothelial cells. Meanwhile, using ICAM-1, NHE1 and acid sphingomyelinase knockout or knockdown lymphocytes with wild-type endothelial cells will further help elucidate the role of endothelial CAM-mediated endocytosis in transmigration.

Time-lapse imaging of leukocyte transmigration *in vivo* after staining endothelial junctions will allow for more physiologically relevant exploration of these phenomena and account for the role of blood flow and other factors. Such *in vivo* experiments could be performed using the aforementioned mouse knockout strains, if budget permits, after

bone-marrow transplantation to allow the *in vivo* interaction between wild-type leukocytes and knockout endothelium.

As mentioned earlier, leukocyte transmigration rates differ depending on the endothelial cell type, the leukocyte type, and the activation conditions. Thus, it will be important to extend these studies to other leukocytes, including macrophages and neutrophils. Also, future work should look at other endothelial cell types, such as brain endothelial cells and endothelial cells from high endothelial venules, which are thought to exhibit higher rates of transcellular transmigration. Furthermore, it is known that leukocytes can migrate across non-endothelial cells, and it has been recently shown that they can migrate transcellularly across fibroblasts [273]. The mechanisms behind these events, and whether or not they relate to CAM-mediated endocytosis, will be important to consider, particularly with the knowledge that the CAM-mediated pathway occurs in other cell types including fibroblasts [274] and epithelial cells [10].

Regarding clot remnant uptake, our model did not vary the properties of fibrin meshes, which could affect clot resolution, degradation and trafficking itinerary. Thus, future studies could observe fibrin mesh endocytosis using different ratios of thrombin to fibrinogen to vary mesh size, density and level of cross-linking. In particular, our data suggest that particles directed to the epitope on ICAM-1 bound by fibrin ( $\gamma 3$  particles) could be internalized in a size-restrictive manner. Furthermore, we have observed that particle size can regulate lysosome trafficking versus transport across cells. Thus, developing a system that permits systematic probing of different clot fragment sizes and how this might affect their uptake, degradation and possible transport across the endothelium, will be important. Finally, it will be crucial to determine the functional

significance of CAM-mediated clearance of blood clot remnants in mouse models by performing time-lapse experiments that measure blood flow as an indicator of vessel blockade, and also in well-established mouse models of clot-related pathologies, such as ischemia-reperfusion, deep-vein thrombosis, and atherosclerosis. In addition to this, our experimental design was such that mice were injected with thrombin-containing fibrin microemboli formulations, which may have affected the integrity of the endothelium and confounded our results [275]. Thus, future work should account for this by measuring endothelial permeability under the thrombin concentrations found in our fibrin microemboli formulations, or add thrombin-inhibiting agents to the formulation prior to injection.

It is possible that ICAM-1-triggered CAM-mediated endocytosis has other functions beyond those explored in this dissertation. Primarily, some pathogens bind to ICAM-1, including rhinovirus, poliovirus, HIV [276], and *Plasmodium falciparum*-infected erythrocytes during malarial infection [277]. In addition, some bacteria may bind to glycosylated residues of ICAM-1 [278] and exploit CAM-mediated transcytosis across the gastrointestinal or lung epithelium. Future work should address potential subversion of CAM-mediated endocytosis by these pathogens for cell/tissue invasion, eventually leading to the development of therapeutic interventions.

## Literature Cited

1. Aird, W.C., *Endothelium as an organ system*. Crit Care Med, 2004. **32**(5 Suppl):S271-9.
2. Dustin, M.L., et al., *Induction by IL 1 and interferon-gamma: tissue distribution, biochemistry, and function of a natural adherence molecule (ICAM-1)*. J Immunol, 1986. **137**(1):245-54.
3. Dustin, M. and T. Springer, *Lymphocyte function-associated antigen-1 (LFA-1) interaction with intercellular adhesion molecule-1 (ICAM-1) is one of at least three mechanisms for lymphocyte adhesion to cultured endothelial cells*. J Cell Biol, 1988. **107**(1):321-31.
4. Lisby, S., et al., *Intercellular adhesion molecule-1 (ICAM-1) expression correlated to inflammation*. Br J Dermatol, 1989. **120**(4):479-84.
5. Serrano, D. and S. Muro, *Endothelial cell adhesion molecules and drug delivery applications*, in *Mechanobiology of the Endothelium*, H. Aranda-Espinoza, Editor. 2014, CRC Press: Boca Raton. In press.
6. Muro, S., et al., *A novel endocytic pathway induced by clustering endothelial ICAM-1 or PECAM-1*. J Cell Sci, 2003. **116**(8):1599-609.
7. Serrano, D., et al., *Intercellular adhesion molecule 1 engagement modulates sphingomyelinase and ceramide, supporting uptake of drug carriers by the vascular endothelium*. Arterioscler Thromb Vasc Biol, 2012. **32**(5):1178-85.

8. Muro, S., et al., *Control of intracellular trafficking of ICAM-1-targeted nanocarriers by endothelial Na<sup>+</sup>/H<sup>+</sup> exchanger proteins*. *Am J Physiol Lung Cell Mol Physiol*, 2006. **290**(5):L809-17.
9. Muro, S., et al., *ICAM-1 recycling in endothelial cells: a novel pathway for sustained intracellular delivery and prolonged effects of drugs*. *Blood*, 2005. **105**(2):650-8.
10. Ghaffarian, R., T. Bhowmick, and S. Muro, *Transport of nanocarriers across gastrointestinal epithelial cells by a new transcellular route induced by targeting ICAM-1*. *J Control Release*, 2012. **163**(1):25-33.
11. Hsu, J., J. Rappaport, and S. Muro, *Specific binding, uptake, and transport of ICAM-1-targeted nanocarriers across endothelial and subendothelial cell components of the blood-brain barrier*. *Pharm Res*, 2014. **31**(7):1855-66.
12. Jo, J.H., et al., *Recycling and LFA-1-dependent trafficking of ICAM-1 to the immunological synapse*. *J Cell Biochem*, 2010. **111**(5):1125-37.
13. Grassmé, H., et al., *Rhinoviruses infect human epithelial cells via ceramide-enriched membrane platforms*. *J Biol Chem*, 2005. **280**(28):26256-62.
14. Staunton, D.E., et al., *A cell adhesion molecule, ICAM-1, is the major surface receptor for rhinoviruses*. *Cell*, 1989. **56**(5):849-53.
15. Kurzinger, K., et al., *A novel lymphocyte function-associated antigen (LFA-1): cellular distribution, quantitative expression, and structure*. *J Immunol*, 1981. **127**(2):596-602.
16. Doolittle, R.F., *Fibrinogen and fibrin*. *Annu Rev Biochem*, 1984. **53**:195-229.

17. Wittchen, E.S., *Endothelial signaling in paracellular and transcellular leukocyte transmigration*. Front Biosci, 2009. **14**:2522-45.
18. Tsakadze, N.L., Z. Zhao, and S.E. D'Souza, *Interactions of intercellular adhesion molecule-1 with fibrinogen*. Trends Cardiovasc Med, 2002. **12**(3):101-8.
19. Etienne-Manneville, S., et al., *ICAM-1-coupled cytoskeletal rearrangements and transendothelial lymphocyte migration involve intracellular calcium signaling in brain endothelial cell lines*. J Immunol, 2000. **165**(6):3375-83.
20. Tyagi, N., et al., *Fibrinogen induces endothelial cell permeability*. Mol Cell Biochem, 2008. **307**(1-2):13-22.
21. Rahman, A. and F. Fazal, *Hug tightly and say goodbye: role of endothelial ICAM-1 in leukocyte transmigration*. Antioxid Redox Signal, 2009. **11**(4):823-39.
22. Lam, C.K., et al., *Embolus extravasation is an alternative mechanism for cerebral microvascular recanalization*. Nature, 2010. **465**(7297):478-82.
23. Rothlein, R., et al., *A human intercellular adhesion molecule (ICAM-1) distinct from LFA-1*. J Immunol, 1986. **137**(4):1270-4.
24. Pober, J.S., et al., *Overlapping patterns of activation of human endothelial cells by interleukin 1, tumor necrosis factor, and immune interferon*. J Immunol, 1986. **137**(6):1893-6.
25. Makgoba, M.W., et al., *Functional evidence that intercellular adhesion molecule-1 (ICAM-1) is a ligand for LFA-1-dependent adhesion in T cell-mediated cytotoxicity*. Eur J Immunol, 1988. **18**(4):637-40.

26. Boyd, A. and S. Wawryk, *Intercellular adhesion molecule 1 (ICAM-1) has a central role in cell-cell contact-mediated immune mechanisms*. Proc Natl Acad Sci USA, 1988. **85**(9):3095-99.
27. Siu, G., S.M. Hedrick, and A.A. Brian, *Isolation of the murine intercellular adhesion molecule 1 (ICAM-1) gene. ICAM-1 enhances antigen-specific T cell activation*. J Immunol, 1989. **143**(11):3813-20.
28. Van Seventer, G.A., et al., *The LFA-1 ligand ICAM-1 provides an important costimulatory signal for T cell receptor-mediated activation of resting T cells*. J Immunol, 1990. **144**(12):4579-86.
29. Neumayer, H.P., et al., *Importance of ICAM-1 for accessory cell function of monocytic cells*. Immunobiology, 1990. **180**(4-5):458-66.
30. Dang, L.H., et al., *Role of ICAM-1 in antigen presentation demonstrated by ICAM-1 defective mutants*. J Immunol, 1990. **144**(11):4082-91.
31. Wegner, C., et al., *Intercellular adhesion molecule-1 (ICAM-1) in the pathogenesis of asthma*. Science, 1990. **247**(4941):456-9.
32. Sobel, R.A., M.E. Mitchell, and G. Fondren, *Intercellular adhesion molecule-1 (ICAM-1) in cellular immune reactions in the human central nervous system*. Am J Pathol, 1990. **136**(6):1309-16.
33. Cosimi, A.B., et al., *In vivo effects of monoclonal antibody to ICAM-1 (CD54) in nonhuman primates with renal allografts*. J Immunol, 1990. **144**(12):4604-12.
34. Rothlein, R., et al., *A form of circulating ICAM-1 in human serum*. J Immunol, 1991. **147**(11):3788-93.

35. Casasnovas, J.M., et al., *A dimeric crystal structure for the N-terminal two domains of intercellular adhesion molecule-1*. Proc Natl Acad Sci USA, 1998. **95**(8):4134-9.
36. Staunton, D.E., et al., *Primary structure of ICAM-1 demonstrates interaction between members of the immunoglobulin and integrin supergene families*. Cell, 1988. **52**(6):925-33.
37. Casasnovas, J.M., J.K. Bickford, and T.A. Springer, *The domain structure of ICAM-1 and the kinetics of binding to rhinovirus*. J Virol, 1998. **72**(7):6244-6.
38. Marlin, S.D. and T.A. Springer, *Purified intercellular adhesion molecule-1 (ICAM-1) is a ligand for lymphocyte function-associated antigen 1 (LFA-1)*. Cell, 1987. **51**(5):813-9.
39. Pluskota, E., Y. Chen, and S.E. D'Souza, *Src homology domain 2-containing tyrosine phosphatase 2 associates with intercellular adhesion molecule 1 to regulate cell survival*. J Biol Chem, 2000. **275**(39):30029-36.
40. Federici, C., et al., *Association of the cytoplasmic domain of intercellular-adhesion molecule-1 with glyceraldehyde-3-phosphate dehydrogenase and beta-tubulin*. Eur J Biochem, 1996. **238**(1):173-80.
41. Carpen, O., et al., *Association of intercellular adhesion molecule-1 (ICAM-1) with actin-containing cytoskeleton and alpha-actinin*. J Cell Biol, 1992. **118**(5):1223-34.

42. Sans, E., E. Delachanal, and A. Duperray, *Analysis of the roles of ICAM-1 in neutrophil transmigration using a reconstituted mammalian cell expression model: implication of ICAM-1 cytoplasmic domain and Rho-dependent signaling pathway*. J Immunol, 2001. **166**(1):544-51.
43. Pattillo, C.B., et al., *ICAM-1 cytoplasmic tail regulates endothelial glutathione synthesis through a NOX4/PI3-kinase-dependent pathway*. Free Radic Biol Med, 2010. **49**(6):1119-28.
44. Qi, J., D.L. Kreutzer, and T.H. Piela-Smith, *Fibrin induction of ICAM-1 expression in human vascular endothelial cells*. J Immunol, 1997. **158**(4):1880-6.
45. Rahman, A., et al., *Thrombin-induced p65 homodimer binding to downstream NF-kappa B site of the promoter mediates endothelial ICAM-1 expression and neutrophil adhesion*. J Immunol, 1999. **162**(9):5466-76.
46. Myers, C.L., et al., *Induction of ICAM-1 by TNF-alpha, IL-1 beta, and LPS in human endothelial cells after downregulation of PKC*. Am J Physiol, 1992. **263**(4 Pt 1):C767-72.
47. Nie, Z., et al., *Expression and regulation of intercellular adhesion molecule-1 on airway parasympathetic nerves*. J Allergy Clin Immunol, 2007. **119**(6):1415-22.
48. Kusterer, K., et al., *Soluble ICAM-1 reduces leukocyte adhesion to vascular endothelium in ischemia-reperfusion injury in mice*. Am J Physiol, 1998. **275**(2 Pt 1):G377-80.
49. Diamond, M.S., et al., *ICAM-1 (CD54): a counter-receptor for Mac-1 (CD11b/CD18)*. J Cell Biol, 1990. **111**(6 Pt 2):3129-39.

50. D'Souza, S.E., et al., *Identification of an active sequence within the first immunoglobulin domain of intercellular cell adhesion molecule-1 (ICAM-1) that interacts with fibrinogen.* J Biol Chem, 1996. **271**(39):24270-7.
51. Duperray, A., et al., *Molecular identification of a novel fibrinogen binding site on the first domain of ICAM-1 regulating leukocyte-endothelium bridging.* J Biol Chem, 1997. **272**(1):435-41.
52. Greve, J.M., et al., *The major human rhinovirus receptor is ICAM-1.* Cell, 1989. **56**(5):839-47.
53. Berendt, A.R., et al., *Intercellular adhesion molecule-1 is an endothelial cell adhesion receptor for Plasmodium falciparum.* Nature, 1989. **341**(6237):57-9.
54. Kondo, N. and G.B. Melikyan, *Intercellular adhesion molecule 1 promotes HIV-1 attachment but not fusion to target cells.* PLoS One, 2012. **7**(9):e44827.
55. Selinka, H.C., A. Zibert, and E. Wimmer, *Poliovirus can enter and infect mammalian cells by way of an intercellular adhesion molecule 1 pathway.* Proc Natl Acad Sci USA, 1991. **88**(9):3598-602.
56. Heiska, L., et al., *Association of ezrin with intercellular adhesion molecule-1 and -2 (ICAM-1 and ICAM-2). Regulation by phosphatidylinositol 4, 5-bisphosphate.* J Biol Chem, 1998. **273**(34):21893-900.
57. Wójciak-Stothard, B., L. Williams, and A.J. Ridley, *Monocyte adhesion and spreading on human endothelial cells is dependent on Rho-regulated receptor clustering.* J Cell Biol, 1999. **145**(6):1293-307.

58. Thompson, P.W., A.M. Randi, and A.J. Ridley, *Intercellular adhesion molecule (ICAM)-1, but not ICAM-2, activates RhoA and stimulates c-fos and rhoA transcription in endothelial cells.* J Immunol, 2002. **169**(2):1007-13.
59. Oh, H.-M., et al., *RKIKK Motif in the Intracellular Domain Is Critical for Spatial and Dynamic Organization of ICAM-1 : Functional Implication for the Leukocyte Adhesion and Transmigration.* Mol Biol Cell, 2007. **18**(6):2322-35.
60. Etienne, S., et al., *ICAM-1 signaling pathways associated with Rho activation in microvascular brain endothelial cells.* J Immunol, 1998. **161**(10):5755-61.
61. Holland, J. and T. Owens, *Signaling through intercellular adhesion molecule 1 (ICAM-1) in a B cell lymphoma line. The activation of Lyn tyrosine kinase and the mitogen-activated protein kinase pathway.* J Biol Chem, 1997. **272**(14):9108-12.
62. Durieu-Trautmann, O., et al., *Intercellular adhesion molecule 1 activation induces tyrosine phosphorylation of the cytoskeleton-associated protein cortactin in brain microvessel endothelial cells.* J Biol Chem, 1994. **269**(17):12536-40.
63. Wang, Q., G.R. Pfeiffer, and W.A. Gaarde, *Activation of SRC tyrosine kinases in response to ICAM-1 ligation in pulmonary microvascular endothelial cells.* J Biol Chem, 2003. **278**(48):47731-43.
64. Adamson, P., et al., *Lymphocyte migration through brain endothelial cell monolayers involves signaling through endothelial ICAM-1 via a rho-dependent pathway.* J Immunol, 1999. **162**(5):2964-73.
65. Greenwood, J., et al., *Intracellular domain of brain endothelial intercellular adhesion molecule-1 is essential for T lymphocyte-mediated signaling and migration.* J Immunol, 2003. **171**(4):2099-108.

66. Wang, Q. and C.M. Doerschuk, *The p38 mitogen-activated protein kinase mediates cytoskeletal remodeling in pulmonary microvascular endothelial cells upon intracellular adhesion molecule-1 ligation*. J Immunol, 2001. **166**(11):6877-84.
67. Wang, Q., et al., *MKK3 and -6-dependent activation of p38alpha MAP kinase is required for cytoskeletal changes in pulmonary microvascular endothelial cells induced by ICAM-1 ligation*. Am J Physiol Lung Cell Mol Physiol, 2005. **288**(2):L359-69.
68. Amos, C., et al., *Cross-linking of brain endothelial intercellular adhesion molecule (ICAM)-1 induces association of ICAM-1 with detergent-insoluble cytoskeletal fraction*. Arterioscler Thromb Vasc Biol, 2001. **21**(5):810-6.
69. Wang, Q. and C.M. Doerschuk, *Neutrophil-induced changes in the biomechanical properties of endothelial cells: roles of ICAM-1 and reactive oxygen species*. J Immunol, 2000. **164**(12):6487-94.
70. Wang, Q., et al., *Changes in the biomechanical properties of neutrophils and endothelial cells during adhesion*. Blood, 2001. **97**(3):660-8.
71. Lawson, C. and S. Wolf, *ICAM-1 signaling in endothelial cells*. Pharmacol Rep, 2009. **61**(1):22-32.
72. Pluskota, E. and S.E. D'Souza, *Fibrinogen interactions with ICAM-1 (CD54) regulate endothelial cell survival*. Eur J Biochem, 2000. **267**(15):4693-704.
73. Lee, S.J., et al., *ICAM-1-induced expression of proinflammatory cytokines in astrocytes: involvement of extracellular signal-regulated kinase and p38 mitogen-activated protein kinase pathways*. J Immunol, 2000. **165**(8):4658-66.

74. Sano, H., et al., *Cross-linking of intercellular adhesion molecule-1 induces interleukin-8 and RANTES production through the activation of MAP kinases in human vascular endothelial cells*. *Biochem Biophys Res Commun*, 1998. **250**(3):694-8.
75. van Buul, J.D., et al., *Inside-out regulation of ICAM-1 dynamics in TNF-alpha-activated endothelium*. *PLoS ONE*, 2010. **5**(6):e11336.
76. Bollinger, C.R., V. Teichgräber, and E. Gulbins, *Ceramide-enriched membrane domains*. *Biochim Biophys Acta*, 2005. **1746**(3):284-94.
77. Muro, S., et al., *Control of endothelial targeting and intracellular delivery of therapeutic enzymes by modulating the size and shape of ICAM-1-targeted carriers*. *Mol Ther*, 2008. **16**(8):1450-8.
78. Clayton, A., et al., *Cellular activation through the ligation of intercellular adhesion molecule-1*. *J Cell Sci*, 1998. **111**(4):443-53.
79. Krunkosky, T.M. and C.L. Jarrett, *Selective regulation of MAP kinases and chemokine expression after ligation of ICAM-1 on human airway epithelial cells*. *Respir Res*, 2006. **7**:12.
80. Ding, B.S., et al., *Advanced drug delivery systems that target the vascular endothelium*. *Mol Interv*, 2006. **6**(2):98-112.
81. Holopainen, J.M., M.I. Angelova, and P.K. Kinnunen, *Vectorial budding of vesicles by asymmetrical enzymatic formation of ceramide in giant liposomes*. *Biophys J*, 2000. **78**(2):830-8.

82. Holopainen, J.M., M. Subramanian, and P.K. Kinnunen, *Sphingomyelinase induces lipid microdomain formation in a fluid phosphatidylcholine/sphingomyelin membrane*. *Biochemistry*, 1998. **37**(50):17562-70.
83. Zha, X., et al., *Sphingomyelinase treatment induces ATP-independent endocytosis*. *J Cell Biol*, 1998. **140**(1):39-47.
84. Tam, C., et al., *Exocytosis of acid sphingomyelinase by wounded cells promotes endocytosis and plasma membrane repair*. *J Cell Biol*, 2010. **189**(6):1027-38.
85. Utermöhlen, O., et al., *Fusogenicity of membranes: the impact of acid sphingomyelinase on innate immune responses*. *Immunobiology*, 2008. **213**(3-4):307-14.
86. Rogasevskaia, T. and J.R. Coorssen, *Sphingomyelin-enriched microdomains define the efficiency of native Ca(2+)-triggered membrane fusion*. *J Cell Sci*, 2006. **119**(13):2688-94.
87. Mebarek, S., et al., *Inhibition of de novo ceramide synthesis upregulates phospholipase D and enhances myogenic differentiation*. *J Cell Sci*, 2007. **120**(3):407-16.
88. Zeidan, Y.H., R.W. Jenkins, and Y.A. Hannun, *Remodeling of cellular cytoskeleton by the acid sphingomyelinase/ceramide pathway*. *The Journal of Cell Biology*, 2008. **181**(2):335-50.
89. Muro, S., et al., *Slow intracellular trafficking of catalase nanoparticles targeted to ICAM-1 protects endothelial cells from oxidative stress*. *Am J Physiol, Cell Physiol*, 2003. **285**(5):C1339-47.

90. Hauck, C.R., et al., *Acid sphingomyelinase is involved in CEACAM receptor-mediated phagocytosis of Neisseria gonorrhoeae*. FEBS Lett, 2000. **478**(3):260-6.
91. Gulbins, E., et al., *Ceramide, membrane rafts and infections*. J Mol Med, 2004. **82**(6):357-63.
92. Caron, E. and A. Hall, *Phagocytosis*, in *Endocytosis*, M. Marsh, Editor. 2001, Oxford University Press: Oxford. 58-77.
93. Rejman, J., et al., *Size-dependent internalization of particles via the pathways of clathrin- and caveolae-mediated endocytosis*. Biochem J, 2004. **377**(1):159-69.
94. Swanson, J.A., *Macropinocytosis*. Trends Cell Biol, 1995. **5**:424-8.
95. Vieira, O.V., R.J. Botelho, and S. Grinstein, *Phagosome maturation: aging gracefully*. Biochem J, 2002. **366**(3):689-704.
96. Koval, M., et al., *Size of IgG-opsionized particles determines macrophage response during internalization*. Exp Cell Res, 1998. **242**(1):265-73.
97. Yoo, J.-W., N. Doshi, and S. Mitragotri, *Endocytosis and intracellular distribution of PLGA particles in endothelial cells: effect of particle geometry*. Macromol Rapid Comm, 2010. **31**(2):142-48.
98. Wiewrodt, R., et al., *Size-dependent intracellular immunotargeting of therapeutic cargoes into endothelial cells*. Blood, 2002. **99**(3):912-22.
99. Chithrani, B.D. and W.C.W. Chan, *Elucidating the mechanism of cellular uptake and removal of protein-coated gold nanoparticles of different sizes and shapes*. Nano Lett, 2007. **7**(6):1542-50.
100. Gratton, S.E.A., et al., *The effect of particle design on cellular internalization pathways*. Proc Natl Acad Sci USA, 2008. **105**(33):11613-8.

101. Garnacho, C., et al., *Differential intra-endothelial delivery of polymer nanocarriers targeted to distinct PECAM-1 epitopes*. J Control Release, 2008. **130**(3):226-33.
102. Smith, C.W., et al., *Cooperative interactions of LFA-1 and Mac-1 with intercellular adhesion molecule-1 in facilitating adherence and transendothelial migration of human neutrophils in vitro*. J Clin Invest, 1989. **83**(6):2008-17.
103. Diamond, M.S., et al., *Binding of the Integrin Mac-1 ( CD11b / CD18 ) to the Third Immunoglobulin-like Domain of ICAM-1 ( CD54 ) and Its Regulation by Glycosylation*. Cell, 1991. **65**(6):961-71.
104. Hermand, P., et al., *Binding sites of leukocyte beta 2 integrins (LFA-1, Mac-1) on the human ICAM-4/LW blood group protein*. J Biol Chem, 2000. **275**(34):26002-10.
105. Barreiro, O., et al., *Dynamic interaction of VCAM-1 and ICAM-1 with moesin and ezrin in a novel endothelial docking structure for adherent leukocytes*. J Cell Biol, 2002. **157**(7):1233-45.
106. Hubbard, A.K. and R. Rothlein, *Intercellular adhesion molecule-1 (ICAM-1) expression and cell signaling cascades*. Free Radic Biol Med, 2000. **28**(9):1379-86.
107. Muro, S., *Intercellular adhesion molecule-1 and vascular cell adhesion molecule-1*, in *Endothelial Biomedicine*, W.C. Aird, Editor. 2007, Cambridge University Press: New York. 1058-70.
108. Lee, B.P. and B.A. Imhof, *Lymphocyte transmigration in the brain: a new way of thinking*. Nat Immunol, 2008. **9**(2):117-8.

109. Muller, W.A., *Getting leukocytes to the site of inflammation*. Vet Pathol, 2013. **50**(1):7-22.
110. Dejana, E., E. Tournier-Lasserre, and B.M. Weinstein, *The control of vascular integrity by endothelial cell junctions: molecular basis and pathological implications*. Dev Cell, 2009. **16**(2):209-21.
111. Ley, K., et al., *Getting to the site of inflammation: the leukocyte adhesion cascade updated*. Nat Rev Immunol, 2007. **7**(9):678-89.
112. Engelhardt, B. and H. Wolburg, *Transendothelial migration of leukocytes: through the front door or around the side of the house?* Eur J Immunol, 2004. **34**(11):2955-63.
113. Serrano, D., *Role of acid sphingomyelinase in ICAM-1/NHE1-dependent endocytosis: implications in leukocyte transmigration*, in *Cell Biology & Molecular Genetics*. 2010, University of Maryland: College Park.
114. Ley, K., et al., *Sequential contribution of L- and P-selectin to leukocyte rolling in vivo*. J Exp Med, 1995. **181**(2):669-75.
115. Zarbock, A., et al., *PSGL-1 engagement by E-selectin signals through Src kinase Fgr and ITAM adapters DAP12 and FcR gamma to induce slow leukocyte rolling*. J Exp Med, 2008. **205**(10):2339-47.
116. Kunkel, E.J., et al., *Absence of trauma-induced leukocyte rolling in mice deficient in both P-selectin and intercellular adhesion molecule 1*. J Exp Med, 1996. **183**(1):57-65.

117. Kunkel, E.J. and K. Ley, *Distinct phenotype of E-selectin-deficient mice. E-selectin is required for slow leukocyte rolling in vivo.* Circ Res, 1996. **79**(6):1196-204.
118. Elices, M.J., et al., *VCAM-1 on activated endothelium interacts with the leukocyte integrin VLA-4 at a site distinct from the VLA-4/fibronectin binding site.* Cell, 1990. **60**(4):577-84.
119. Cinamon, G., et al., *Novel chemokine functions in lymphocyte migration through vascular endothelium under shear flow.* J Leukoc Biol, 2001. **69**(6):860-6.
120. Luu, N.T., G.E. Rainger, and G.B. Nash, *Kinetics of the different steps during neutrophil migration through cultured endothelial monolayers treated with tumour necrosis factor-alpha.* J Vasc Res, 1999. **36**(6):477-85.
121. Carman, C.V., et al., *Transcellular diapedesis is initiated by invasive podosomes.* Immunity, 2007. **26**(6):784-97.
122. Carman, C.V., *Mechanisms for transcellular diapedesis: probing and pathfinding by 'invadosome-like protrusions'.* J Cell Sci, 2009. **122**(17):3025-35.
123. Carman, C.V. and T.A. Springer, *A transmigratory cup in leukocyte diapedesis both through individual vascular endothelial cells and between them.* J Cell Biol, 2004. **167**(2):377-88.
124. Carman, C.V., et al., *Endothelial cells proactively form microvilli-like membrane projections upon intercellular adhesion molecule 1 engagement of leukocyte LFA-1.* J Immunol, 2003. **171**(11):6135-44.

125. Phillipson, M., et al., *Endothelial domes encapsulate adherent neutrophils and minimize increases in vascular permeability in paracellular and transcellular emigration*. PLoS ONE, 2008. **3**(2):e1649.
126. van Buul, J.D., et al., *RhoG regulates endothelial apical cup assembly downstream from ICAM1 engagement and is involved in leukocyte trans-endothelial migration*. J Cell Biol, 2007. **178**(7):1279-93.
127. Yang, L., et al., *ICAM-1 regulates neutrophil adhesion and transcellular migration of TNF-alpha-activated vascular endothelium under flow*. Blood, 2005. **106**(2):584-92.
128. Tilghman, R.W. and R.L. Hoover, *E-selectin and ICAM-1 are incorporated into detergent-insoluble membrane domains following clustering in endothelial cells*. FEBS Lett, 2002. **525**(1-3):83-7.
129. Privratsky, J.R., et al., *Relative contribution of PECAM-1 adhesion and signaling to the maintenance of vascular integrity*. J Cell Sci, 2011. **124**(9):1477-85.
130. Mamdouh, Z., A. Mikhailov, and W.A. Muller, *Transcellular migration of leukocytes is mediated by the endothelial lateral border recycling compartment*. J Exp Med, 2009. **206**(12):2795-808.
131. Mamdouh, Z., G.E. Kreitzer, and W.A. Muller, *Leukocyte transmigration requires kinesin-mediated microtubule-dependent membrane trafficking from the lateral border recycling compartment*. J Exp Med, 2008. **205**(4):951-66.
132. Mamdouh, Z., et al., *Targeted recycling of PECAM from endothelial surface-connected compartments during diapedesis*. Nature, 2003. **421**(6924):748-53.

133. Dejana, E., *Endothelial cell-cell junctions: happy together*. Nat Rev Mol Cell Biol, 2004. **5**(4):261-70.
134. Vockel, M. and D. Vestweber, *How T cells trigger the dissociation of the endothelial receptor phosphatase VE-PTP from VE-cadherin*. Blood, 2013. **122**(14):2512-22.
135. Sumagin, R., E. Lomakina, and I.H. Sarelius, *Leukocyte-endothelial cell interactions are linked to vascular permeability via ICAM-1-mediated signaling*. Am J Physiol Heart Circ Physiol, 2008. **295**(3):H969-77.
136. Marchesi, V.T. and J.L. Gowans, *The migration of lymphocytes through the endothelium of venules in lymph nodes: an electron microscope study*. Proc R Soc London, 1964. **159**:283-90.
137. Williamson, J. and J. Grisham, *Electron microscopy of leukocytic margination and emigration in acute inflammation in dog pancreas*. Am J Pathol, 1961. **39**(2):239-56.
138. Millán, J., et al., *Lymphocyte transcellular migration occurs through recruitment of endothelial ICAM-1 to caveola- and F-actin-rich domains*. Nat Cell Biol, 2006. **8**(2):113-23.
139. Hashimoto, K., et al., *Live-cell visualization of the trans-cellular mode of monocyte transmigration across the vascular endothelium, and its relationship with endothelial PECAM-1*. J Physiol Sci, 2012. **62**(1):63-9.
140. Nourshargh, S., P.L. Hordijk, and M. Sixt, *Breaching multiple barriers: leukocyte motility through venular walls and the interstitium*. Nat Rev Mol Cell Biol, 2010. **11**(5):366-78.

141. Woodfin, A., et al., *The junctional adhesion molecule JAM-C regulates polarized transendothelial migration of neutrophils in vivo*. Nat Immunol, 2011. **12**(8):761-9.
142. Marmon, S., et al., *Caveolin-1 expression determines the route of neutrophil extravasation through skin microvasculature*. Am J Pathol, 2009. **174**(2):684-92.
143. Dvorak, A.M. and D. Feng, *The vesiculo-vacuolar organelle (VVO). A new endothelial cell permeability organelle*. J Histochem Cytochem, 2001. **49**(4):419-32.
144. Kollman, J.M., et al., *Crystal structure of human fibrinogen*. Biochemistry, 2009. **48**(18):3877-86.
145. Altieri, D.C., et al., *Structural recognition of a novel fibrinogen gamma chain sequence (117-133) by intercellular adhesion molecule-1 mediates leukocyte-endothelium interaction*. J Biol Chem, 1995. **270**(2):696-9.
146. Mosesson, M.W., *Fibrinogen and fibrin structure and functions*. J Thromb Haemost, 2005. **3**(8):1894-904.
147. Bach, T.L., et al., *Endothelial cell VE-cadherin functions as a receptor for the beta15-42 sequence of fibrin*. J Biol Chem, 1998. **273**(46):30719-28.
148. Cheresh, D.A., *Human endothelial cells synthesize and express an Arg-Gly-Asp-directed adhesion receptor involved in attachment to fibrinogen and von Willebrand factor*. Proc Natl Acad Sci USA, 1987. **84**(18):6471-5.
149. Charo, I.F., L.S. Bekeart, and D.R. Phillips, *Platelet glycoprotein IIb-IIIa-like proteins mediate endothelial cell attachment to adhesive proteins and the extracellular matrix*. J Biol Chem, 1987. **262**(21):9935-8.

150. Bae, J.-S., L. Yang, and A.R. Rezaie, *Receptors of the protein C activation and activated protein C signaling pathways are colocalized in lipid rafts of endothelial cells*. Proc Natl Acad Sci USA, 2007. **104**(8):2867-72.
151. Horvat, R. and G.E. Palade, *Thrombomodulin and thrombin localization on the vascular endothelium; their internalization and transcytosis by plasmalemmal vesicles*. Eur J Cell Biol, 1993. **61**(2):299-313.
152. Altieri, D.C., et al., *Oligospecificity of the cellular adhesion receptor Mac-1 encompasses an inducible recognition specificity for fibrinogen*. J Cell Biol, 1988. **107**(5):1893-900.
153. Harmening, D.M., *Clinical hematology and fundamentals of hemostasis*. D.M. Harmening, Editor. 2001, F. A. Davis Co.: Philadelphia.
154. Rosenberg, R. and W. Aird, *Vascular-bed-specific hemostasis and hypercoagulable states*. N Engl J Med, 1999. **340**(20):1555-64.
155. Aird, W.C., *Coagulation*. Crit Care Med, 2005. **33**(12 Suppl):S485-7.
156. Adams, R.L.C. and R.J. Bird, *Review article: coagulation cascade and therapeutics update: relevance to nephrology. Part 1: overview of coagulation, thrombophilias and history of anticoagulants*. Nephrology, 2009. **14**(5):462-70.
157. Bavendiek, U., et al., *Induction of tissue factor expression in human endothelial cells by CD40 ligand is mediated via activator protein 1, nuclear factor kappa B, and Egr-1*. J Biol Chem, 2002. **277**(26):25032-9.
158. Yang, Y. and J. Loscalzo, *Regulation of tissue factor expression in human microvascular endothelial cells by nitric oxide*. Circulation, 2000. **101**(18):2144-48.

159. Parry, G.C.N. and N. Mackman, *Transcriptional regulation of tissue factor expression in human endothelial cells*. *Arterioscler Thromb Vasc Biol*, 1995. **15**(5):612-21.
160. Kolev, K. and R. Machovich, *Molecular and cellular modulation of fibrinolysis*. *Thromb Haemost*, 2003. **89**(4):610-21.
161. Cines, D.B., et al., *Endothelial cells in physiology and in the pathophysiology of vascular disorders*. *Blood*, 1998. **91**(10):3527-61.
162. Blombäck, B., et al., *Native fibrin gel networks observed by 3D microscopy, permeation and turbidity*. *Biochimica Biophys Acta*, 1989. **997**(1-2):96-110.
163. Kadish, J.L., C.E. Butterfield, and J. Folkman, *The effect of fibrin on cultured vascular endothelial cells*. *Tissue Cell*, 1979. **11**(1):99-108.
164. Ribes, J.A., C.W. Francis, and D.D. Wagner, *Fibrin induces release of von Willebrand factor from endothelial cells*. *J Clin Invest*, 1987. **79**(1):117-23.
165. Ruggeri, Z.M., *Functional domains of von Willebrand factor involved in interactions with platelets and the subendothelium*. *Prog Clin Biol Res*, 1988. **283**:219-53.
166. Kaufman, R.J., *Biological regulation of factor VIII activity*. *Annu Rev Med*, 1992. **43**:325-39.
167. Harley, S.L., J. Sturge, and J.T. Powell, *Regulation by fibrinogen and its products of intercellular adhesion molecule-1 expression in human saphenous vein endothelial cells*. *Arterioscler Thromb Vasc Biol*, 2000. **20**(3):652-8.
168. Martinez, J., et al., *Interaction of fibrin with VE-cadherin*. *Ann NY Acad Sci*, 2006. **936**:386-405.

169. Liu, H.H., et al., *Interaction of fibrin and VE-cadherin in regulating cytoskeleton change of endothelial cell in angiogenesis*. Eur J Neurol, 2008. **15**(s3):258-59.
170. Chang, M.C., et al., *Integrin alpha v beta 3 and phospholipase C regulate prostacyclin formation of endothelial cells caused by ancrod-generated fibrin*. Eur J Pharmacol, 1996. **297**(1-2):129-36.
171. Xu, Q., et al., *Integrin alphavbeta3-RGDS interaction mediates fibrin-induced morphological changes of glomerular endothelial cells*. Kidney Int, 1999. **56**(4):1413-22.
172. Languino, L.R., et al., *Fibrinogen mediates leukocyte adhesion to vascular endothelium through an ICAM-1-dependent pathway*. Cell, 1993. **73**(7):1423-34.
173. van de Stolpe, A., et al., *Fibrinogen binding to ICAM-1 on EA.hy 926 endothelial cells is dependent on an intact cytoskeleton*. Thromb Haemost, 1996. **75**(1):182-9.
174. Gardiner, E.E. and S.E. D'Souza, *Sequences within fibrinogen and intercellular adhesion molecule-1 (ICAM-1) modulate signals required for mitogenesis*. J Biol Chem, 1999. **274**(17):11930-6.
175. Ichinose, A. and N. Aoki, *The initiation of fibrinolysis in alpha 2-plasmin inhibitor deficient plasma. Role of fibrin*. Thromb Res, 1986. **41**(6):847-54.
176. Levin, E.G., L. Santell, and K.G. Osborn, *The expression of endothelial tissue plasminogen activator in vivo: a function defined by vessel size and anatomic location*. J Cell Sci, 1997. **110**(2):139-48.
177. Gualandris, A. and M. Presta, *Transcriptional and posttranscriptional regulation of urokinase-type plasminogen activator expression in endothelial cells by basic fibroblast growth factor*. J Cell Physiol, 1995. **162**(3):400-9.

178. Cesarman-Maus, G. and K.A. Hajjar, *Molecular mechanisms of fibrinolysis*. Br J Haematol, 2005. **129**(3):307-21.
179. Brogren, H., et al., *Platelets synthesize large amounts of active plasminogen activator inhibitor 1*. Blood, 2004. **104**(13):3943-8.
180. Walker, J. and M. Nesheim, *The molecular weights, mass distribution, chain composition, and structure of soluble fibrin degradation products released from a fibrin clot perfused with plasmin*. J Biol Chem, 1999. **274**(8):5201-12.
181. Jennewein, C., et al., *Novel aspects of fibrin(ogen) fragments during inflammation*. Mol Med, 2011. **17**(5-6):568-73
182. Collet, J.P., et al., *Influence of fibrin network conformation and fibrin fiber diameter on fibrinolysis speed : dynamic and structural approaches by confocal microscopy*. Arterioscler Thromb Vasc Biol, 2000. **20**(5):1354-61.
183. Veklich, Y., et al., *Structural studies of fibrinolysis by electron microscopy*. Blood, 1998. **92**(12):4721-9.
184. Vassalli, J.D., A.P. Sappino, and D. Belin, *The plasminogen activator/plasmin system*. J Clin Invest, 1991. **88**(4):1067-72.
185. Fukao, H. and O. Matsuo, *Antithrombotic regulation in human endothelial cells by fibrinolytic factors*. Semin Thromb Hemost, 2000. **26**(1):33-8.
186. Kirsch, R., et al., *Fibrinogen is degraded and internalized during incubation with neutrophils, and fibrinogen products localize to electron lucent vesicles*. Biochem J, 2002. **364**(Pt 2):403-12.

187. Simon, D.I., et al., *Fibrin(ogen) is internalized and degraded by activated human monocytoïd cells via Mac-1 (CD11b/CD18): a nonplasmin fibrinolytic pathway.* Blood, 1993. **82**(8):2414-22.
188. Smalberg, J.H., et al., *Hypercoagulability and hypofibrinolysis and risk of deep vein thrombosis and splanchnic vein thrombosis: similarities and differences.* Arterioscler, Thromb Vascular Biology, 2011. **31**(3):485-93.
189. Ansar, M., et al., *Biological functionalization of drug delivery carriers to bypass size restrictions of receptor-mediated endocytosis independently from receptor targeting.* ACS Nano, 2013. **7**(12):10597-611.
190. Muro, S., et al., *Endothelial targeting of high-affinity multivalent polymer nanocarriers directed to intercellular adhesion molecule 1.* J Pharmacol Exp Ther, 2006. **317**(3):1161-9.
191. Papademetriou, I.T., et al., *In vivo performance of polymer nanocarriers dually-targeted to epitopes of the same or different receptors.* Biomaterials, 2013. **34**(13):3459–66.
192. Cernuda-Morollon, E., S. Gharbi, and J. Millan, *Discriminating between the paracellular and transcellular routes of diapedesis.* Methods Mol Biology (Clifton, N.J.), 2010. **616**:69-82.
193. Humphries, W.H.t., C.J. Szymanski, and C.K. Payne, *Endo-lysosomal vesicles positive for Rab7 and LAMP1 are terminal vesicles for the transport of dextran.* PLoS One, 2011. **6**(10):e26626.
194. Ghaffarian, R. and S. Muro, *Models and methods to evaluate transport of drug delivery systems across cellular barriers.* J Vis Exp, 2013. (80):e50638.

195. Hsu, J., et al., *Enhanced endothelial delivery and biochemical effects of alpha-galactosidase by ICAM-1-targeted nanocarriers for Fabry disease*. J Control Release, 2011. **149**(3):323-31.
196. Jerome, W.G., S. Handt, and R.R. Hantgan, *Endothelial cells organize fibrin clots into structures that are more resistant to lysis*. Microsc Microanal, 2005. **11**(3):268-77.
197. Horinouchi, K., et al., *Acid sphingomyelinase deficient mice: a model of types A and B Niemann-Pick disease*. Nat. Genet., 1995. **10**(3):288-93.
198. Langer, R., *Drug delivery and targeting*. Nature, 1998. **392**(6679 Suppl):5-10.
199. Tiwari, G., et al., *Drug delivery systems: An updated review*. Intern J Pharm Investig, 2012. **2**(1):2-11.
200. Yoo, J.-W., et al., *Bio-inspired, bioengineered and biomimetic drug delivery carriers*. Nat Rev Drug Discov, 2011. **10**(7):521-35.
201. Muro, S., *Challenges in design and characterization of ligand-targeted drug delivery systems*. J Control Release, 2012. **164**(2):125-37.
202. Eniola, A.O., et al., *I-Domain of Lymphocyte Function-Associated Antigen-1 Mediates Rolling of Polystyrene Particles on ICAM-1 under Flow*. Biophys J, 2005. **89**(5):3577-88.
203. Eniola, A.O. and D.A. Hammer, *In vitro characterization of leukocyte mimetic for targeting therapeutics to the endothelium using two receptors*. Biomaterials, 2005. **26**(34):7136-44.
204. Eniola, A.O. and D.A. Hammer, *Artificial polymeric cells for targeted drug delivery*. J Control Release, 2003. **87**(1-3):15-22.

205. Eniola, A.O., P.J. Willcox, and D.A. Hammer, *Interplay between rolling and firm adhesion elucidated with a cell-free system engineered with two distinct receptor-ligand pairs*. Biophys J, 2003. **85**(4):2720-31.
206. Schmid-Schonbein, G.W., Y.Y. Shih, and S. Chien, *Morphometry of human leukocytes*. Blood, 1980. **56**(5):866-75.
207. Dittrich, R., M.A. Ritter, and D.W. Droste, *Microembolus detection by transcranial doppler sonography*. Eur J Ultrasound, 2002. **16**(1-2):21-30.
208. Chigaev, A., et al., *Real-time analysis of the inside-out regulation of lymphocyte function-associated antigen-1 revealed similarities to and differences from very late antigen-4*. J Biol Chem, 2011. **286**(23):20375-86.
209. van Kooyk, Y., et al., *Activation of LFA-1 through a Ca<sup>2+</sup>(+)-dependent epitope stimulates lymphocyte adhesion*. J Cell Biol, 1991. **112**(2):345-54.
210. van Kooyk, Y., S.J. van Vliet, and C.G. Figdor, *The actin cytoskeleton regulates LFA-1 ligand binding through avidity rather than affinity changes*. J Biol Chem, 1999. **274**(38):26869-77.
211. Brown, V.I. and M.I. Greene, *Molecular and cellular mechanisms of receptor-mediated endocytosis*. DNA Cell Biol, 1991. **10**(6):399-409.
212. Neelamegham, S., et al., *Hydrodynamic shear shows distinct roles for LFA-1 and Mac-1 in neutrophil adhesion to intercellular adhesion molecule-1*. Blood, 1998. **92**(5):1626-38.
213. Chames, P., et al., *Therapeutic antibodies: successes, limitations and hopes for the future*. Br J Pharmacol, 2009. **157**(2):220-33.

214. Tchesnokova, V., et al., *Type 1 fimbrial adhesin FimH elicits an immune response that enhances cell adhesion of Escherichia coli*. *Infect Immun*, 2011. **79**(10):3895-904.
215. Oyen, D., et al., *Mechanistic analysis of allosteric and non-allosteric effects arising from nanobody binding to two epitopes of the dihydrofolate reductase of Escherichia coli*. *Biochim Biophys Acta*, 2013. **1834**(10):2147-57.
216. Garnacho, C., D. Serrano, and S. Muro, *A fibrinogen-derived peptide provides intercellular adhesion molecule-1-specific targeting and intraendothelial transport of polymer nanocarriers in human cell cultures and mice*. *J Pharmacol Exp Ther*, 2012. **340**(3):638-47.
217. Medina, D.L., et al., *Transcriptional activation of lysosomal exocytosis promotes cellular clearance*. *Dev Cell*, 2011. **21**(3):421-30.
218. Schenkel, A.R., Z. Mamdouh, and W.A. Muller, *Locomotion of monocytes on endothelium is a critical step during extravasation*. *Nat Immunol*, 2004. **5**(4):393-400.
219. Steiner, O., et al., *Differential roles for endothelial ICAM-1, ICAM-2, and VCAM-1 in shear-resistant T cell arrest, polarization, and directed crawling on blood-brain barrier endothelium*. *J Immunol*, 2010. **185**(8):4846-55.
220. Yang, L., et al., *Endothelial cell cortactin coordinates intercellular adhesion molecule-1 clustering and actin cytoskeleton remodeling during polymorphonuclear leukocyte adhesion and transmigration*. *J Immunol*, 2006. **177**(9):6440-9.

221. Barreiro, O., et al., *Endothelial adhesion receptors are recruited to adherent leukocytes by inclusion in preformed tetraspanin nanoplateforms*. J Cell Biol, 2008. **183**(3):527-42.
222. Barreiro, O., et al., *Endothelial tetraspanin microdomains regulate leukocyte firm adhesion during extravasation*. Blood, 2005. **105**(7):2852-61.
223. Phillipson, M., et al., *Intraluminal crawling of neutrophils to emigration sites: a molecularly distinct process from adhesion in the recruitment cascade*. J Exp Med, 2006. **203**(12):2569-75.
224. Shulman, Z., et al., *Lymphocyte crawling and transendothelial migration require chemokine triggering of high-affinity LFA-1 integrin*. Immunity, 2009. **30**(3):384-96.
225. Shaw, S.K., et al., *Reduced expression of junctional adhesion molecule and platelet/endothelial cell adhesion molecule-1 (CD31) at human vascular endothelial junctions by cytokines tumor necrosis factor-alpha plus interferon-gamma does not reduce leukocyte transmigration under flow*. Am J Pathol, 2001. **159**(6):2281-91.
226. Allingham, M.J., J.D. van Buul, and K. Burridge, *ICAM-1-mediated, Src- and Pyk2-dependent vascular endothelial cadherin tyrosine phosphorylation is required for leukocyte transendothelial migration*. J Immunol, 2007. **179**(6):4053-64.
227. Kleyman, T.R. and E.J. Cragoe, *Amiloride and its analogs as tools in the study of ion transport*. J Membr Biol, 1988. **105**(1):1-21.

228. Masereel, B., L. Pochet, and D. Laeckmann, *An overview of inhibitors of Na(+)/H(+) exchanger*. Eur J Med Chem, 2003. **38**(6):547-54.
229. von Bismarck, P., et al., *Improved pulmonary function by acid sphingomyelinase inhibition in a newborn piglet lavage model*. Am J Respir Crit Care Med, 2008. **177**(11):1233-41.
230. Jbeily, N., et al., *Hyperresponsiveness of mice deficient in plasma-secreted sphingomyelinase reveals its pivotal role in early phase of host response*. J Lipid Res, 2012. **54**(2):410-24.
231. Altura, B.M., et al., *Sphingomyelinase and ceramide analogs induce vasoconstriction and leukocyte-endothelial interactions in cerebral venules in the intact rat brain: Insight into mechanisms and possible relation to brain injury and stroke*. Brain Res Bull, 2002. **58**(3):271-8.
232. Ding, Z., K. Xiong, and T.B. Issekutz, *Regulation of chemokine-induced transendothelial migration of T lymphocytes by endothelial activation: differential effects on naive and memory T cells*. J Leukoc Biol, 2000. **67**(6):825-33.
233. Faveeuw, C., et al., *Roles of alpha(4) integrins/VCAM-1 and LFA-1/ICAM-1 in the binding and transendothelial migration of T lymphocytes and T lymphoblasts across high endothelial venules*. Int Immunol, 2000. **12**(3):241-51.
234. Schrage, A., et al., *Enhanced T cell transmigration across the murine liver sinusoidal endothelium is mediated by transcytosis and surface presentation of chemokines*. Hepatology, 2008. **48**(4):1262-72.

235. Denker, S.P., et al., *Direct binding of the Na<sup>+</sup>-H exchanger NHE1 to ERM proteins regulates the cortical cytoskeleton and cell shape independently of H<sup>+</sup> translocation*. Mol Cell, 2000. **6**(6):1425-36.
236. Vicente-Manzanares, M., C.K. Choi, and A.R. Horwitz, *Integrins in cell migration--the actin connection*. J Cell Sci, 2009. **122**(2):199-206.
237. Denker, S.P. and D.L. Barber, *Ion transport proteins anchor and regulate the cytoskeleton*. Curr Opin Cell Biol, 2002. **14**(2):214-20.
238. Kunishima, M., et al., *Spontaneous membrane fusion induced by chemical formation of ceramides in a lipid bilayer*. J Am Chem Soc, 2006. **128**(45):14452-3.
239. Hoffman, M. and D. Monroe, *A Cell-based Model of Hemostasis*. Thromb Haemost, 2001. **85**(6):958-65.
240. Komorowicz, E., et al., *Flow rate-modulated dissolution of fibrin with clot-embedded and circulating proteases*. Circ Res, 1998. **82**(10):1102-8.
241. Gonda, S.R. and J.R. Shainoff, *Adsorptive endocytosis of fibrin monomer by macrophages: evidence of a receptor for the amino terminus of the fibrin alpha chain*. Proc Natl Acad Sci USA, 1982. **79**(15):4565-9.
242. Emeis, J.J., J. Lindeman, and W. Nieuwenhuizen, *Immunoenzyme histochemical localization of fibrin degradation products in tissues*. Am J Pathol, 1981. **103**(3):337-44.
243. Garcia, J.G., R.F. Dodson, and K.S. Callahan, *Effect of environmental particulates on cultured human and bovine endothelium. Cellular injury via an oxidant-dependent pathway*. Lab Invest, 1989. **61**(1):53-61.

244. Garcia, J.G., et al., *Asbestos-induced endothelial cell activation and injury. Demonstration of fiber phagocytosis and oxidant-dependent toxicity*. Am Rev Respir Dis, 1988. **138**(4):958-64.
245. Kirsch, T., et al., *Engulfment of apoptotic cells by microvascular endothelial cells induces proinflammatory responses*. Blood, 2007. **109**(7):2854-62.
246. Stan, R.V., *Endocytosis pathways in endothelium: how many?* Am J Physiol Lung Cell Mol Physiol, 2006. **290**(5):L806-8.
247. Muro, S., M. Koval, and V. Muzykantov, *Endothelial endocytic pathways: gates for vascular drug delivery*. Curr Vasc Pharmacol, 2004. **2**(3):281-99.
248. Oh, P., et al., *Live dynamic imaging of caveolae pumping targeted antibody rapidly and specifically across endothelium in the lung*. Nat Biotechnol, 2007. **25**(3):327-37.
249. Harley, S.L. and J.T. Powell, *Interaction of fibrinogen with saphenous vein endothelial cells stimulates tyrosine phosphorylation of cortactin*. Endothelium, 2000. **7**(2):149-54.
250. Guo, M., et al., *Fibrinogen-gamma C-terminal fragments induce endothelial barrier dysfunction and microvascular leak via integrin-mediated and RhoA-dependent mechanism*. Arterioscler Thromb Vasc Biol, 2009. **29**(3):394-400.
251. Ricard, I., M.D. Payet, and G. Dupuis, *VCAM-1 is internalized by a clathrin-related pathway in human endothelial cells but its alpha(4)beta(1) integrin counter-receptor remains associated with the plasma membrane in human T lymphocytes*. Eur J Immunol, 1998. **28**(5):1708-18.

252. Xiao, K., et al., *p120-Catenin Regulates Clathrin-dependent Endocytosis of VE-Cadherin*. Mol Biol Cell, 2005. **16**(11):5141-51.
253. Odrliin, T.M., et al., *Integrin alphavbeta3-mediated endocytosis of immobilized fibrinogen by A549 lung alveolar epithelial cells*. Am J Respir Cell Mol Biol, 2001. **24**(1):12-21.
254. Seglen, P.O., B. Grinde, and A.E. Solheim, *Inhibition of the lysosomal pathway of protein degradation in isolated rat hepatocytes by ammonia, methylamine, chloroquine and leupeptin*. Eur J Biochem, 1979. **95**(2):215-25.
255. Atochin, D.N., et al., *Mouse model of microembolic stroke and reperfusion*. Stroke, 2004. **35**(9):2177-82.
256. Verheugt, F.W., et al., *Reocclusion: the flip side of coronary thrombolysis*. J Am Coll Cardiol, 1996. **27**(4):766-73.
257. Davalos, D. and K. Akassoglou, *Fibrinogen as a key regulator of inflammation in disease*. Semin Immunopathol, 2012. **34**(1):43-62.
258. Calderon, A.J., et al., *Optimizing endothelial targeting by modulating the antibody density and particle concentration of anti-ICAM coated carriers*. J Control Release, 2011. **150**(1):37-44.
259. Bhowmick, T., et al., *Effect of flow on endothelial endocytosis of nanocarriers targeted to ICAM-1*. J Control Release, 2012. **157**(3):485-92.
260. Garnacho, C., et al., *RhoA activation and actin reorganization involved in endothelial CAM-mediated endocytosis of anti-PECAM carriers: critical role for tyrosine 686 in the cytoplasmic tail of PECAM-1*. Blood, 2008. **111**(6):3024-33.

261. Simon, S.I. and G.W. Schmid-Schönbein, *Biophysical aspects of microsphere engulfment by human neutrophils*. Biophys J, 1988. **53**(2):163-73.
262. Rudt, S. and R. Muller, *Invitro phagocytosis assay of nanoparticles and microparticles by chemiluminescence. 1. Effect of analytical parameters, particle-size and particle concentration*. J Control Release, 1992. **22**(3):263-271.
263. Champion, J.A. and S. Mitragotri, *Role of target geometry in phagocytosis*. Proc Natl Acad Sci USA, 2006. **103**(13):4930-4.
264. Fernandes, M.C., et al., *Trypanosoma cruzi subverts the sphingomyelinase-mediated plasma membrane repair pathway for cell invasion*. J Exp Med, 2011. **208**(5):909-21.
265. Suzuki, Y., et al., *SM-20220, a Na(+)/H(+) exchanger inhibitor: effects on ischemic brain damage through edema and neutrophil accumulation in a rat middle cerebral artery occlusion model*. Brain Res, 2002. **945**(2):242-8.
266. Wang, Y., et al., *Mice with a null mutation in the NHE1 Na<sup>+</sup>-H<sup>+</sup> exchanger are resistant to cardiac ischemia-reperfusion injury*. Circ Res, 2003. **93**(8):776-82.
267. Teichgräber, V., et al., *Ceramide accumulation mediates inflammation, cell death and infection susceptibility in cystic fibrosis*. Nat Med, 2008. **14**(4):382-91.
268. Wedmore, C.V. and T.J. Williams, *Control of vascular permeability by polymorphonuclear leukocytes in inflammation*. Nature, 1981. **289**(5799):646-50.
269. Vestweber, D., *Relevance of endothelial junctions in leukocyte extravasation and vascular permeability*. Ann NY Acad Sci, 2012. **1257**:184-92.

270. Masedunskas, A., et al., *Activated leukocyte cell adhesion molecule is a component of the endothelial junction involved in transendothelial monocyte migration*. FEBS Lett, 2006. **580**(11):2637-45.
271. Huang, M.-T., et al., *ICAM-2 mediates neutrophil transmigration in vivo: evidence for stimulus specificity and a role in PECAM-1-independent transmigration*. Blood, 2006. **107**(12):4721-7.
272. Azcutia, V., et al., *Endothelial CD47 promotes vascular endothelial-cadherin tyrosine phosphorylation and participates in T cell recruitment at sites of inflammation in vivo*. J Immunol, 2012. **189**(5):2553-62.
273. Couture, P., et al., *Adhesion and transcellular migration of neutrophils and B lymphocytes on fibroblasts*. Exp Cell Res, 2009. **315**(13):2192-206.
274. Muro, S., E.H. Schuchman, and V.R. Muzykantov, *Lysosomal enzyme delivery by ICAM-1-targeted nanocarriers bypassing glycosylation- and clathrin-dependent endocytosis*. Mol Ther, 2006. **13**(1):135-41.
275. Rabiet, M.J., et al., *Thrombin-induced endothelial permeability is associated with changes in cell-to-cell junction organization*. Arterioscler Thromb Vasc Biol, 1996, **16**(3):488-96.
276. Hopkins, A.M., A.W. Baird, and A. Nusrat, *ICAM-1: targeted docking for exogenous as well as endogenous ligands*. Adv Drug Deliv Rev, 2004. **56**(6):763-78.
277. Ockenhouse, C.F., et al., *Plasmodium falciparum-infected erythrocytes bind ICAM-1 at a site distinct from LFA-1, Mac-1, and human rhinovirus*. Cell, 1992. **68**(1):63-9.

278. Avadhanula, V., et al., *Nontypeable Haemophilus influenzae adheres to intercellular adhesion molecule 1 (ICAM-1) on respiratory cells and upregulates ICAM-1 expression*. Infect Immun, 2006, **74**(2):830-8.